CONCEPTUAL INTERNAL DESIGN AND COMPUTATIONAL FLUID DYNAMICS ANALYSIS OF A SUPERSONIC INLET

A THESIS SUBMITTED TO

THE GRADUATE SCHOOL OF NATURAL AND APPLIED SCIENCES OF

MIDDLE EAST TECHNICAL UNIVERSITY

BY

MİNE ALEMDAROĞLU

IN PARTIAL FULFILLMENT OF THE REQUIREMENTS

FOR

THE DEGREE OF MASTER OF SCIENCE

IN

AEROSPACE ENGINEERING

MAY 2005

Approval of the Graduate School of Natural and Applied Sciences

_____

Prof. Dr. Canan ÖZGEN

Director

I certify that this thesis satisfies all the requirements as a thesis for the degree of Master of Science.

_____

Prof. Dr. Nafiz ALEMDAROĞLU

Head of Department

This is to certify that we have read this thesis and that in our opinion it is fully adequate in scope and quality, as a thesis for the degree of Master of Science.

_____	_____
Dr. Sartuk KARASOY	Prof. Dr. Yusuf ÖZYÖRÜK
Co-Supervisor	Supervisor

Examining Committee Members:

Prof. Dr. İ. Hakkı TUNCER	(METU-AEE)	_____
Prof. Dr. Yusuf ÖZYÖRÜK	(METU-AEE)	_____
Prof. Dr. Kahraman ALBAYRAK	(METU- ME)	_____
Assoc. Prof. Dr. Sinan EYİ	(METU-AEE)	_____
Dr. Sartuk KARASOY	(ROKETSAN)	_____

I hereby declare that all information in this document has been obtained and presented in accordance with academic rules and ethical conduct. I also declare that, as required by these rules and conduct, I have fully cited and referenced all material and results that are not original to this work.

Name, Last name : Mine Alemdaroğlu

Signature :

ABSTRACT

CONCEPTUAL INTERNAL DESIGN AND COMPUTATIONAL FLUID DYNAMICS ANALYSIS OF A SUPERSONIC INLET

ALEMDAROĞLU, Mine
M. S., Department of Aerospace Engineering
Supervisor: Prof. Dr. Yusuf ÖZYÖRÜK

May 2005, 144 pages

In this thesis, the conceptual internal design of the air inlet of a supersonic, high altitude, solid propellant ramjet cruise missile is performed. Inviscid, compressible CFD analysis of the designed inlet is made in order to obtain qualitative and quantitative performance characteristics of the inlet at different operating conditions.

The conceptual design of the inlet is realized by using analytical relations and equations, correlations derived from numerous available past experimental data and state-of-the-art design examples. The performance estimation of the designed inlet at different operating conditions is done by using one and two dimensional gas dynamics equations. The results of the performance estimation study are compared with the results of the CFD analysis and these results are discussed in detail. A commercial tool, CFD-FASTRAN®, is used for the CFD analysis. Inlet flow phenomena such as, different shock patterns and shock positions, performance degradation at off-design operating conditions and inlet unstart are observed.

Keywords: Supersonic Inlet, Ramjet, CFD, Inlet Performance Characteristics, Operating Conditions, Unstart

ÖZ

SESÜSTÜ BİR HAVA ALIĞININ KAVRAMSAL İÇ TASARIMI VE SAYISAL AKIŞKANLAR DİNAMİĞİ ANALİZİ

ALEMDAROĞLU, Mine
Yüksek Lisans, Havacılık ve Uzay Mühendisliği Bölümü
Tez Yöneticisi: Prof. Dr. Yusuf ÖZYÖRÜK

Mayıs 2005, 144 sayfa

Bu tezde, sesüstü, yüksek irtifada seyir eden, katı yakıtlı ramjet motorlu bir seyir füzesinin hava alığının kavramsal iç tasarımı yapılmıştır. Tasarlanan bu sesüstü hava alığının değişik çalışma durumlarındaki nitel ve nicel performans özelliklerinin belirlenmesi amacıyla, viskositesiz, sıkıştırılabilir Sayısal Akışkanlar Dinamiği analizi gerçekleştirilmiştir.

Hava alığının kavramsal tasarımının gerçekleştirilmesi sırasında, analitik bağıntılardan ve denklemlerden, korelasyonlardan ve güncel tasarım örneklerinden yararlanılmıştır. Bir ve iki boyutlu gaz dinamiği denklemleri kullanılarak, tasarlanan hava alığının değişik çalışma koşullarındaki performansı tahmin edilmiştir. Bu çalışmasının sonuçları Sayısal Akışkanlar Dinamiği analizinin sonuçları ile karşılaştırılmıştır. Bu sonuçlar detaylı olarak tartışılmıştır. Sayısal Akışkanlar Dinamiği analizi CFD-FASTRAN® ticari yazılımı kullanılarak yapılmıştır. Bu analizlerin sonucunda, değişik şok düzenleri ve şok konumları, tasarım dışı çalışma koşullarında performans azalması ve hava alığının başlamaması gibi çeşitli hava alığı akışı ile ilgili olgular gözlemlenmiştir.

Anahtar Kelimeler: Sesüstü Hava Alığı, Ramjet, Sayısal Akışkanlar Dinamiği, Performans Özellikleri, Çalışma Koşulları, Başlamama

To my family, for their endless love , patience and support ...

ACKNOWLEDGEMENTS

I would like to express my deepest thanks and gratitude to Prof. Dr. Yusuf Özyörük for his supervision, encouragement, patience, understanding and constant guidance during all stages of this thesis.

I would also like to express my deepest thanks and gratitude to Dr. Sartuk Karasoy who spread me his enthusiasm, for his co-supervision, understanding, encouragement, and innovative ideas.

I would like to express my deepest gratitude and special thanks to my true friend Özgür Demir for being a savior in stages of desperation of the thesis.

I would like to express my sincere appreciation to my colleagues from ROKETSAN, Tolga Avcıoğlu, Cengizhan Bahar, Ercan Örücü, Alper Kahvecioğlu, Alp Marangoz, Atılgan Toker, Nevzat Sarışın, Görkem Ertürk and Selma Şimşek for their crucial advises.

I would also like to thank my friend Emre Öztürk for his support and valuable advise.

I would like to express my thanks to Fırat Temel for his support and for his help in the editing of the thesis.

My gratitude, thanks and love is endless for my family who this thesis is devoted to. Without them, and all they have done for me, everything would be impossible.

TABLE OF CONTENTS

LIST OF TABLES

TABLE

LIST OF FIGURES

FIGURE

LIST OF SYMBOLS

a	Speed of sound
A_i	Cross sectional area at station i
C_F	Thrust Coefficient
C_{NM}	Nozzle mass flow coefficient
D_t	Steady state flow distortion
F	Thrust
g	Gravitational acceleration
H	Height or Altitude
I_s	Specific Impulse
L	Length
M_i	Mach number at station i
$\dot{m}_i$	Mass flow rate of air at station i
$\dot{m}_f$	Mass flow rate of fuel
P_i	Static pressure at station i
P_{ti}	Total pressure at station i
PR	Total pressure recovery
q_0	Dynamic pressure at freestream
T_i	Static temperature at station i
T_{ti}	Total temperature at station i
U	Velocity in the x direction
V_i	Total velocity at station i

Greek Symbols

α	Angle of attack
η_n	Nozzle efficiency
η_σ	Ram compression efficiency

η , η_p	Total pressure recovery
ϕ	Equivalence ratio
δ_i	ith wedge angle
θ_i , δ_i	ith oblique shock angle
θ_{sd}	Subsonic diffuser inner body divergence angle
∞	Freestream
γ_i	Specific heat ratio at station i
ρ_i	Density at station i
Σ	Critical area ratio

Subscripts

0, 1, 2, 3, 4, 5, 6	represent the station numbers
R	reference
c	cowl or capture
n	normal component
stoich	stoichiometric
ch	combustion chamber entrance station
s	upstream of terminal normal shock station
sub	subsonic diffuser

Acronyms

CFD	Computational Fluid Dynamics
CFL	Courant-Fredrichs-Lewy number
CPU	Central Processing Unit
SFC	Specific Fuel Consumption

CHAPTER 1

INTRODUCTION

1.1 Objective of the Thesis

The objective of the thesis is twofold. The first objective is to perform the aerodynamic internal conceptual design of a supersonic inlet for an air to ground, high altitude, supersonic, integrated-rocket ramjet cruise missile operating on a solid propellant ramjet at its sustain phase. This objective consists of applying a conceptual design methodology based on analytical methods and correlations, starting from a set of overall system design requirements. The second objective is to perform the inviscid Computational Fluid Dynamics (CFD) study in order to obtain major performance parameters, shock patterns and flow properties at on-design and various off-design operating conditions. The results of the CFD study will be compared to the analytical results, which will be discussed along with the found trends in flowfield behavior.

1.2 Motivation and Overview

Cruise Missiles are guided weapon systems in which aerodynamic lift is used to cruise at a certain altitude during a long period of their flight. Powered by air-breathing engines, they have the advantages of long range, short flight time and high terminal speed which also have advantageous consequences in terms of effectiveness against air defense systems. In today's world, the necessity of being in the right place at the right time is pin-pointed through the threat of mobile weapons that can be driven to a suitable launch site, set up, launched and departed

before sufficient time to respond. These highly mobile and difficult to locate weapons have dwell times of under 10 minutes. Such “Time Critical Target” threats can be eliminated by high altitude supersonic cruise missiles capable of high supersonic speeds with rapid reaction capabilities. The advantage of launching these missiles from air, surface or under-sea platforms beyond the range of relevant defense systems is defined as stand-off capability [1].

Ramjet propulsion has gained importance as sustainer of supersonic cruise missiles, which have to satisfy the requirement of combining long range and high speed. The major advantages of ramjet propulsion is its simple construction and high specific impulse whereas its drawback is that the ramjet engine cannot be started at zero velocity. This disadvantage can be resolved with the addition of an integrated boost motor generating a sufficient thrust which can accelerate the missile to its ramjet take-over speed. This could be achieved by means of a booster motor which would be separated at burn-out. However this design configuration has the disadvantage of added inert mass as well as the additional design complexity of a reliable stage separation system. In order to overcome this drawback, the Integrated Rocket Ramjet was introduced. This concept consists of a combustor that serves initially as a rocket combustion chamber for the integral booster, and after booster burnout as a ramjet combustor [2].

Inlets are principle components of all air-breathing engines which are used to inhale air from freestream. Inlets are used to diffuse air from freestream velocity to a lower velocity required by the engine for accomplishing efficient combustion. The inlet design goal is to diffuse the exact amount of air required by the engine at the required thermodynamic state; to perform this diffusion process with a minimum loss in total pressure; to deliver the air to the engine with tolerable amounts of flow distortion at the combustion chamber entrance plane; and to minimize the inlets contribution to the external drag of the aircraft [3].

Supersonic inlets are composed of supersonic diffuser, throat and subsonic diffuser components. These components are located in this order in the streamwise direction. Inlets may be grouped under nine different categories: their operating Mach number regime, family, geometry, supersonic diffuser form, supersonic compression complexity, supersonic compression direction, location on vehicle body, number and interface with combustor [3].

Inlet performance parameters are closely related to the overall design goals of the inlet. In industrial applications, these performance parameters are measured by the inlet aerodynamicist and are of interest to the engine designer who is concerned about designing an engine to operate on the airflow delivered by the inlet and a following duct. The most important performance parameters are the total pressure recovery, the capture area ratio, the flow distortion and the drag force on the inlet. All of these inlet performance parameters are closely coupled with the operating characteristics of the inlet. For prescribed freestream conditions, the supersonic inlet could be operating under subcritical, critical or supercritical conditions depending on the position of the terminal normal shock Operational characteristics are also classified depending on the operating Mach number: On-design Mach number operation, above-design Mach number operation and below-design Mach number operation [3, 4].

Conventional inlet design process generally consists of designing the inlet at one design point. The selection of this design point is based on the trajectory analyses and the engineering experience of the designers. Performance analysis is the indispensable stage of the design process. At this stage the inlet performance is mapped at various deviation conditions from the design point and idealized standard day conditions. By means of these analyses, the performance at different points of the trajectory can also be determined. It may clearly be interpreted from the operational characteristics of the inlet, that in general the inlet performance is very sensitive to changes in its operating conditions. Analyses to determine the performance of an inlet should be performed at different operating conditions in

order to understand the performance trends and flowfield behavior at various cases that can be encountered during missile flight.

Before the flight test of the missile, test procedures that can be accomplished on the ground are applied. Analytical, empirical or experimental procedures can be used in the solution of inlet development problems. Ground tests are usually very time-consuming and are associated with high cost. Nevertheless, with the advent of more sophisticated computers and progress in computer capability, choice of engineers has shifted to maximizing the analytical and computational procedures. By this means, it is possible to save a significant amount of time and money [5].

1.3 Literature Survey

Valuable text books and working group reports that cover a broad range of information in a wide context of subjects on supersonic missile inlets are available [3, 4, 6] and are most helpful for the understanding of concepts closely investigated hereby.

Research studies that deal with inlets focus on different aspects of the subject matter depending on their specific research objectives. Therefore it is rather difficult to classify them under more general headings. Only some selected studies related to the subject are presented here as follows:

Fleeman [7] presented valuable information about ramjet inlet/airframe integration and conceptual design sizing criteria for supersonic inlets. In this same context, Goldsmith [8] discussed general principles of intake design, performance and integration with the airframe and emphasized research on internal and external flow in pitot intakes.

The development of different methods in order to quantify the total pressure recovery of inlets is a quite common focus of interest for researchers. A study was conducted by Azevedo et al [9]. with the purpose of quantifying the inviscid total pressure losses associated with shock wave systems existing in high Mach number flows.

For many inlets, the supersonic diffuser is composed of several wedges. The problem of optimizing the wedge angles to obtain minimum total pressure loss was investigated by Safarik and Polak [10].

An alternative to using analytical methods or simple correlations during the design process, instead of using analytical methods or simple correlations viscous or inviscid computational tools or semi-empirical flow solvers can be used. Ahsun [11] used viscous and inviscid computational tools to design an actively stabilized supersonic internal compression inlet that can withstand flight velocity, temperature and angle of attack perturbations encountered in atmospheric flight. Details and validation methodology for the Euler semiempirical simulation for three dimensional inlets (2ES3D) were presented by Knight et al. [12].

In a series of studies, Knight et al. [13, 14, 15, 16] performed inlet design using automated optimization. They linked together a semi-empirical flow solver and an improved Genetic Algorithm within an automated loop [13, 14]. They obtained a geometry model for a supersonic missile inlet by combining an efficient simple physical model analysis tool and a sophisticated CFD Navier-Stokes analysis tool [15]. They performed three dimensional optimization of a supersonic inlet by linking together an optimizer and a simulation tool into an automated optimization loop. They verified the results by using a full Navier-Stokes solver [16].

Inlet buzz (or unstart) is an extremely important aspect that should be carefully avoided in the control of an inlet for ramjet application. Related to this subject matter, some aspects of supersonic inlet stability along with the consideration of

buzz-triggering mechanisms and the problem of stable flow regulation were discussed by Connor [17]. Pordal [18] presented information on the transient behavior of supersonic flow through inlets via time varying analysis. Pamadi [19] conducted an experimental study on a two dimensional external compression supersonic inlet and determined its stable flow range and derived a correlation relating inlet geometry, shock stand-off distance and freestream Mach number. Unsteady pressure behavior in a Ramjet/Scramjet Inlet was analyzed by Rodi and Texler [20] by obtaining time accurate pressure measurements during and after inlet unstart. Miller and Smith [21] numerically investigated the unstart caused by back pressure on a high speed inlet and compared the results with Schlieren images. New boundary conditions, that allow to implement Boundary Layer bleed and compressor face conditions and to be used for increasing the accuracy of numerical unsteady supersonic inlet analyses were developed by Mayer and Paynter [22]. Knight et al. [23] examined the angle of attack induced unstart of the High Speed Civil Transport Inlet by using a three-dimensional time-accurate Navier Stokes solver. They presented the results along with the qualitative comparison of the flowfield phenomena with the experimental observations.

The inlet operability with angle of attack has also been an important matter of consideration to researchers. Knight et al. [24] determined the maximum angle of attack value that a High Speed Civil Transport Inlet can sustain before unstart by using a three dimensional Navier-Stokes solver and this value was compared with the experimental results. A computational fluid dynamics analysis of the X-29 Inlet at very high angles of attack (50-90 degrees) in which flow calculations were compared with wind tunnel data was performed by Tindell and Hill [25].

Several more numerical studies were conducted with the purpose of obtaining important inlet performance parameters. Chan and Liang [26] performed a numerical investigation of a Supersonic Mixed Compression Inlet in order to obtain relations between combustion chamber entrance face pressure and total pressure recovery and to analyze flow distortion levels. The variance of inlet performance

parameters with leading edge sweep and freestream Mach number was investigated by Holland and Perkins [27]. In their study, they expanded the two dimensional oblique shock theory to account for three dimensional effects and compared the results with other numerical results.

The extension of the ramjet technology to vehicles flying at hypersonic speeds is the supersonic combustion ramjet (scramjet) concept. The study dealing with a number of optimization problems of a ramjet inlet including the optimization to obtain maximum total pressure recovery was previously presented in this section [10]. A study dealing with the optimization of two dimensional scramjet inlets for maximum total pressure recovery was also performed by Smart [28]. Hsia [29] performed an inviscid analysis of a dual mode scramjet inlet and concluded by comparing the results with test data that this inviscid analysis was capable of predicting the inlet performance trend. Ajmani et al. [30] performed a two-dimensional numerical analysis for a hypersonic inlet to compare the performance of different turbulence models. Cockrell and Huebner [31] performed a computational analysis of a body mounted scramjet inlet. They also conducted an internal drag analysis by using the results and experimental data. Ender et al. [32] developed a MATLAB routine that optimizes the two dimensional hypersonic inlet consisting of three fixed ramps and which is also capable of computing effective inlet height, inlet length and nose height values which allow the oblique shock to attach to the cowl lip at the selected design Mach number.

1.4 Outline of the Thesis

Chapter 1 of the thesis gives a brief overview on inlet fundamentals, design and tests. In this chapter, a literature survey on the subject matter is also presented.

In Chapter 2 inlet fundamentals, inlet performance parameters and inlet operating characteristics are briefly defined and discussed.

Chapter 3 is about the design of a specific inlet. It includes the problem definition, the design requirements and specifications, examination of the effect of the inlet size on the engine performance and a competitor study. The selection of the design-to condition and the design parameters and the sizing of the inlet is also explained in this chapter.

Chapter 4 is about performance estimation of the designed inlet. The analytical equations and the procedure applied to obtain the inlet performance parameters and flow variables at certain stations of the inlet at various operating conditions are presented in this chapter.

Chapter 5 describes the CFD method applied and gives brief information on the flow solver used. The model preparation process applied to the inlet flow problem is described in this chapter.

In Chapter 6, the results obtained through the CFD analyses are presented. This chapter also contains comparison of these results with the analytical result and their discussions.

Chapter 7 presents some conclusions about the present study and suggests some future work directions.

CHAPTER 2

THEORY

2.1 Inlet Fundamentals

In order to successfully design an inlet, it is essential to understand the working fundamentals of the inlet components the significance of the inlet performance parameters and the flow phenomena taking place at various operating conditions. This chapter gives brief explanation on these subjects.

Inlets are one of the principle components of all air-breathing engines. They are required to diffuse air from freestream velocity to a lower velocity required by the engine for accomplishing efficient combustion. The inlet is required to supply the exact amount of air required by the engine at desired velocities. It is also required to perform this task with a minimum loss in total pressure, to deliver the air to the engine with tolerable amounts of flow distortion at the combustion chamber entrance plane, and to minimize the inlets contribution to the external drag of the missile [3].

In a ducted rocket, namely solid propellant ram-rocket application, the integrated rocket ramjet concept is applied as follows: The missile is accelerated to ramjet take-over velocity by the rocket motor contained in the ramjet chamber. After burn-out of the rocket motor (end of boost phase) the rocket motor nozzle is ejected. The rocket motor combustion chamber now becomes the ramjet combustor. The oxygen deficient solid propellant burns within the primary combustion chamber (the gas generator) and the fuel rich combustion products are exhausted into the secondary

combustion chamber. Here these fuel rich combustion products mix and afterburn with the air supplied by the air inlets [2]. A sketch of the operation of the integrated rocket ramjet is given in Figure 2.1 [2].

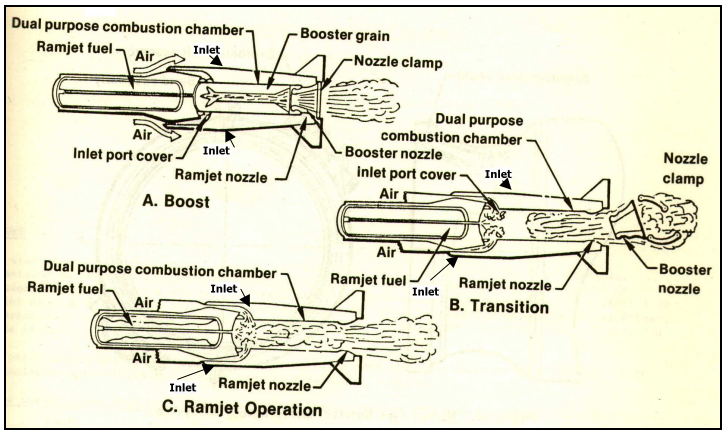

Figure 2.1 Sketch of the operation of the integrated rocket ramjet

It is useful at this point to draw attention to why the ramjet engine cannot be started (cannot produce thrust) at zero velocity. At zero velocity, i.e., when the vehicle is at rest, there is no air flow through the inlet and the internal engine pressure is the same as the ambient pressure. Due to the lack of a compressor component between the inlet and the combustion chamber, unlike turbojet engines, the engine pressure level cannot be raised above the ambient pressure level thus the ramjet engine cannot produce thrust at zero velocity. The total pressure recovery phenomenon of the inlet is also closely related to this fact. For ramjet engines where there is no compressor component, the energy available to do work can be increased by minimizing total pressure losses. This is why the total pressure loss is mostly referred to as the total pressure recovery term of the inlet. An increase in the total pressure recovery, corresponding to a decrease in the total pressure losses, results in an increase in engine thrust. This effect of the total pressure recovery term P_{t2}/P_{t0} is noticed in the non-dimensional thrust coefficient given by Eqn. (2.1) for a ramjet engine. The other equations that describe the ramjet engine performance are the continuity Eqn. (2.2) and the specific fuel consumption Eqn. (2.3).

$$C_F = \frac{2\left(\frac{A_6}{A_R}\right)}{\gamma_0 M_0^{\ 2}}\left\{\frac{\frac{P_{t2}}{P_{t0}}\frac{P_{t4}}{P_{t2}}\eta_N\left[\frac{P_6}{P_{t6}}\left(1+\gamma_6 M_6^{\ 2}\right)_{ideal}\right]}{\frac{P_0}{P_{t0}}}-1\right\}-2\frac{A_0}{A_c}\frac{A_c}{A_R} \qquad (2.1)$$

$$\frac{P_{t5}}{P_{t0}} = \frac{P_{t2}}{P_{t0}}\frac{P_{t4}}{P_{t2}} = \frac{\frac{P_0}{P_{t0}}\dot{m}_0 A_0\left(1+\frac{f}{a}\right)}{\frac{P_5}{P_{t5}}\dot{m}_5 A_5 C_{NM}}\sqrt{\frac{T_{t5}}{T_{t0}}} \qquad (2.2)$$

$$SFC = \frac{3600\dot{m}_f}{C_F q_0 A_R} \qquad (2.3)$$

In Equations (2.1) to (2.3) η_N represents the nozzle efficiency, C_{NM} represents the nozzle mass flow coefficient, f/a represents the fuel to air ratio, q_0 is the freestream dynamic pressure, and $\dot{m}_f$ is the mass flow rate of fuel, $\dot{m}_0$ represents the freestream mass flow rate of air. The term P_{t2}/P_{t0} represents the total pressure ratio across the inlet and the term P_{t4}/P_{t2} represents the total pressure ratio across the combustor.

In order to better illustrate the flow stations that appear in these equations, the Brayton cycle on which the ramjet engine operates on is given in Figure 2.2, and the sketch of a typical ramjet engine consisting of an in-line inlet, a combustor and a nozzle is given in Figure 2.3.

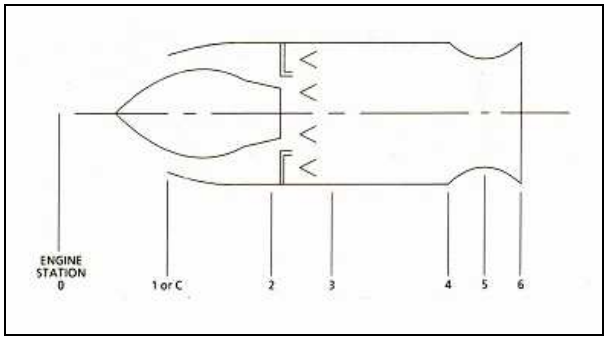

Figure 2.2 Schematic of the engine stations

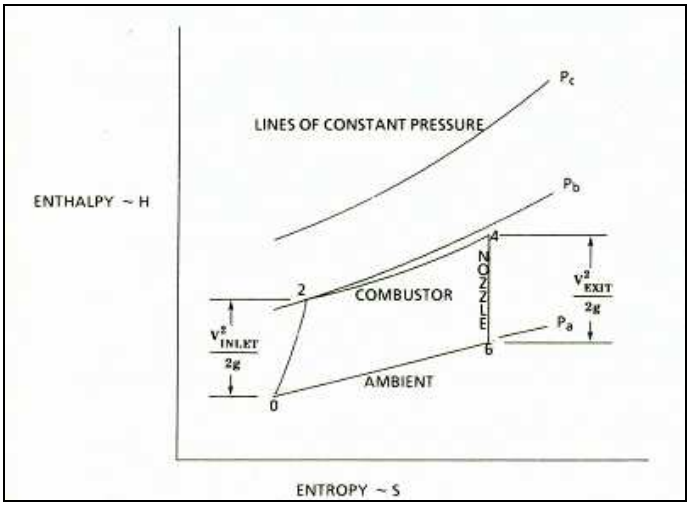

Figure 2.3 The Brayton cycle

Two very important equations related to one-dimensional flow are presented hereby. These two equations are valid under the assumptions of steady, adiabatic, reversible, one-dimensional flow and air is a perfect gas. Along with appropriate modifications they can be applied to the flow through an inlet although, one-dimensional flow techniques are generally insufficient to obtain quantitative measures of the compression process through the inlet. Accordingly, combinations of one and two-dimensional and sometimes three-dimensional techniques are applied when performing complete analyses. For this reason, in this thesis, first

combinations of one and two-dimensional equations are used for the design and performance estimation of the inlet. Then, CFD analyses are conducted to obtain the major performance parameters of the designed inlet.

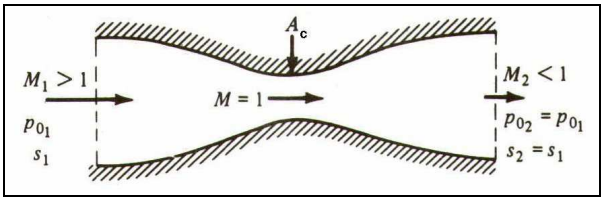

Figure 2.4 Ideal (isentropic) supersonic diffuser

Considering the streamtube shown in Figure 2.4 [33], along which the flow is quasi one-dimensional; we can write:

$$P_t A_c = constant \tag{2.4}$$

The ratio of the critical cross sectional area to any cross sectional area in the streamtube is given by Eqn. (2.5).

$$\frac{A}{A_c} = \Sigma(M,\gamma) = \frac{1}{M}\left(\frac{2+(\gamma-1)M^2}{\gamma+1}\right)^{\frac{\gamma+1}{2(\gamma-1)}} \tag{2.5}$$

During the design process Eqn. (2.4) and Eqn. (2.5) will be combined with the two dimensional Rankine Hugoniot relations to account for the total pressure losses in the supersonic diffuser.

The supersonic inlet is composed of a supersonic diffuser, a throat and a subsonic diffuser. The compression process takes place through the supersonic diffuser. The transition from supersonic to subsonic flow usually takes place across a normal shock that stands in the throat (namely the minimum area) during on-design operating conditions. At the subsonic diffuser the flow is decelerated to an

acceptable Mach number for the combustion chamber. The external wall of the supersonic inlet is called the cowl. The most upstream end of the cowl is called the cowl lip.

2.2 Flow Physics Through the Supersonic Diffuser

Most common supersonic diffuser shapes are presented in Figure 2.5 [3], while three different compression forms are shown in Figure 2.6 [4]. These compression forms are all external, all internal and mixed compression.

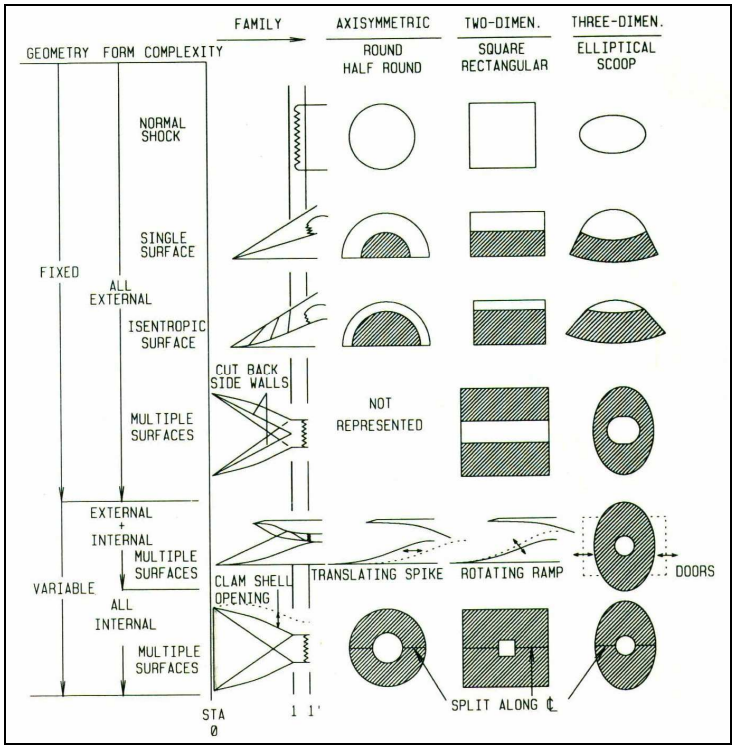

Figure 2.5 Supersonic diffuser shapes

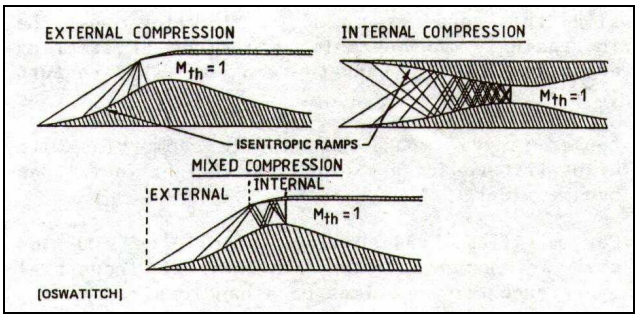

Figure 2.6 Types of compression

Inlet unstart can be described as the flow physics that occurs when the normal shock moves upstream from the throat plane due to some disturbances such as wind gusts or combustor pressure oscillations. The advantage of all external compression is that it allows flow spillage in cases of unstart and the normal shock can be stabilized at an upstream condition where the total pressure recovery value will be nearly the same as the critical total pressure recovery value. If the shock is swallowed by the inlet, this is defined as inlet restart. For the case of all external compression, after the disturbance is removed, the inlet swallows the shock and restart takes place.

If the flow compression process is desired to be both external and internal or desired to be all internal, an implementation of variable geometry is required. In order to start an unstarted inlet, the throat area, must be large enough to pass the entrance area mass flow at a total pressure that corresponds to the value behind a normal shock at the entrance Mach number, allowing swallow of the external shock. On the other hand, if the starting contraction area ratio of an inlet exceeds the required value at a specified Mach number, the inlet will be able to start only with the aid of some variable geometry device.

The third classification of supersonic diffusers is according to their compression complexity. A good parameter for comparing the performance of supersonic inlets with different compression complexity is the total pressure recovery across the supersonic diffuser. In Figure 2.7 [2] the maximum pressure recovery values

through series of oblique or conical shocks and a terminal normal shock in axisymmetric supersonic inlets is plotted against the freestream Mach number.

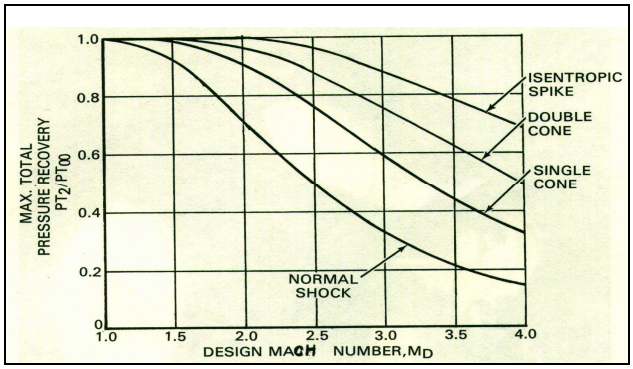

Figure 2.7 Comparison of the total pressure recovery values obtained with different compression complexity

As can be seen from Figure 2.7, for high supersonic Mach numbers and application to compact missiles, multiple compression surfaces and variable geometry diffusers are capable of attaining the highest possible total pressure recovery levels. Nevertheless, their complexity increases weight and cost. In some cases, the designer sacrifices some amount of total pressure recovery to benefit from the advantages of lower weight less cost and simpler design[3].

The fourth and final classification of supersonic diffusers is according to their family. The axisymmetric family consists of round or half-round cross sectional area shapes. The two-dimensional family consists of square or rectangular cross sectional area shapes. The three-dimensional family consists of elliptical or scoop cross sectional area shapes.

2.3 Flow Physics through the Throat and the Subsonic Diffuser

Under normal, design operating conditions, the transition from supersonic to subsonic flow in an inlet occurs across a normal shock that stands at the throat. In inviscid flow the normal shock stands as a single wave or discontinuity. However,

in viscous flow, due to the boundary layer growth along the walls of the supersonic diffuser and the interaction of the normal shock with these boundary layers, a series of discontinuities, called a shock train is formed. This shock train which extends into the subsonic diffuser adds to the unfavorable pressure gradient in the streamwise direction (increases momentum loss in boundary layer) and causes the boundary layer to separate from the walls of the subsonic diffuser. This phenomenon leads to a decrease in total pressure recovery, along with a distorted flow profile that can degrade combustion efficiency. Due to this phenomenon, the subsonic diffuser is generally designed with empirical procedures that must incorporate analytically intractable shock-boundary layer interactions [3]. A sketch of the normal shock interaction with the boundary layer is given in Figure 2.8 [3].

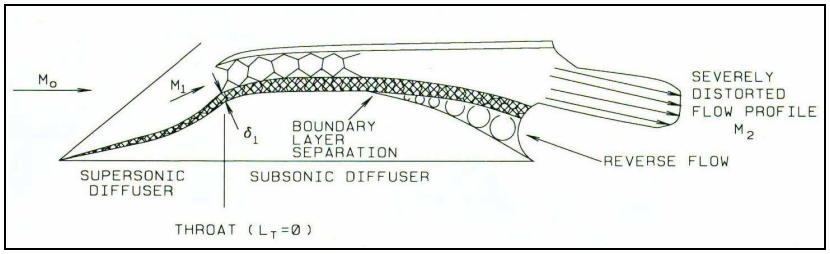

Figure 2.8 Normal shock-boundary layer interaction

The disadvantageous consequences of this problem can be reduced by stretching the throat region in the streamwise direction, to a certain length in which the entire shock train would be contained. The total pressure recovery is maximum for throat lengths equal to or slightly greater than the shock train length. If the throat section length is chosen equal to the shock train length, the boundary layer will be attached to the subsonic diffuser walls and this will yield an attached and a relatively undistorted flow profile.

2.4 Inlet Performance Parameters

Inlet performance parameters related to internal flow are the total pressure recovery, the capture area ratio and the flow distortion. The inlet performance

parameter related to external flow is the drag force on the inlet and the inlets contribution to the missiles lift to drag ratio.

2.4.1 Total pressure recovery

The total pressure recovery term is actually noticed through the understanding of the term defining the efficiency of the compression process taking place in the ramjet engine. The most natural definition of efficiency of the ram compression process is:

$$\eta_\sigma = \frac{work\ done\ in\ compression}{kinetic\ energy\ available} \tag{2.6}$$

At high freestream speeds and particularly for supersonic flow, a more convenient measure than η_σ, is the simple ratio of the mean total pressure at the combustion chamber entrance plane to freestream total pressure. This term, designated as P_{t2}/P_{t0}, is widely known as total pressure recovery and can be sometimes also designated as η, η_p or PR.

The total pressure recovery term has a significant contribution to the engine net thrust. Minimizing total pressure losses in the inlet means increasing total pressure recovery, and accordingly increasing the energy available to do work and the engine thrust. The variation of the thrust coefficient with inlet total pressure recovery is plotted in Figure 2.9. During the generation of this plot constant values were assumed for the other flow variables ($A_6/A_R = 0.8$, $\gamma_0 = 1.4$, $\gamma_6 = 1.2$, $M_0 = 3.5$, $M_6 = 0.27$, $P_{t4}/P_{t2} = 0.9$, $\eta_N = 0.97$, $A_0/A_c = 0.5$, $A_c/A_R = 0.3$).

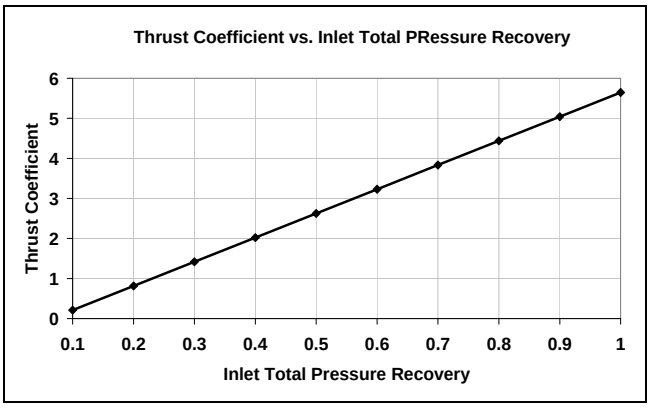

Figure 2.9 Thrust coefficient vs. inlet total pressure recovery graph

2.4.2 Capture area ratio

All important internal flow phenomena and the external drag depend critically on the relative amount of flow through the inlet. Knowing the relative amount of flow through the inlet is important because of several reasons. The first reason is that all performance parameters are functions of the flow through the inlet. The second reason is that, if the flow through the inlet is known, it is possible to avoid undesirable flow physics. Another reason is the possibility of evaluating the one dimensional Mach number at any duct station in order to correlate to subsonic diffuser performance.

The capture area ratio designated by A_0/A_c, also known as mass flow ratio (MFR) is defined as the ratio of flow being ingested to the flow that would be ingested at datum conditions. MFR depends on the operating condition of the inlet. The inlet is required to deliver (to the combustion chamber) the exact amount of air needed by the engine. The capture area is a measure of how well this requirement is satisfied.

2.4.3 Steady state flow distortion

Flow distortion is a performance parameter describing the general health of the inlet flow. The source of total pressure distortion can either be the geometric design, the aerodynamic design or both. The interaction of the inlet shock and the boundary layer on the compression surface may result in flow separation behind the normal shock. Duct flow separation may be caused by the choice of a too high rate of diffusion (cross sectional area change) or the presence of sharp bends. Total pressure distortion can also be caused by missile attitude (incidence or yaw) or by mismatching between engine and inlet airflows which cause departure from critical operation (either subcritical or supercritical operation).

When both the static temperature and pressure are assumed to be constant across the compressor face, both the velocity and Mach number can be considered as functions of total pressure only. Therefore, the distribution of total pressure is the only measurement that needs to be made. The most widespread quantitative distortion parameter used in the inlet design is the steady state flow distortion. This parameter was used in the earliest experiments on inlets conducted in the 1950s [4]. It is designated by D_t and is represented by Eqn. (2.7).

$$D_t = \frac{\Delta P_t}{P_t} = \frac{P_{t2\max} - P_{t2\min}}{P_{t2mean}} \tag{2.7}$$

2.4.4 Drag force on the inlet

Although the drag force on the inlet is composed of pressure drag, viscous drag and momentum drag, the additive (spillage) drag (a subcategory of pressure drag) is the component about which the inlet designer is mostly concerned. Additive (spillage)

drag, includes the drag force applicable to the capture stream tube boundary, experienced during the inlets' operating regime below the design Mach number.

2.5 Operating Characteristics

2.5.1 Operating conditions at 0 degrees incidence and yaw

The operating conditions of a supersonic inlet include the on-design and off-design operating conditions. The on-design operating condition is sometimes also referred to as, the design-to condition in supersonic inlet literature. The design-to condition can be defined as the condition for which the inlet is designed. The on-design condition of a typical ramjet inlet has the following three characteristics:

- **On-design Mach number operation:** Operation at the freestream Mach number for which the compression surfaces were designed.
- **Shock on lip operation:** Operation with the supersonic compression surface shock intersection point on the cowl lip, for inlets containing one or several wedges in the supersonic diffuser component.
- **Critical operation:** Operation with the terminal normal shock located in the throat section of the inlet.

Off-design conditions of a typical ramjet include supercritical operation and subcritical operation.

- **Supercritical operation:** To decrease the engine thrust (namely, to decrease the total pressure recovery below the critical value) the fuel to air ratio must be decreased. At such a condition, the terminal normal shock moves downstream from the throat section into the subsonic diffuser. In the subsonic diffuser, the diverging geometry allows the flow to accelerate to higher Mach

numbers and correspondingly lower total pressure recovery values are yielded. This operating condition is known as “Supercritical Operating Condition”.

- **Subcritical operation:** This condition is attained when the terminal normal shock is positioned forward of the throat. This condition is mostly also referred to as the “inlet unstart” condition. The terminal normal shock moves forward from the throat due to; combustor pressure oscillations, errors in metering fuel flow, perturbations from standard atmosphere, related to hot and cold atmospheric conditions, wind gusts, viscosity effects, differential thermal growth, ablation of thermal protection material.

In subcritical operating condition, as long as the terminal normal shock maintains a stable position in the supersonic diffuser, the subcritical total pressure recovery remains nearly the same as the critical total pressure recovery value [3]. Subcritical operation is carefully avoided in the control of an inlet for the ramjet application. One method to avoid the possibility of subcritical operation during the flight, is to size the exit nozzle throat at a value larger than that for critical pressure recovery. By this means, at heat release values corresponding to the design-to value of the fuel to air ratio, the inlet can achieve a certain amount of its critical total pressure recovery and a supercritical margin is built into the design.

Inlet Buzz: Inlet buzz can be described as the instability of flow in subcritical operation below some value of the flow ratio, in the form of an oscillation of the shock system. Buzz is initiated when the inlet becomes choked because of massive flow separation. The terminal normal shock is pushed upstream, away from the entrance channel on the compression surfaces, in order to spill the unpassed flow. A drastic change takes place in the flow situation causing the separation and attached flow is re-established, yielding, a greatly reduced static pressure created by the starving engine. Correspondingly, the normal shock is sucked back into the subsonic diffuser. Just when the system stabilizes, separation reappears and the whole process repeats itself. This is why buzz is an oscillation and it is

characterized by low frequency and high amplitude [4]. The cause of the separation (the buzz-initiating mechanism) may be the shock wave boundary layer interaction, the diffuser flow separation or the shock wave interference ahead of the inlet [4]. There are several different approaches to what the buzz initiating (triggering) mechanisms are.

The Ferri and Nucci approach is illustrated in Figure 2.10 [2]. Ferri and Nucci's postulate can be summarized as follows. Assuming that the static pressure across the cowl station CLB is uniform, the total pressures of segments CL and LB have different values. The total pressure of segment CL is the one associated with a normal shock at freestream Mach number. The total pressure of segment LB is the one associated with an oblique shock and a strong shock at a Mach number less than the freestream Mach number. The condition leading to instability is the reaching of a compression limit. If the static pressure at the cowl station, becomes equal to the total pressure of segment CL, the flow across CL stagnates. This stagnation requires flow reversal. Hence; instability occurs.

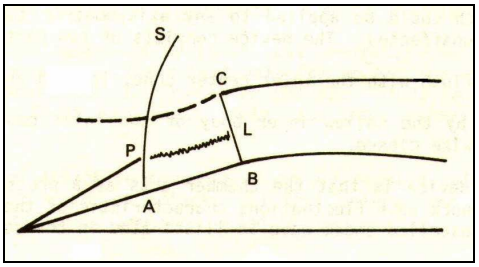

Figure 2.10 Inlet at buzz initiation

A different approach to the inlet instability (inlet buzz) problem, is the Orlin and Dunsworth approach. Orlin and Dunsworth stated that the rate of change of inlet static pressure at the cowl station with mass flow determined the flow stability through the supersonic diffuser. Orlin and Dunsworth defined inlet buzz by introducing the pressure slope criterion. Orlin and Dunsworth postulated that, stable flow broke down when the slope of the static pressure characteristic at entry

passed from negative to positive as flow ratio was reduced [2, 6]. This breakdown condition can be represented as in Eqn. (2.8);

$$\frac{dP_i}{d\left(\frac{A_\infty}{A_i}\right)} = 0 \tag{2.8}$$

It is stated in inlet literature that the *pressure slope* is small and negative throughout the subcritical regime for external-compression inlets as long as the shock intersection point is outside of the entry streamtube [6]. A positive slope is obtained when with increasing flow spillage, the shock intersection point moves inside the entry streamtube and brings air of lower total pressure into the inlet [6].

Buzz can cause structural damage to the inlet, it may also cause compressor surge or ramjet flame out [4]. Therefore attaining stable flow regulation is extremely important. However, the inlet designs which have subcritical stability; yield critical total pressure recovery values less than that can be achieved with “no stability” designs [2]. Since, there is no analytical technique provided to design high stability inlets, the designer has to rely on his/her experience and wind tunnel tests. Of course, this causes great risk and most of the time increases the program cost. Furthermore, most of the times, in industrial applications, due to cost and weight constraints, variable-geometry devices are not implemented into the design. Because of all these reasons, mostly, the inlet designer prefers to design a high performance inlet with no stability in subcritical operation. Meanwhile, the designer implements into the design a shock position control, to ensure supercritical operation and at the same time to avoid subcritical operation.

Hereby completing the discussion on inlet buzz, the nine different operating modes of an all external, isentropic surface, ramjet inlet at 0 degrees incidence and yaw is given in Figure 2.11 [3].

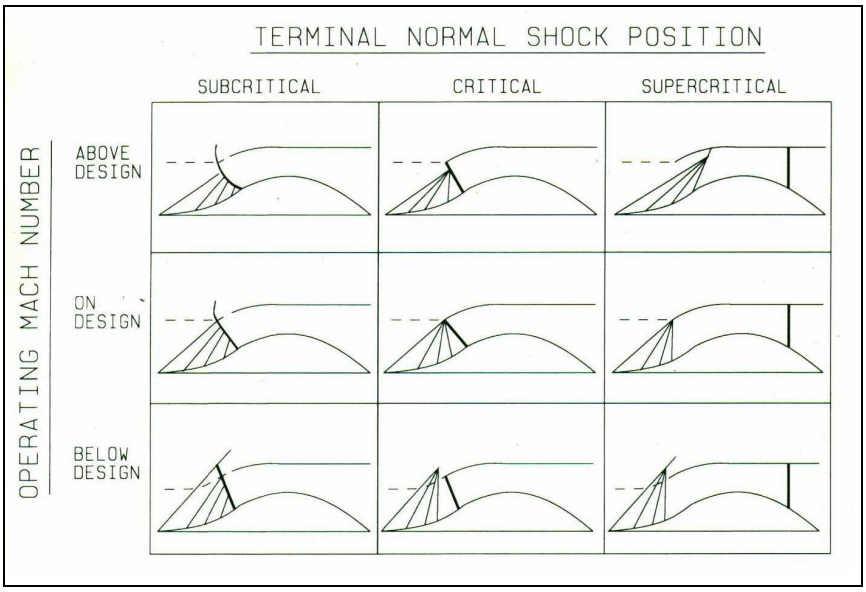

Figure 2.11 The nine operating modes of a typical ramjet inlet

The on-design operating condition is the sketch positioned in the center of the 3 by 3 operating conditions matrix of Figure 2.11. This condition, corresponds to a full capture resulting in no flow spillage and no additive drag. There are 8 possible off-design operating conditions.

Examining Figure 2.11 it is easily noticed that at on-design Mach number supercritical operating conditions the capture area ratio is also equal to 1, and there is no flow spillage or additive drag because the supersonic diffuser flow picture is the same as the on-design critical operating conditions flow picture. During the on design Mach number subcritical operation, if the terminal normal shock maintains a stable position, the uncompressed freestream flow is spilled over the outside of the cowl and the capture area of the inlet is less than 1 and additive drag is present [3].
At above design Mach number, the wedge shock and the compression fan focal point move inside the cowl lip. At this condition the capture streamtube consists of an externally compressed flow along with an uncompressed freestream flow. At above design critical operating condition although the captured freestream tube consists of an externally compressed flow along with an uncompressed freestream

flow, full capture is present and the capture area ratio is equal to 1. During above design supercritical operation, the merger of the wedge shock and the compression fan produces a new shock, which is always stronger than the wedge shock and which can reflect from the cowl wall [3]. Nevertheless, the capture area ratio is equal to 1. At above design subcritical operation, all of the freestream tube cannot be captured, the capture area ratio is less than 1, and the inlet spills air over the cowl lip, causing additive drag.

At below design Mach number, the wedge shock and the compression fan focal point merge outside of the cowl lip, correspondingly the capture area ratio is less than one. The inlet spills air over the cowl lip and additive drag is present. The external flow picture is the same for the below design critical and below design supercritical cases. At the below design subcritical operating case the amount of flow spillage is increased when compared to the below design critical and supercritical cases. This is because of the curved normal shock standing upstream of the cowl lip.

To summarize, the qualitative performance of a supersonic inlet as a function of the terminal normal shock position and the freestream Mach number is given in Figure 2.12 [3].

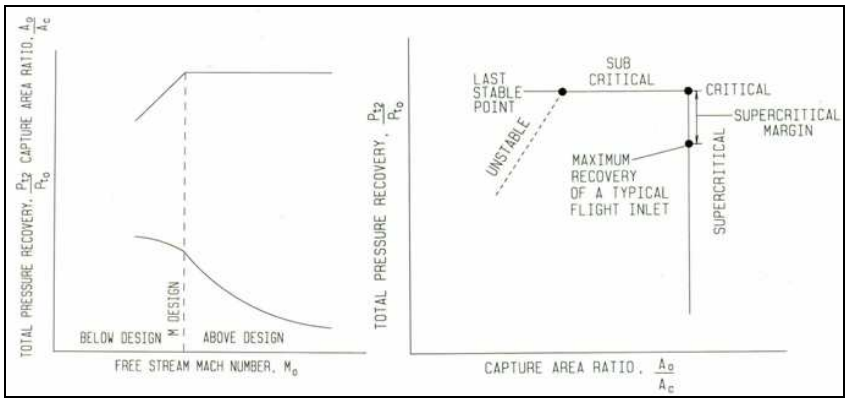

Figure 2.12 Qualitative performance as a function of terminal normal shock position

2.5.2 Operation at incidence

Operation at incidence is common to high altitude, highly maneuverable air-to-air missiles. In such attitude, the inlets behavior is dominated by the state of flow around the entry lip.

Firstly, the characteristics of axisymmetric inlets operating at angle of attack will be discussed. Interpretation from Figure 2.13 [3] leads to the understanding that, though the flow picture is symmetric at zero degrees angle of attack, this symmetry is destroyed when the inlet is rotated to angle of attack with the freestream direction [3].

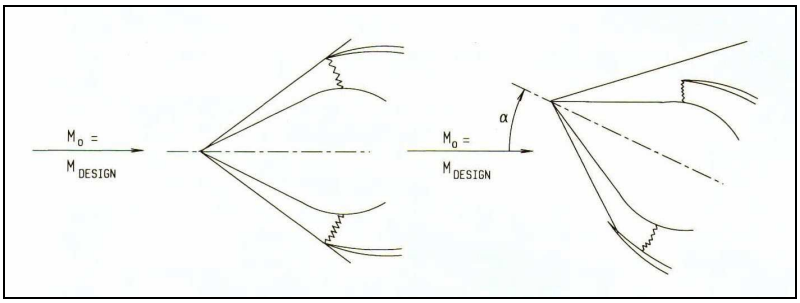

Figure 2.13 Axisymmetric inlet at incidence

The windward side of the shock sheet crosses the cowl lip plane in a manner similar to operation above the design Mach number [3]. The leeward side of the shock sheet lies forward of the cowl lip plane similar to operation below the design Mach number [3]. Hence, the inlet spills air on the leeward side. Because the flow will adjust to produce a constant strength shock, the terminal normal shock is skewed, so that critical total pressure recovery is achieved with the leeward side of the shock in the throat and the windward side of the shock in the subsonic diffuser [3]. There is a loss in inlet performance and this is why axisymmetric inlets are not preferred for any mission where maneuvering flight is required.

Second, and finally the characteristics of two dimensional inlets operating at angle of attack will be examined. Figure 2.14 [6] shows the measured pressure recovery of a representative double-wedge intake over a range of positive and negative angles of attack and at two Mach numbers. In Figure 2.14, the analytically calculated critical total pressure recovery values are shown with dashed lines and the measured values are shown by solid lines.

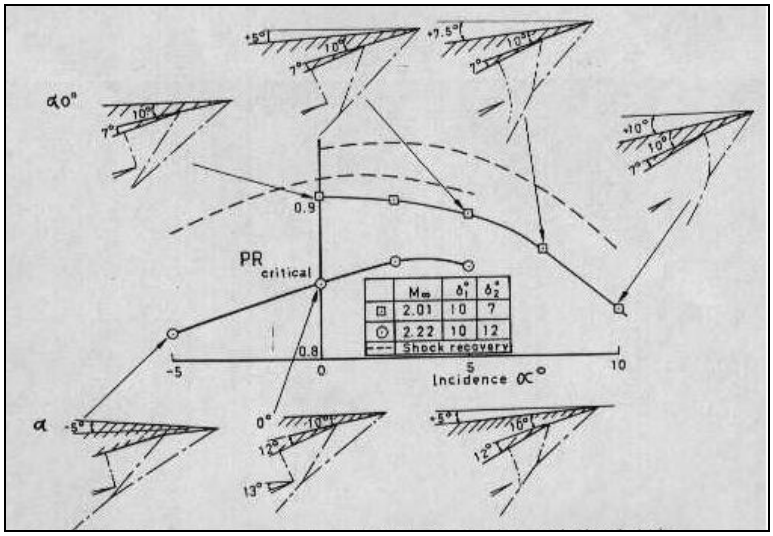

Figure 2.14 Total pressure recovery and shock wave patterns of a 2-D double wedge inlet at incidence

Depending on the operating Mach number and the incidence angle 2-D Double wedge inlets may exhibit increasing performance during operation at incidence this is why 2-D inlets are preferred for missions where maneuvering flight is required.

CHAPTER 3

DESIGN

3.1 Problem Definition

The inlet to be designed, is the inlet of a guided, high altitude, supersonic, air-to-surface cruise missile. The propulsion system of this missile is an integrated rocket ramjet. After being launched from the carrier aircraft, the climb phase begins and the missile is accelerated to ramjet takeover velocity by the solid propellant rocket booster. After burnout of the solid-propellant booster the solid-propellant ramjet engines operation begins. The climb and acceleration phase continues (with the ramjet engine operating) until the cruise altitude is reached. Then, the cruise flight phase which is the phase with the longest duration begins. At the end of the cruise phase the ramjet engines operation is terminated and the power-off dive flight phase begins. The design of the supersonic inlet of such a missile will be realized by using analytical relations and equations, correlations derived from numerous past experimental data and state-of-the-art design examples. The conceptual trajectory of the missile is given in Figure 3.1 and Figure 3.2.

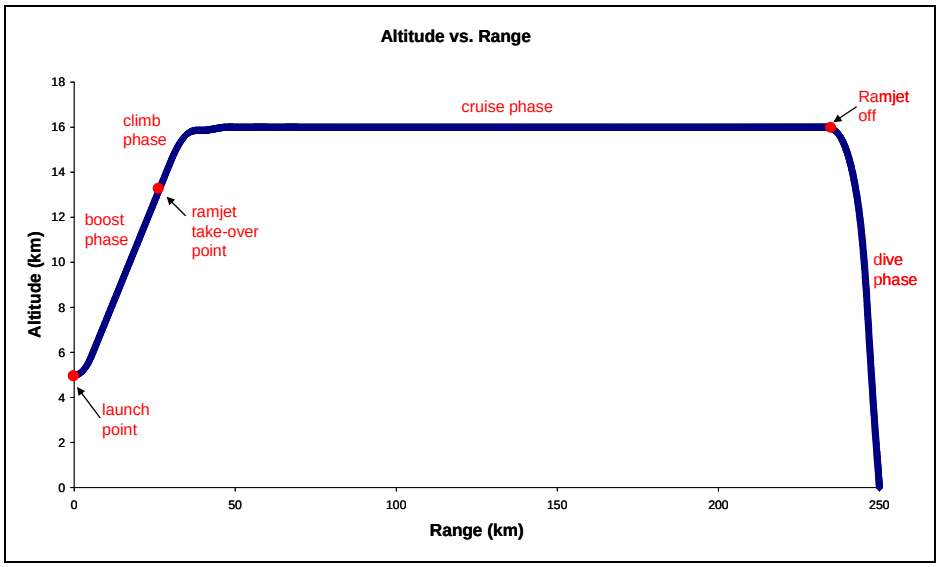

Figure 3.1 Conceptual altitude vs. range graph of the missile

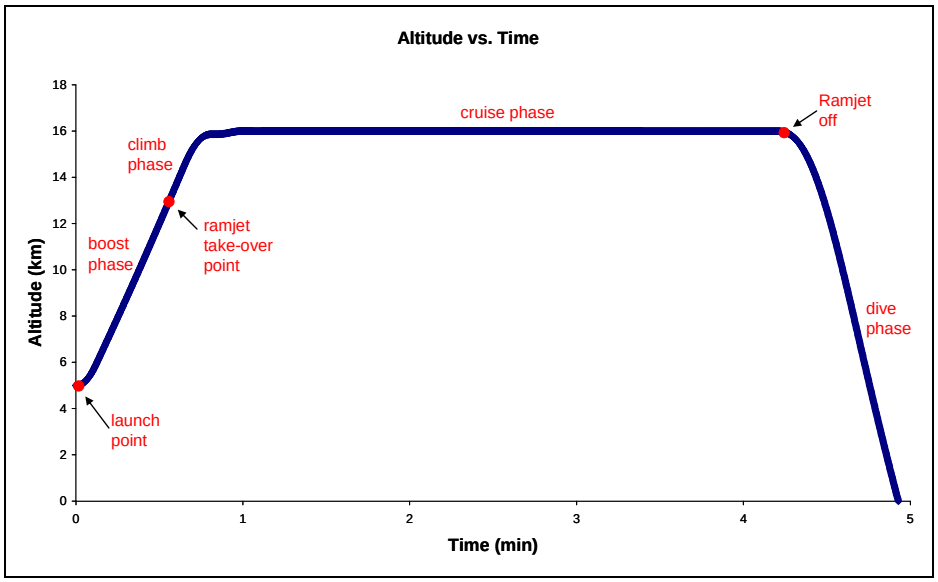

Figure 3.2 Conceptual altitude vs. time graph of the missile

The inlet design parameters that will be decided on are the following:

- **Family:** axisymmetrical, two-dimensional or three-dimensional
- **Geometry:** fixed or variable
- **Supersonic Diffuser Form:** all external compression, all internal compression or combination
- **Supersonic Compression Complexity:** normal shock, single surface, isentropic surface or multiple surfaces
- **Supersonic Compression Direction:** outward, inward or downward
- **Location on the Vehicle Body:** nose, chin, cheek, top, bottom, side, forward, mid or aft
- **Number:** single, dual, three or four
- **Interface with Combustor:** in-line or off-set.

After deciding on the design parameters listed above, the sizing of the inlet will be realized. After sizing is completed, in order to validate the design (to determine whether the requirements are satisfied) a performance estimation study will be conducted by utilizing analytical relations, equations and correlations. In order to provide more reliable and realistic values of performance parameters a CFD analysis will be performed. This analysis will also provide insight to flow behavior via resulting flow pictures.

3.2 Requirements

As in all design processes, the inlet design process is also governed by the requirements. The total system (missile) design requirements impose the engine design requirements. In turn, the inlet design requirements are derived from the engine design requirements. These derived inlet design requirements are:

- Capture of exact amount of air.
- Minimum loss in total pressure.
- Tolerable amount of flow distortion.
- Least possible external drag to the system.

3.3 Total System Design Specifications and Selection of the Design-To Condition

The designed inlet should work in accordance with the ramjet engine throughout the ramjet powered flight phase. If the missile was launched directly at its cruise altitude, then the inlet design-to condition would be obviously the cruise condition. Nevertheless, in the case where the missile is boosted from launch altitude to a ramjet takeover altitude the selection of the design-to condition is not so obvious. The methodology followed for the selection of this design condition, is as follows in most industrial applications: Three or more design-to conditions are chosen. The inlet is designed at these design-to conditions, and the performance of the missile with these designed inlets is investigated by trajectory analyses. As a result the optimum design-to condition is determined. Thus, the inlet designer cannot determine this optimum design-to condition solely by him/herself. This is an iterative procedure between the inlet designer and the trajectory planner. In the context of the present design study, only the first loop of this iteration will be performed, since the aim is simply to provide a methodology for design.

From the desired trajectory of the missile given in Figure 3.2, it is seen that the dive phase is the power off phase of the mission. Therefore, selection of the design-to condition according to the dive phase is irrelevant. Nevertheless, the power on cruise phase is the longest duration flight phase of the mission. During cruise, the missile travels at its highest velocity and highest altitude. Therefore, as the starting and first point of the iterative loop, it is reasonable to select the cruise condition as the design-to condition. After performing total system (missile) performance

analyses with the inlet designed according to this condition, if it is seen that this design does not satisfy the climb phase requirements of the mission, several solutions to this problem can be implemented. One solution is to increase the mass of the booster by extending the weight limits, in order to increase the altitude of the ramjet takeover point. Then, to work with the trajectory planner to see if this solution improves the total system performance. Another solution is to impose some constraints on the launch altitude of the carrier aircraft, so that launch is realized from a higher altitude and the altitude of the ramjet takeover point is increased.

There are no currently available analytical methods to perform a high stability design. Due to this reason, in this study, the methodology that will be used, is to design an inlet that will yield maximum total pressure recovery at the design-to condition and then to investigate this inlets stability at various operating conditions. In this scope, the performance of the inlet at angle of attack will also be investigated.

In the light of above discussions, the cruise Mach number, the cruise altitude, and zero degrees angle of attack parameters are selected as the design-to condition.

The total system (the missile and the launching platform) design specifications, that will be an input to the inlet design problem are the following:

- Cruise altitude = 16 km
- Cruise Mach number = 3.5
- Circular missile body, dimensions as shown in Figure 3.3

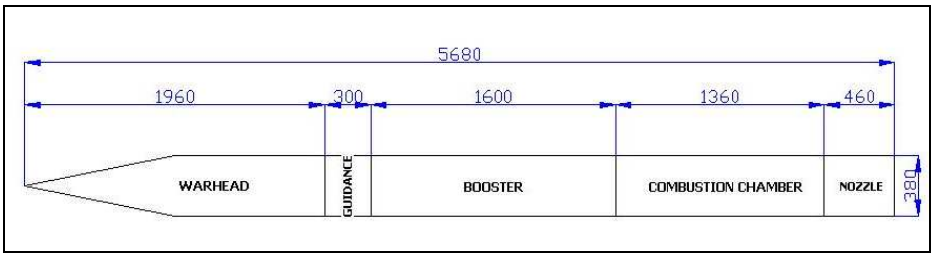

Figure 3.3 Side view drawing of the missile body (dimensions in mm)

- Due to launcher constraints, missile width< 0.69 m; missile height< 0.39 m
- Cruise thrust = 5000 N
- Solid propellant: hydroxyl terminated polybutadiene, aluminum, magnesium and boroncarbide and its chemical composition is %35 Mg, %35 B_4C and %30 HTPB ($C_4H_6O_{0.15}$) [36]
- Equivalence ratio = 0.8. [36]
- Specific impulse = 800 s^{-1}.
- Combustion chamber entrance Mach number = 0.3.

3.4 The Effect of Inlet Size on Engine Performance

Before performing the inlet competitor study and the sizing of the inlet, it is found useful to perform a trade study to obtain an idea about how the inlet size affects the engine performance.

For any combination of freestream Mach number, pressure and temperature values, along with the selection of the fuel, and the size of the ramjet engine and inlet, it is possible to map the performance of the ramjet engine at any possible fuel flow rate. This performance map consists of the non-dimensional thrust coefficient, the ratio of total pressure at the engine throat to the total pressure at freestream, and the Specific Fuel Consumption.

With the purpose of obtaining the performance comparison of two different ramjet engines, one having a relatively smaller inlet, the following analysis is conducted. The Thrust Coefficient versus Engine Total Pressure Ratio graph is generated both for the engine with the small inlet and for the engine with the relatively larger inlet. For common Thrust Coefficient and Engine Total Pressure Ratio values, the total temperature at the engines nozzle throat, and the engine nozzle throat area is obtained for both the engine with the smaller inlet and the engine with the larger inlet. Once these values are obtained, the specific fuel consumption values of each engine are calculated.

The engine having the smaller inlet, will further on be notated as Engine 1 and is assumed to be composed of an inlet having a cowl area to reference area ratio of 0.3. The engine having the larger inlet, will further on be notated as Engine 2 and is assumed to be composed of an inlet having a cowl area to reference area ratio of 0.35.

The calculations are done for a freestream Mach number of 2.5, a sea level static pressure value of 10353Pa and a sea level static temperature value of 288.15K. The specific heat ratio of air at the freestream (γ_0) is 1.4 and specific heat ratio of air at the nozzle exit station (γ_6) is assumed to be 1.2. The nozzle mass flow coefficient value (C_{nm}) is assumed to be 0.97. The nozzle efficiency value (η_n) is assumed to be 0.97. The capture area ratio (A_0/A_c), of the inlets of both engines is assumed to be 0.9. The exit area and the reference area of both engines are assumed to be $1m^2$. The selected fuel is the JP-5 fuel, and its temperature rise curves are given in Figure 3.4 [3]. These curves are used to determine the fuel-to-air ratio and the engine total temperature ratio.

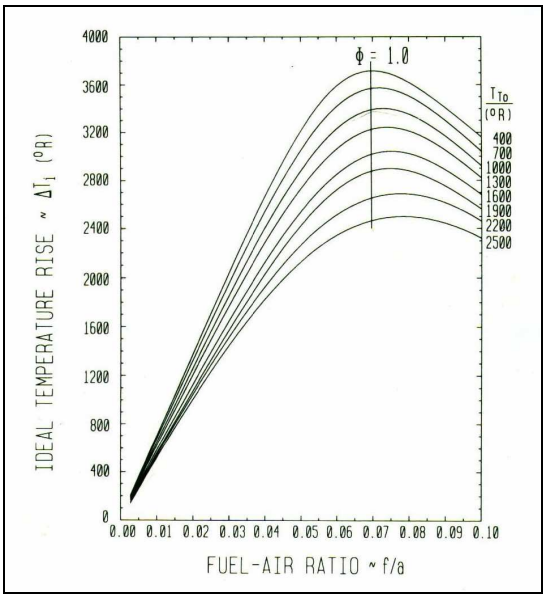

Figure 3.4 Temperature rise curves of JP-5 Fuel

In order to generate the thrust coefficient versus engine total pressure ratio graph, the thrust coefficient and total pressure ratio values of Engine 1, are calculated for 4 different total temperature values at the nozzle throat, coupled with 3 different nozzle throat area to reference area ratios. Similarly, the thrust coefficient and total pressure ratio values of Engine 2, are calculated for 4 different total temperature values at the nozzle throat, coupled with 4 different nozzle throat area to reference area ratios. These values are represented for each engine in Table 3.1.

Table 3.1 Nozzle throat total temperature and area ratio values for Engine 1 and Engine 2

Engine 1 (A_c/A_R=0.30)		**Engine 2 (A_c/A_R=0.35)**	
Nozzle Throat Total Temperature (T_{t5})	Nozzle Throat Area to Reference Area Ratio (A_5/A_R)	Nozzle Throat Total Temperature (T_{t5})	Nozzle Throat Area to Reference Area Ratio (A_5/A_R)
1759 K	0.3	1759 K	0.35
1981 K	0.325	1981 K	0.40
2203 K	0.35	2203 K	0.45
2426 K		2426 K	0.50

Eqn. (2.1) and Eqn. (2.2) is used to obtain the values of the thrust coefficient and the engine total pressure recovery for each of the cases given in Table 3.1.

A *MATHCAD* code is developed for performing the calculations. The thrust coefficient versus engine total pressure ratio graphs obtained for Engine 1 and Engine 2 are given in Figure 3.5 and Figure 3.6.

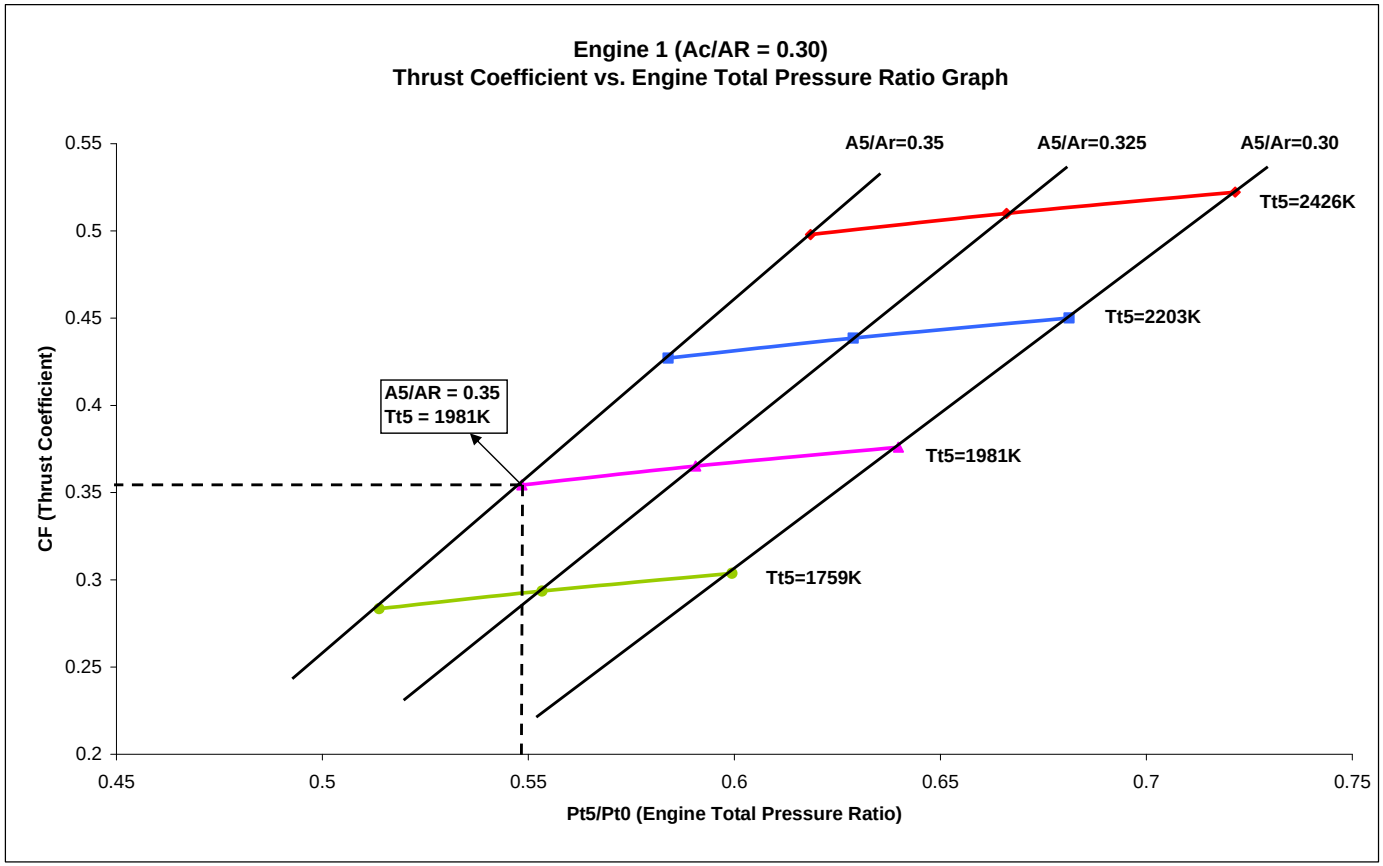

Figure 3.5 Thrust coefficient vs. engine total pressure ratio graph of Engine 1

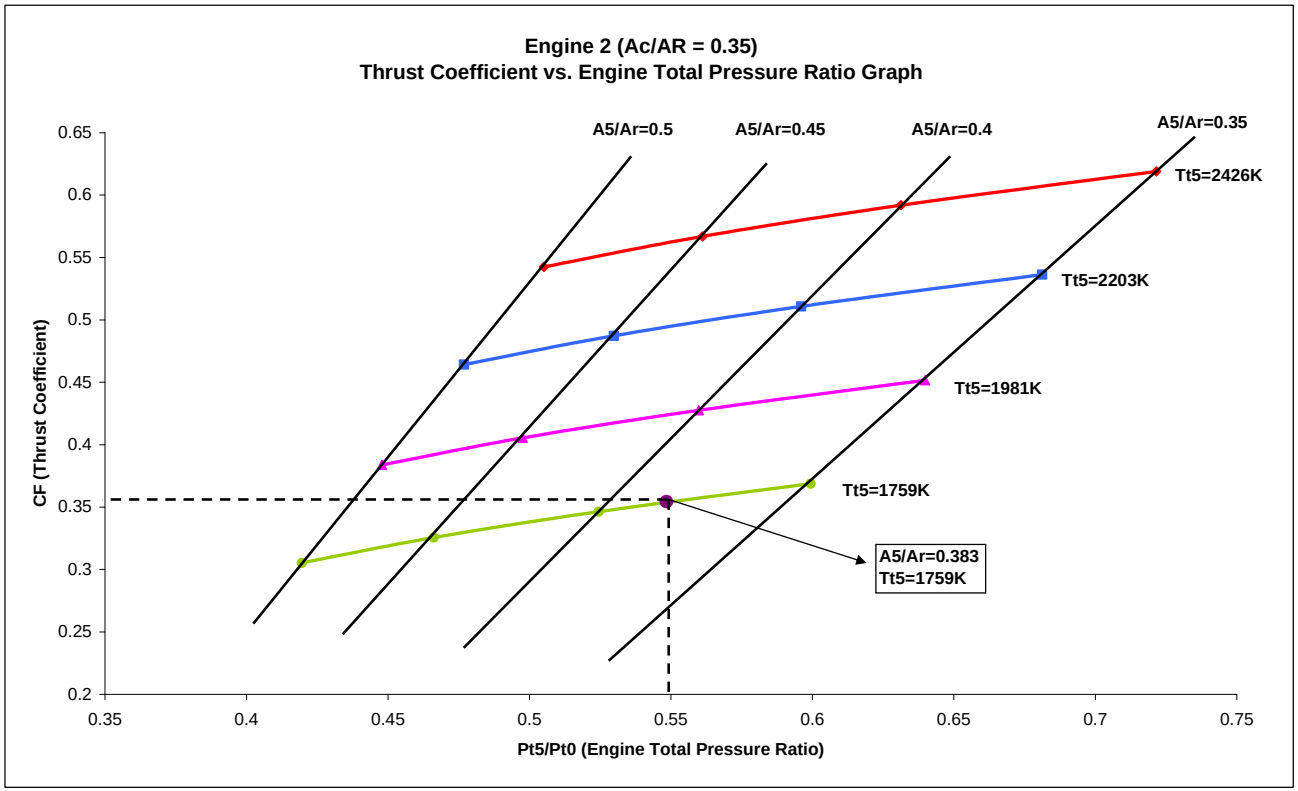

Figure 3.6 Thrust coefficient vs. engine total pressure ratio graph of Engine 2

At the points marked on both Figure 3.5 and Figure 3.6, corresponding to a thrust coefficient value of 0.356 and an engine total pressure ratio of 0.549, the specific fuel consumption values are calculated for both Engine 1 and Engine 2 using Eqn. (2.3). The results are given on Table 3.2.

Table 3.2 SFC values of Engine 1 and 2 at common thrust coefficient and total pressure recovery point

Calculated Properties	**Engine 1** **(A_c/A_R = 0.30)**	**Engine 2** **(A_c/A_R = 0.35)**
Thrust Coefficient (C_F)	0.356	0.356
Engine Total Pressure Ratio (P_{t5}/P_{t0})	0.549	0.549
Nozzle Throat Total Temperature (T_{t5})	1981 K	1759 K
Nozzle Throat Area to Reference Area Ratio (A_5/A_R)	0.35	0.383
Specific Fuel Consumption (SFC)	2.8 ((kg/hr)/N)	2.4 ((kg/hr)/N)

Assuming that, the Thrust Coefficient required to maintain a cruise condition is 0.356, and the maximum allowable engine total pressure ratio is 0.549, it can easily be depicted from the results on Table 3.2 that; for the smaller inlet an engine nozzle throat size smaller than the engine nozzle throat size required for the larger inlet is sufficient. It is also understood that, the smaller inlet requires the engine to operate with a higher fuel flow rate (a higher nozzle throat total temperature value) and correspondingly, with a higher specific fuel consumption.

The inlet designer has an important choice to make. The inlet designer either chooses to design a larger and more economical engine (in terms of fuel consumption), or a smaller, presumably lighter in weight more economical engine with the potential for less drag. The advantages and disadvantages of the smaller and larger engines (Engine 1 and Engine 2 respectively) are summarized in Table 3.3.

Table 3.3 Trade study for engines 1 and 2

Properties	Engine 1		Engine 2	
	Advantage	**Disadvantage**	**Advantage**	**Disadvantage**
Size	Smaller			Larger
Weight	Lighter			Heavier
Specific Fuel Consumption		More	Less	
Potential For Drag	Less			More

3.5 Competitor Study

The purpose of performing a competitor study is to benefit from the existing designs of the inlets of ramjet missiles under deployment. The inlets of ramjet missiles are classified in this competitor study according to the missions of the missiles.

3.5.1 Surface-to-air ramjet missiles and their inlets

The BOMARC B of the United States Air Force is a 710 km ranged missile. Its propulsion system, consists of a solid-fuel rocket for the boost and ramjet engine for sustain phases. The BOMARC is capable of a maximum velocity of 3.0 Mach. It has two axisymmetric inlets each mounted in-line with the two ramjet engines.

The TALOS is also a U.S anti-aircraft missile. Its propulsion system consists of a sustainer ramjet and a separate booster. This missile has a nose mounted axisymmetric inlet.

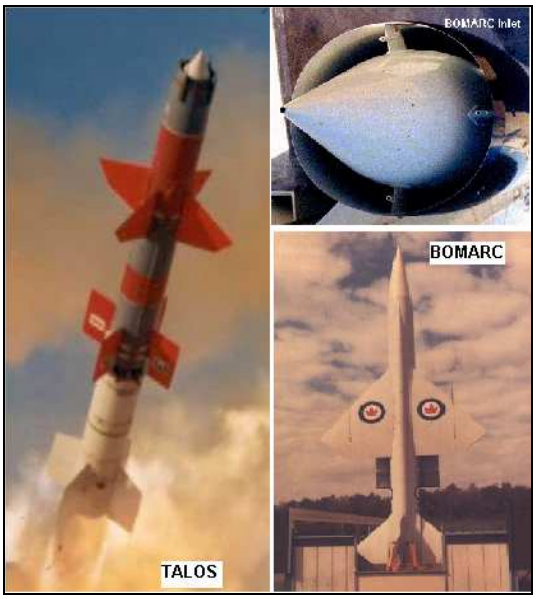

Figure 3.7 Surface-to-air ramjet missiles and their inlets

3.5.2 Air-to-surface ramjet missiles and their inlets

The advanced strategic air launched missile (ASALM) of the U.S, had a major innovation, which was its integrated rocket/ramjet propulsion system. It had a chin mounted three-dimensional inlet and high maneuvering capability. The cruise speed for ASALM missions was planned to be Mach 4.5 for a range of 480 km.

The Russian Krypton missile, one of the first to use the integrated rocket ramjet concept, allows a supersonic speed of Mach 2 during the flight and utilizes 4 axisymmetric inlets. The Krypton has a range of 70 km.

The Russian Moskit, is propelled by a dual (rocket-jet) engine operating by the same principle as the Krypton's engine. It utilizes 4 axisymmetric inlets. The ramjet enables the Moskit to achieve speeds as high as Mach 3. The system has a range of 150-250 km.

The French ASMP missile also uses the integrated rocket ramjet concept. It has high maneuverability. It utilizes dual, side mounted two-dimensional inlets. It has a maximum velocity of Mach 3 and its range is 100 to 300km.

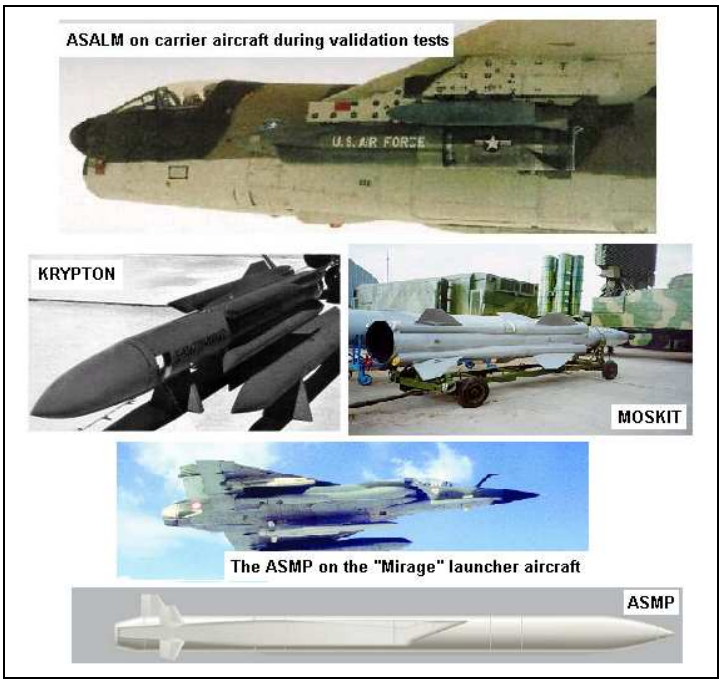

Figure 3.8 Air-to-surface ramjet missiles and their inlets

3.5.3 Air-to-air ramjet missiles and their inlets

The ALVRJ (air launched low volume ramjet) of the U.S, used the concept of an “integral rocket” to reduce volume. The ALVRJ demonstrated successful transition from rocket to ramjet operation with cruise at a speed in excess of Mach 2.5 and flights at sea level and 10000 m. It utilizes 4 axisymmetric inlets and it has a range of 160 km.

The METEOR is a missile being developed under a current program in the U.S. Meteor is a new concept in air-to-air weapons, employing advanced air breathing motor technology. It will provide Eurofighter with the capability to deal with

projected air-to-air threats. The METEOR will have a minimum range of 100km and a maximum velocity of Mach 4. Due to the high angle of attack and high maneuver capability requirements, it will use dual, cheek mounted, two-dimensional inlets.

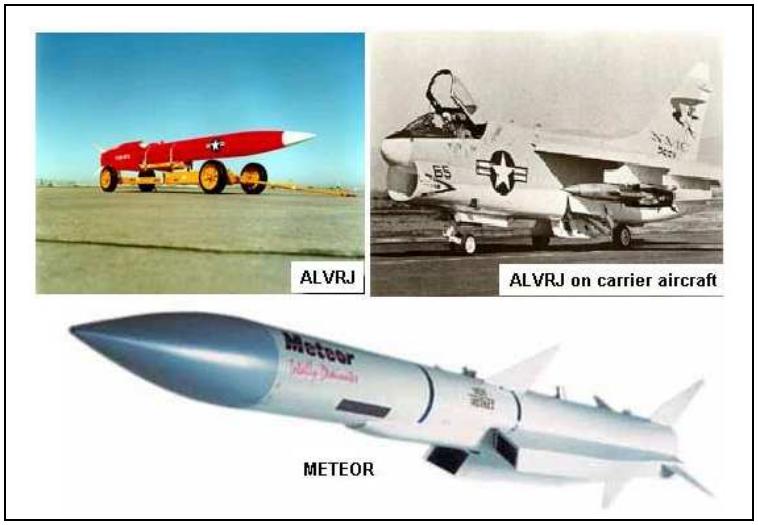

Figure 3.9 Air-to-air ramjet missiles and their inlets

3.6 Selection of the Design Parameters

- **Family**

In Figure 3.10 [2] it can be seen that axisymmetric inlet performance decreases rapidly with increasing angle of attack. In contrast to the axisymmetric inlet, the two-dimensional and chin inlet designs show increasing inlet performance with increasing angle of attack.

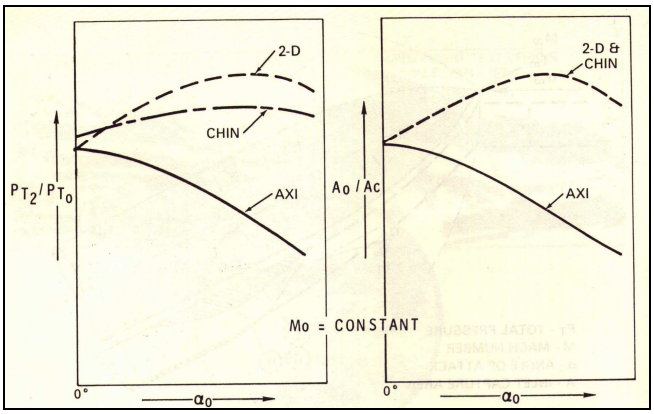

Figure 3.10 Performance comparison of 2-D, chin and axisymmetric inlets

It is also recognized in the Competitor Study Section that missiles with high maneuverability capabilities have two-dimensional inlets, such as the ASMP and the METEOR due to higher attainable total pressure recovery values during operation at incidence. Therefore it is decided that, the designed inlet will be a two-dimensional inlet.

- **Geometry**

It is known that variable geometry devices can greatly improve the performance and stability of the inlet. Nevertheless, they increase the weight, the complexity of the design and the design cost. In order to benefit from the advantages of low weight and cost and to keep the design simple, as a starting point, it is decided that the designed inlet will be a fixed geometry inlet.

- **Supersonic diffuser form**

It is known that, the advantage of all external type compression over all internal or mixed type compression is that the flow can be spilled in the cases of unstart, causing a stabilizing effect. Whereas, with all internal or mixed compression type inlets, if the contraction area ratio limit is exceeded the inlet can only be started with the aid of variable geometry devices. Therefore, it is decided that the designed inlet will be an all external compression type inlet.

- **Supersonic compression complexity**

It is known that for supersonic inlets, the highest total pressure recovery values are obtained with inlets having isentropic supersonic diffusers because the compression process is achieved through a series of compression waves. Nevertheless, the manufacturing of this type of diffuser is very difficult and the manufacturing cost is high. It is also known that the total pressure recovery level closest to the level of isentropic inlets can be obtained with multiple wedge supersonic diffusers.

Efficient inlet integration for supersonic missiles requires at least one oblique shock prior to the inlet normal shock, for good inlet total pressure recovery at Mach numbers greater than 3. In Reference [7] it is also suggested that, for Mach numbers greater than 3.5, two oblique shocks prior to the inlet normal shock are desirable for total pressure recovery. Therefore, it is decided that, in the present study, the supersonic diffuser of the designed inlet will be a double wedge supersonic diffuser.

- **Supersonic compression direction**

In Figure 3.11 [4], the effect of inlet inversion is shown. It can be seen that inversion increases the total pressure recovery level of the two-dimensional inlet during angle of attack operation. It is decided that the inlet will be a downward compression inlet.

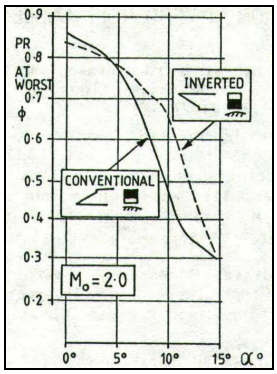

Figure 3.11 Increase in total pressure recovery with inlet inversion

- **Location on the vehicle body and number of inlets**

The inlets location on the vehicle body should be decided on according to the number of inlets. The number of inlets is determined during the sizing study, in accordance with the engines airflow requirement and is constrained by the missile diameter and launcher interfaces. It can be concluded from the results of the Competitor Study that, two-dimensional downward compression inlets are either dual side mounted or dual cheek mounted. Side mounted inlets used in the ASMP yield good performance during the angle of attack operation which is required during the air-to-surface mission. However for air-to-air missions, a wider angle of attack operating range is required and cheek mounted inlets are used as in the case of METEOR. This characteristic is also justified by Figure 3.12 [4].

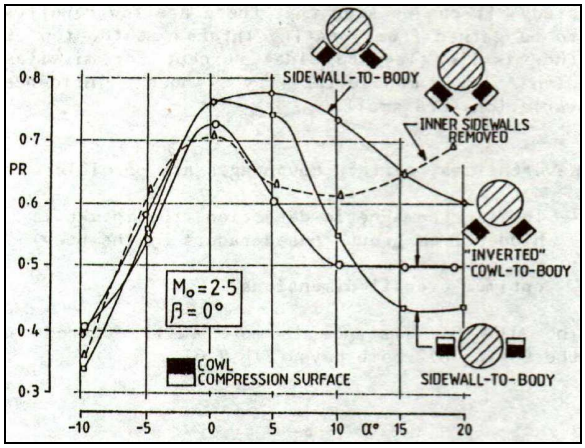

Figure 3.12 Total pressure recovery levels at angle of attack of side and cheek mounted dual inlet configurations

Another important parameter in the design of a supersonic inlet is the lift-to-drag ratio. Side mounted inlets have the advantage of providing a higher lift-to drag ratio (by means of contributing to the body lift) when compared to axisymmetric inlets. It is advantageous to benefit from this feature especially in order to increase the range that can be traveled during the cruise flight phase.

It is most probable that the designed inlet configuration of the air-to-surface missile will be dual, side mounted but the decision will be finalized with the sizing study.

- **Interface with the combustor**

Since the inlet to be designed is not an axisymmetric inlet, rather it is a two-dimensional inlet, it will be off-set and the interface with the combustor will be a dump pipe.

3.7 Sizing of the Inlet

3.7.1 Calculation of the mass flow rate of air at the design-to condition

The design-to condition is the cruise condition. The Mach number at this condition is 3.5, the altitude is 16000 m and the thrust value is 5000N. The chemical reaction that occurs in the combustion chamber is,

$$0.35\ Mg + 0.35\ B_4C + 0.3\ C_4H_6O_{0.15} + \boldsymbol{X}\ O_2 \rightarrow 0.35\ MgO + 0.7\ B_2O_3 + 1.55\ CO_2 + 1.8\ H_2O$$

Where the value of $\boldsymbol{X}$ is calculated as:

$$X = \frac{0.35 + 3 \cdot 0.7 + 2 \cdot 1.55 + 1.8 - 0.3 \cdot 0.15}{2} = 3.6525\ moles$$

Therefore, it is determined that for **1 mole** of fuel **3.6525 moles** of oxygen is needed. Next, the molecular weight of 1 mole of fuel and 1 mole of oxygen is calculated from the atomic weights of the elements given below.

Atomic weight of Mg : 24.305 gr, atomic weight of B:10.811 gr, atomic weight of C:12.011 gr, atomic weight of H:1.00794 gr, atomic weight of O:15.9994 gr. Thus,

Molecular weight of 1 mole of fuel = 0.35 x (24.3050) + 0.35 x (4 x 10.811 + 12.011) + 0.3 x (4 x 12.011 + 6 x 1.00794 + 0.15 x 15.9994) = 44.8 gr

Molecular weight of 1 mole of O_2 = 2 x 15.9994 = 32.0 gr

Thus, for 44.8 gr of fuel, 116.9 gr of O_2 is needed.

The mass flow rate of fuel required at the design-to condition is determined from the cruise thrust level using Eqn. (3.1).

$$F = \dot{m}_f \cdot I_s \cdot g \tag{3.1}$$

$$\dot{m}_f = \frac{5000\ N}{800\ s^{-1} \cdot 9.7575\ m/s^2} = 0.6405\ kg/s$$

Where, the value of the gravitational constant at 16,000 m altitude, is obtained from the US76 Standard Atmosphere Model [37].

It is readily determined that for 44.8 gr of fuel 116.9 gr of O_2 is needed. Correspondingly, the mass flow rate of O_2 needed for 640.5 g/s of fuel flow rate is calculated.

$$\dot{m}_{O_2}\ needed\ \ for\ cruise\ level = \frac{640.5 \times 116.9}{44.8} = 1671.3\ g/s$$

This value corresponds to $\frac{1671.3}{32} = 52.2\ moles/s$ of O_2.

Next, the amount of air which contains 52.2 moles of O_2 is calculated. For this purpose the chemical composition of air at 16,000 m is obtained from the US76 Standard Atmosphere Model [37] and is given below.

Chemical composition of 1 mole of air at 16,000 m altitude is; 0.78084 moles N_2, 0.20948 moles O_2, 0.00934 moles Ar, 0.00032 mol CO_2 and 0.00002 moles Ne.

The amount of air which contains 52.2 moles of O_2 is calculated.

$$number\ of\ \ moles\ of\ air\ which\ contains\ required\ amount\ of\ \ O_2 = \frac{52.2}{0.20948} = 249.3\ moles$$

The molecular weight of 1 mole of air is first calculated in order to obtain the weight of 249.3 moles of air by using the atomic weights of the constituents.

Molecular weight of 1 mole of air = 0.78084 x (2 x 14) + 0.20948 x (2 x 16) + 0.00934 x (39.95) + 0.00032 x (12 + 2 x 16) + 0.00002 x (20.18) = 29.0 gr

Thus, weight of 249.3 moles of air = 7222 gr

Therefore, the required mass flow rate of air at cruise is; $\dot{m}_{air} = 7.222\ kg/s$

The obtained values of the mass flow rate of fuel $(\dot{m}_f)$ and mass flow rate of air $(\dot{m}_{air})$, are stoichiometric values. By using these values, the stoichiometric fuel to air ratio can be determined.

$$\left(\frac{f}{a}\right)_{stoich} = \frac{(\dot{m}_f)_{stoich}}{(\dot{m}_{air})_{stoich}} = \frac{0.6405\ kg/s}{7.222\ kg/s} = 0.089 \qquad (3.2)$$

The equivalence ratio of a fuel is described as the ratio of the realized fuel to air ratio to the stoichiometric fuel to air ratio. It's formula is given in Eqn. (3.3).

$$\phi = \frac{\left(\frac{f}{a}\right)}{\left(\frac{f}{a}\right)_{stoich}} \tag{3.3}$$

The realized mass flow rate of air is calculated by using Eqn. (3.3).

$$\dot{m}_{air} = \frac{\dot{m}_f}{\phi\left(\frac{f}{a}\right)_{stoich}} = \frac{0.6405}{0.8 \times 0.089} = 9.027\ kg/s$$

Thus, the mass flow rate of air $(\dot{m}_{air})$ required by the engine is obtained to be about **9.027** kg/s.

3.7.2 Calculation of the freestream tube area at the design-to condition

The freestream tube area corresponding to 9.027 kg/s of air is calculated by using Eqn. (3.4).

$$A_0 = \frac{\dot{m}_{air}}{\rho_0 U_0} = \frac{\dot{m}_{air}}{\rho_0 M_0 a_0} \tag{3.4}$$

The values of the freestream density and freestream speed of sound at 16000 m altitude are obtained from the US76 Standard Atmosphere Model [37].

$$A_0 = \frac{9.027}{0.166 \times 3.5 \times 295.07} = 0.0525\ m^2$$

Therefore, the cross-sectional area of the captured streamtube at the design-to condition should be 0.0525 m^2.

Given that the missile diameter is 0.38 m, a single inlet with a cross sectional area of 0.0525 m^2 would be too voluminous. However, two inlets each with cross sectional areas of 0.0262 m^2 would fit and not be too voluminous. Therefore, it is hereby decided, in accordance with Section 3.6, that there will be two side mounted inlets. It is observed from competitor study that the heights of side mounted inlets are smaller than the missile diameter. It is decided that this feature will also be implemented into this design. Nevertheless, it is also known that, in order to reduce parasitic side wall surface area it is preferred to choose the width to height ratio larger than 1 [3]. In this design case this corresponds to an inlet width larger than 0.16 m. Unfortunately, the maximum possible inlet width, due to launcher constraints is 0.155 m. Therefore implementing an inlet width to height ratio larger than 1 is impossible. Due to these reasons, the chosen inlet width is 0.15 m and the chosen inlet height is $\frac{0.0262}{0.15} = 0.175\ m.$

3.7.3 Sizing of the supersonic diffuser

The supersonic diffuser is a double wedge diffuser. Firstly, the wedge angles that would yield a maximum total pressure recovery through two oblique shocks and a terminal normal shock located in the entrance plane, is calculated. For this purpose, a *MATLAB* code is written. In this code the values of the ramp angles δ_1 and δ_2 (shown in Figure 3.13) are varied from 1° to 90°, and the total pressure recovery values through two oblique shocks and a terminal normal shock, corresponding to each respective combination of δ_1 and δ_2 is calculated. The calculations are done at the design-to condition. The inlet stations in the notation of the “Wedge Angles” MATLAB Code are also shown in Figure 3.13.

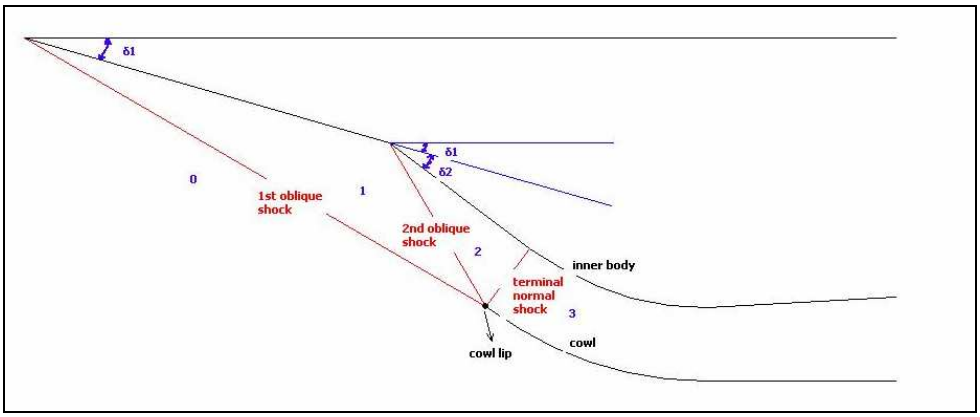

Figure 3.13 Supersonic diffuser wedge angles and stations

For calculating the Mach numbers and the total pressure ratio values at each station the Rankine-Hugoniot Relations given in Eqn. (3.5) to (3.9) are used.

$$\tan\theta_i = 2\cot\beta_i \frac{M_i^{\,2}\sin^2\beta_i - 1}{M_i^{\,2}(\gamma + \cos 2\beta_i) + 2} \tag{3.5}$$

$$M_{n,i} = M_i \sin\beta_i \tag{3.6}$$

$$M_{n,i+1}^{\,2} = \frac{1 + \frac{(\gamma-1)}{2} M_{n,i}^{\,2}}{\gamma M_{n,i}^{\,2} - \frac{(\gamma-1)}{2}} \tag{3.7}$$

$$M_{i+1} = \frac{M_{n,i+1}}{\sin(\beta_i - \theta_i)} \tag{3.8}$$

$$\frac{P_{t,i+1}}{P_{t,i}} = \left[\left(\frac{\gamma-1}{\gamma+1} + \frac{2}{(\gamma+1)M_{n,i}^{\,2}}\right)^{\gamma}\left(\frac{2\cdot\gamma}{\gamma+1}M_{n,i}^{\,2} - \frac{\gamma-1}{\gamma+1}\right)\right]^{\frac{-1}{(\gamma-1)}} \tag{3.9}$$

The results are given in Figure 3.14 where the total pressure recovery value (P_{t3}/P_{t0}) is plotted for combinations of wedge angles (δ_1 and δ_2). It can be seen that the maximum total pressure recovery is obtained with a first wedge angle (δ_1) of 16°, along with a second wedge angle (δ_2) of 21° and the value of the maximum total pressure recovery is 0.6099. The results are given in Table 3.4.

Table 3.4 Design parameters of the supersonic diffuser

First Wedge Angle (δ_1)	16°
Second Wedge Angle (δ_2)	21°
First Oblique Shock Angle (β_1)	30.22°
Second Oblique Shock Angle (β_2)	43.61°
Freestream Mach Number (M_0)	3.5
Mach Number Behind 1st Oblique Shock (M_1)	2.5446
Mach Number Behind 2nd Oblique Shock (M_2)	1.6304
Mach Number Behind Terminal Normal Shock (M_3)	0.6595
Total Pressure Ratio Through 1st Oblique Shock (P_{t1}/P_{t0})	0.8294
Total Pressure Ratio Through 2nd Oblique Shock (P_{t2}/P_{t1})	0.8323
Total Pressure Ratio Through Terminal Normal Shock (P_{t3}/P_{t2})	0.8836
Overall Total Pressure Ratio (P_{t3}/P_{t0})	0.6099

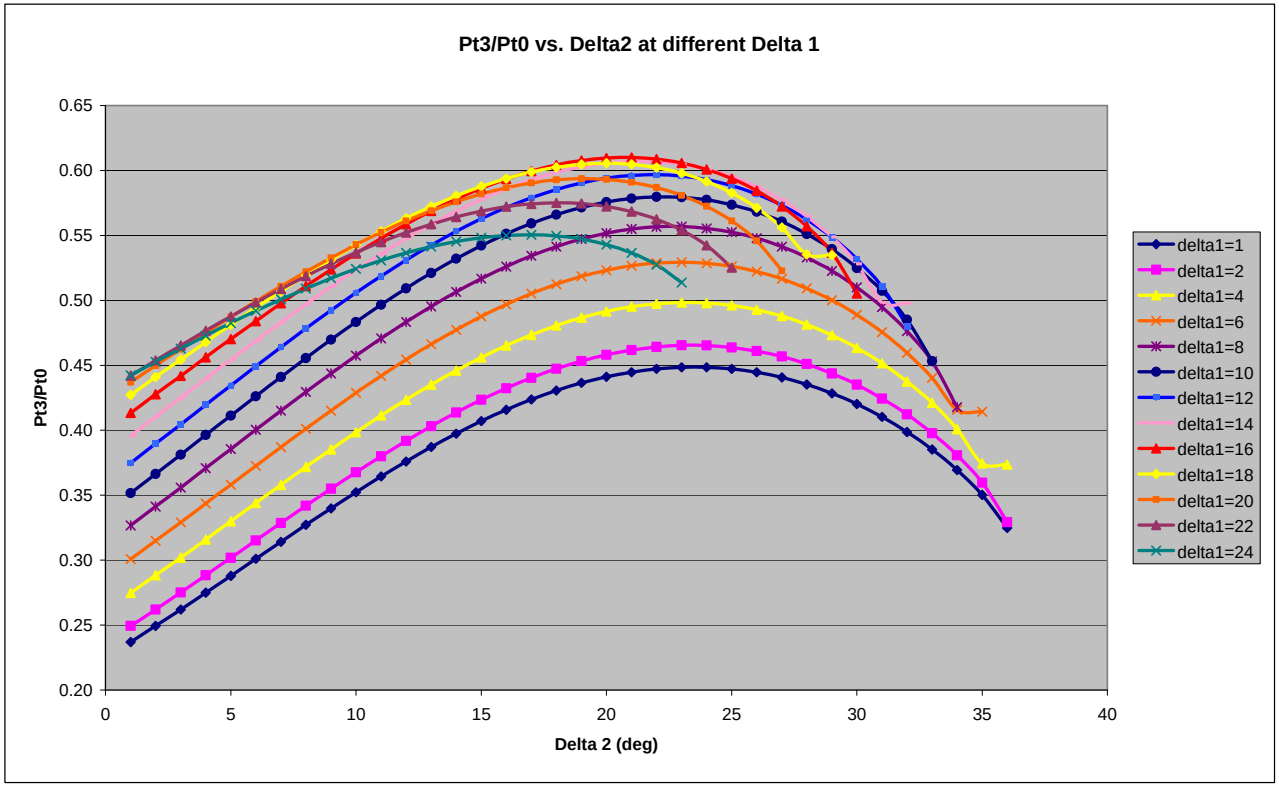

Figure 3.14 Total pressure recovery with different wedge angles

Now that the wedge angles are selected (δ_1=16° and δ_2=21°) the supersonic diffuser can be sized. Recalling that, at the design-to conditions the intersection point of the oblique shocks should be at the cowl lip and by using the geometric relations derived from Figure 3.15:

$$H_0 = \frac{A_0}{w} = 0.175\ m$$

$$L_{lip} = \frac{H_0}{\tan\beta_1} = 0.300\ m$$

$$L_{\sup wedge1} = \frac{L_{lip}\tan(\beta_2+\theta_1) - H_0}{\tan(\beta_2+\theta_1) - \tan\theta_1} = 0.238\ m$$

$$L_{\sup wedge2a} = L_{lip} - L_{\sup wedge1} = 0.063\ m$$

$$A_1 = \frac{A_0}{\cos(90-\beta_1)} = 0.052154\ m^2$$

$$A_2 = \frac{A_1\sin(\beta_1-\theta_1)}{\sin(180-\beta_2)} = 0.01858\ m^2$$

$$A_{th} = A_2\sin(\beta_2-\theta_2) = 0.0071435\ m^2$$

$$H_{th} = \frac{A_{th}}{w} = 0.048\ m$$

$$L_{\sup wedge2b} = \frac{H_{th}}{\tan(90-(\theta_1+\theta_2))}\cos(\theta_1+\theta_2) = 0.029\ m$$

$$L_{\sup} = L_{\sup wedge1} + L_{\sup wedge2a} + L_{\sup wedge2b} = 0.329\ m$$

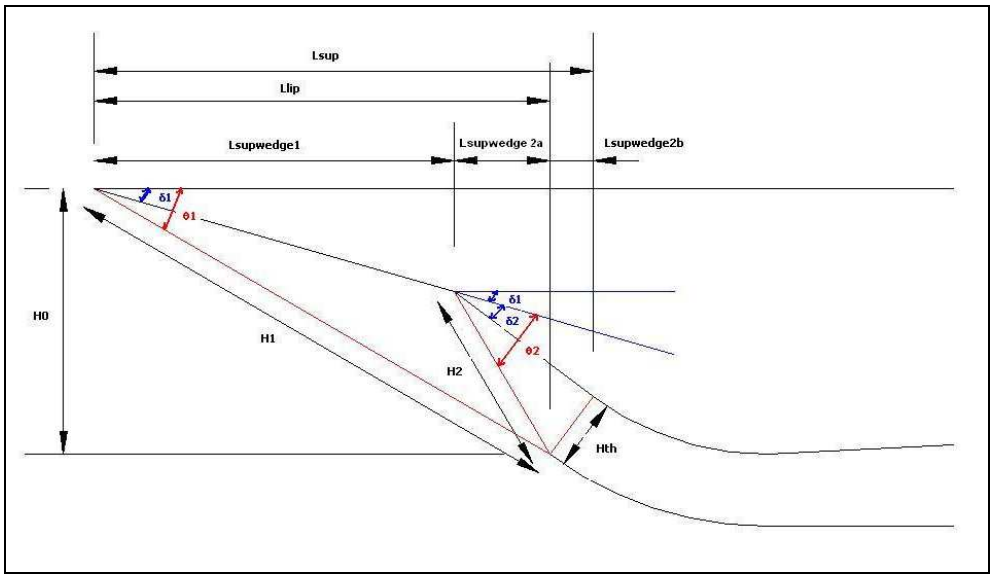

Figure 3.15 Associated dimensions of the supersonic diffuser

3.7.4 Sizing of the constant area throat

In order to minimize disadvantageous effects of the shock-boundary layer interaction, a constant area throat is implemented into the design. Experimental data for obtaining the shock train length of this particular design condition is not available. Nevertheless, in scores of other experiments, it was determined that a minimum radius of curvature equal to four channel heights provides the shortest practical axial distance in which to complete the turn [3]. This distance is claimed to yield the minimum possible external drag, and since it minimizes the axial distances, it introduces an advantage of low weight. Therefore, a radius of curvature equal to four channel heights is implemented into the design. However, during viscous CFD analyses and wind tunnel tests, it should be checked whether the length of this constant area turn is longer than the shock train length.

The inlet is an all external compression type inlet. Thus, to avoid any internal contraction the inner body must also be turned at the same rate as the inner cowl surface. Using the geometric relations derived from Figure 3.16 the constant area

throat is sized. The resulting side view sketch of the supersonic diffuser with the throat is given in Figure 3.17.

$$cx = \left(H_{th} + 4H_{th}\right)\sin\left(\delta_1 + \delta_2\right) = 0.143\ m$$

$$cy = \left(H_{th} + 4H_{th}\right) - \left(H_{th} + 4H_{th}\right)\cos\left(\delta_1 + \delta_2\right) = 0.048\ m$$

$$ix = 4H_{th}\sin\left(\delta_1 + \delta_2\right) = 0.115\ m$$

$$iy = 4H_{th} - 4H_{th}\cos\left(\delta_1 + \delta_2\right) = 0.038\ m$$

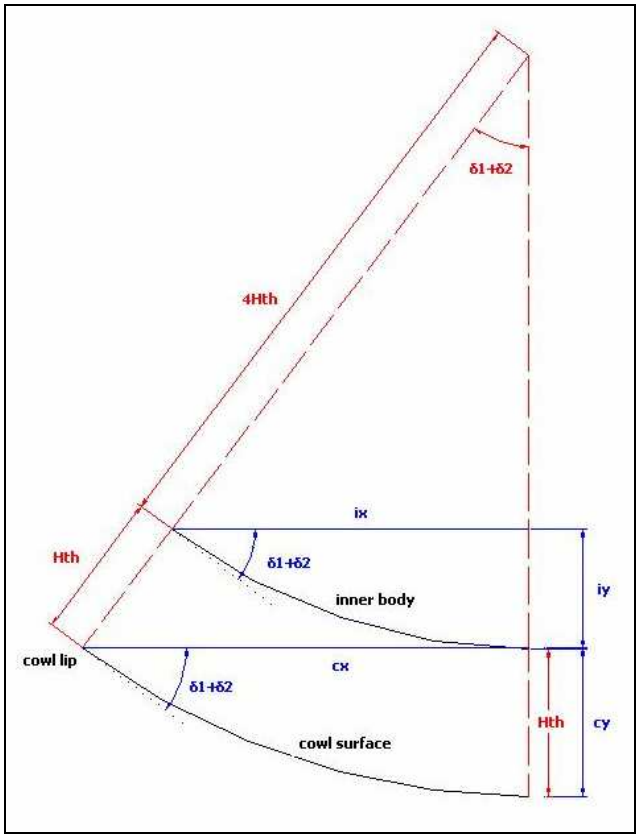

Figure 3.16 Schematic of the dimensions of the constant area throat

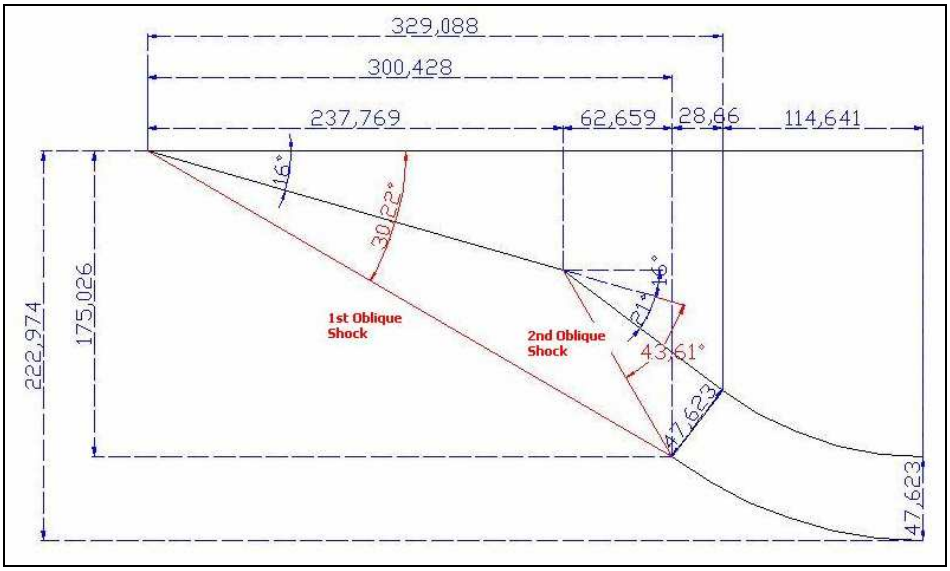

Figure 3.17 The supersonic diffuser and the throat (dimensions in mm)

3.7.5 Sizing of the subsonic diffuser

In order to size the subsonic diffuser, it is first necessary to calculate the combustion chamber entrance area (or namely the inlet exit area). This area is obtained by using Eqn. (2.4). However, it was stated in Section 2.1 that, one dimensional flow techniques are generally insufficient to obtain quantitative measures of the compression process through the inlet and that accordingly combinations of one and two dimensional and sometimes three dimensional techniques are applied when performing complete analyses. Therefore, when calculating the total pressure ratio value by Eqn. (2.4), two dimensional Rankine-Hugoniot relations are used. By this means, a combination of one dimensional and two dimensional flow techniques is incorporated into the design.

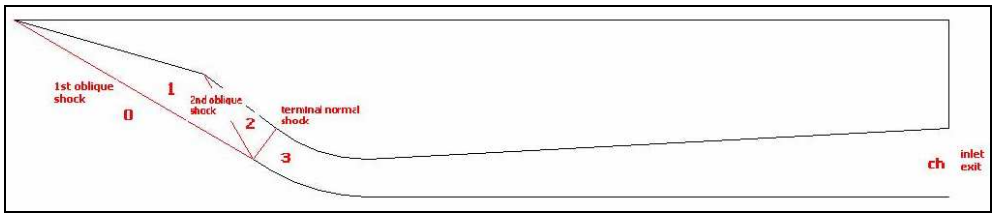

Figure 3.18 Schematic of the inlet stations

Eqn. (2.4) is written between stations 0 and "ch" shown in Figure 3.18.

$$P_{t0} A_{c0} = P_{tch} A_{cch} \tag{3.10}$$

where from Eqn. (2.5),

$$A_{c0} = \frac{A_0}{\Sigma_0} = \frac{A_0}{\frac{1}{M_0}\left(\frac{2+(\gamma-1)M_0^{\,2}}{\gamma+1}\right)^{\frac{\gamma+1}{2(\gamma-1)}}} \tag{3.11}$$

Inserting Eqn. (3.11) into Eqn. (3.10),

$$A_{ch} = \frac{\Sigma_{ch}}{\Sigma_0} \cdot \frac{P_{t0}}{P_{tch}} \cdot A_0 \tag{3.12}$$

Where;

$$\frac{P_{tch}}{P_{t0}} = \frac{P_{tch}}{P_{t3}} \cdot \frac{P_{t3}}{P_{t2}} \cdot \frac{P_{t2}}{P_{t1}} \cdot \frac{P_{t1}}{P_{t0}} \tag{3.13}$$

In Eqn. (3.13), $P_{tch}/P_{t3} = 1$, with the inviscid assumption used for conceptual sizing. Calculated from Rankine-Hugoniot Relations and given in Table 3.4 $P_{t3}/P_{t2} = 0.8836$, $P_{t2}/P_{t1} = 0.8323$ and $P_{t1}/P_{t0} = 0.8294$.

And also from Eqn. (2.5); $\Sigma_{ch} = 2.035$ and $\Sigma_0 = 6.790$.

Now evaluating Eqn. (3.12),

$A_{ch} = 0.0129\ m^2$

Thus, the corresponding height of the combustion chamber is;

$$H_{ch} = \frac{A_{ch}}{w} = 0.086\ m$$

Now, in order to calculate the length of the subsonic diffuser, the value of the inner body's divergence angle is decided on. In Figure 3.19 [3], the schematic of a conical subsonic diffuser is given.

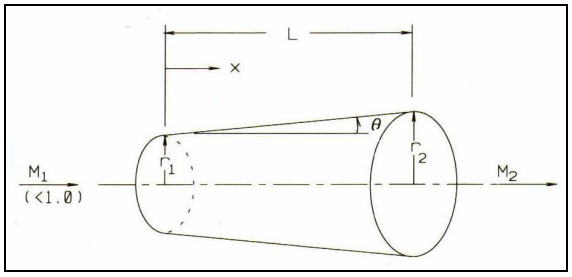

Figure 3.19 Schematic of a conical subsonic diffuser

It is known that, experiments conducted with subsonic diffusers of all shapes with an overall area change, limited by an equivalent conical half-angle of 3 degrees, have shown a compression process total pressure recovery approaching unity [3]. Therefore, it is decided that the subsonic diffusers inner body divergence angle will be 3 degrees. Thus, now the length of the subsonic diffuser can be calculated by using Eqn. (3.14).

$$L_{sub} = \frac{H_{ch} - H_{th}}{\tan \theta_{sd}} = 0.732\ m \tag{3.14}$$

Hereby, the sizing of the inlet is completed. Although the process is presented here step by step, a *MATLAB* code has been developed for this purpose and the sizing has been done by using this *MATLAB* code, which is the inlet sizing tool used for the present procedure.

The side view and the front view drawings of the designed inlet is given in Figure 3.20. The three dimensional solid model of the inlet is given in Figure 3.21.

Figure 3.22 is the side view drawing of the inlet installed on the missile. It can be observed from Figure 3.22 that when the inlet is installed on the missile, the inlet is not too lengthy and voluminous. The extension part of the inlet, which extends from the start of the combustion chamber section until the end of the nozzle section is the fairing part and it provides surfaces for the tail control fins to be mounted on.

A summary of important geometry design parameters are given in Table 3.5.

Table 3.5 Summary of important design parameters

Important Design Parameters	
Family	2-D
Geometry	Fixed
Supersonic diffuser form	All external compression
Supersonic Compression Complexity	Double wedge
Supersonic compression direction	Downward
Location on the vehicle body	Side mounted
Number of inlets	2
Interface with the combustor	Off-set
First wedge angle	16 °
Second wedge angle	21 °
Radius of curvature of the throat section	4 entrance channel heights
Subsonic diffusers inner body divergence angle	3 °

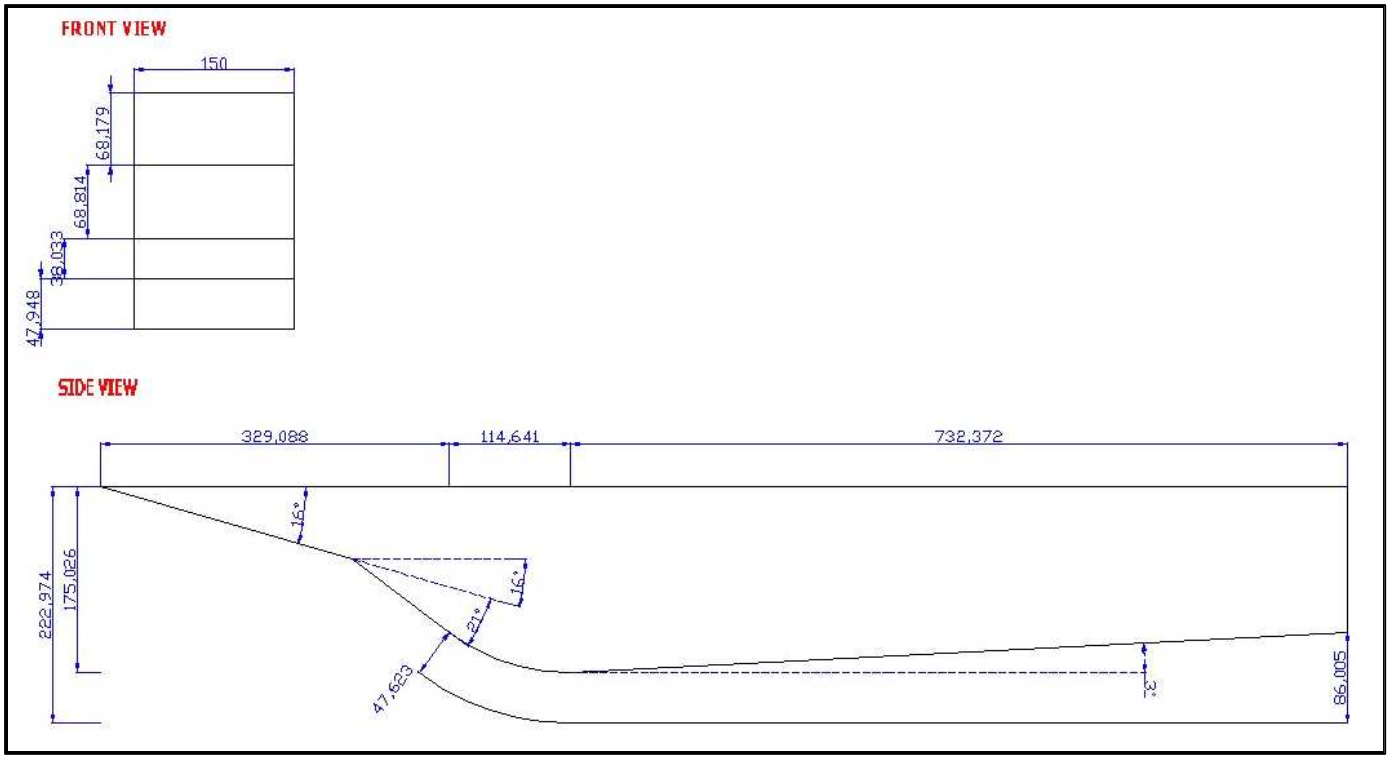

Figure 3.20 Front and side view drawings of the designed inlet (dimensions in mm)

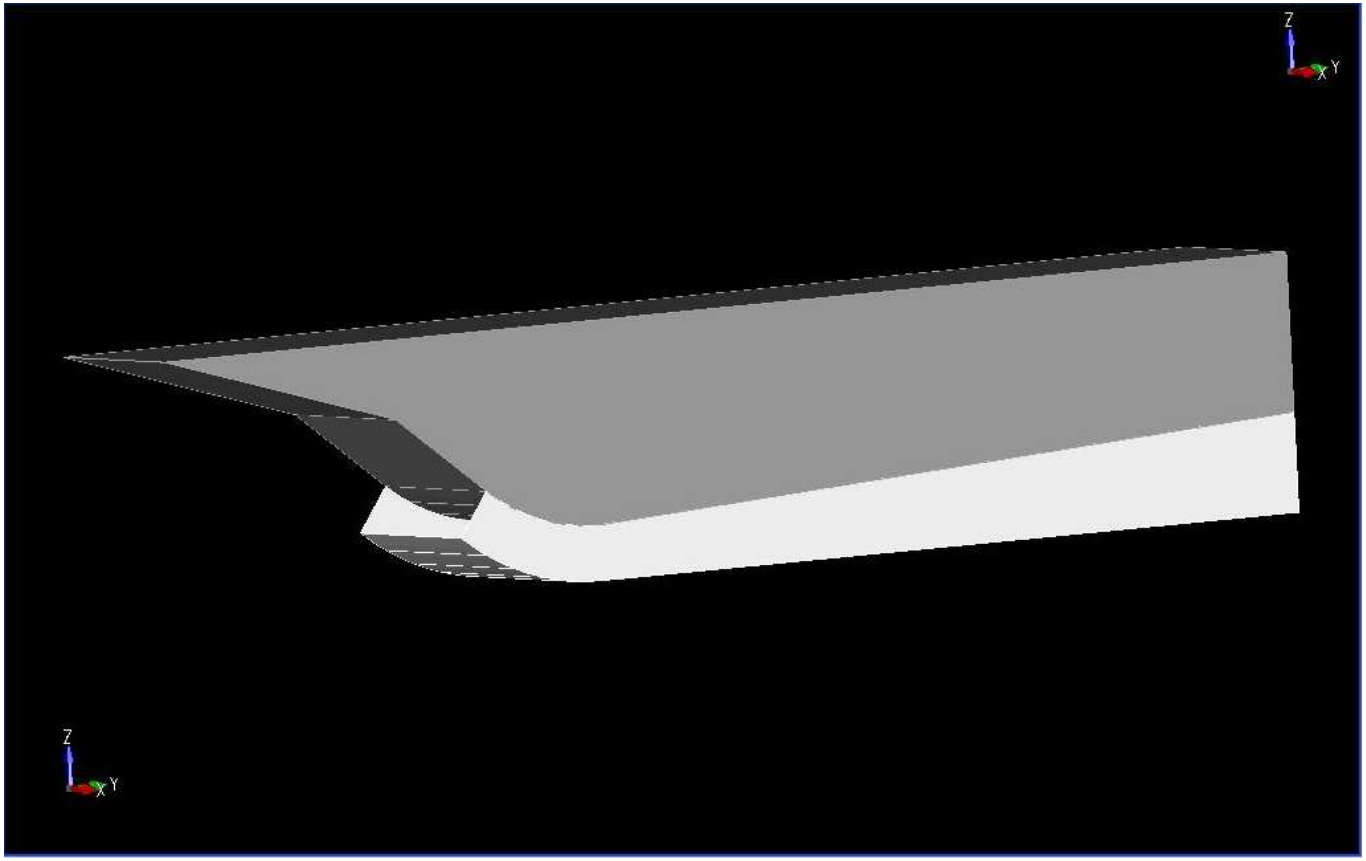

Figure 3.21 Three dimensional drawing of the designed inlet

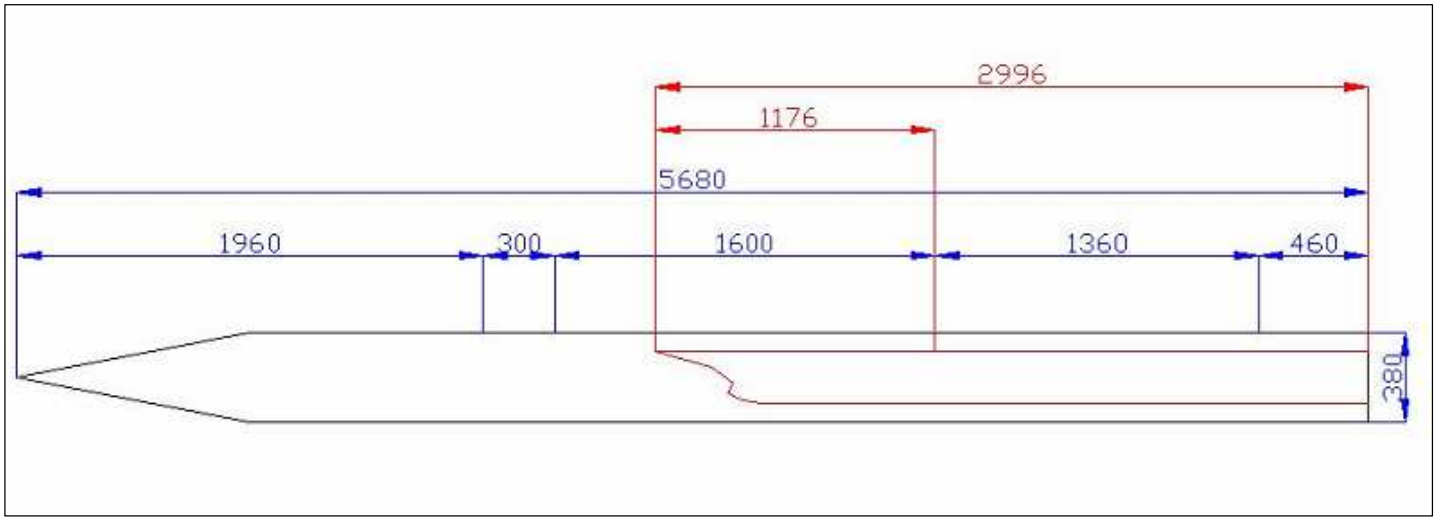

Figure 3.22 Side view drawing of the inlet installed on the missile body (dimensions in mm)

CHAPTER 4

PERFORMANCE ESTIMATION

4.1 Estimated Performance Parameters and the Cases

The performance of the designed inlet is estimated at various operating conditions. The aim of this study is to obtain some preliminary values of the flow variables and ideas about flowfield behavior at different operating conditions before performing CFD analyses. The analytically calculated (estimated) values resulting from this study can later on be compared with the results of the CFD analyses.

There are 13 cases for which performance estimation is made. The description of these cases are given in Table 4.1, Table 4.2 and Table 4.3.

Table 4.1 Descriptions of cases 1 to 9

Cases for which angle of attack = 0deg		TERMINAL NORMAL SHOCK POSITION		
		SUBCRITICAL	CRITICAL	SUPERCRITICAL
MACH NUMBER	ABOVE DESIGN MACH NUMBER	case 6	case 4	case 5
	ON DESIGN MACH NUMBER	case 3	case 1	case 2
	BELOW DESIGN MACH NUMBER	case 9	case 7	case 8

Table 4.2 Descriptions of case 10 and case 11

Cases for which angle of attack > 0deg		TERMINAL NORMAL SHOCK POSITION	
		CRITICAL	SUPERCRITICAL
MACH NUMBER	ON DESIGN MACH NUMBER	case 10	case 11

Table 4.3 Descriptions of case 10 and case 11

Cases for which angle of attack < 0deg		TERMINAL NORMAL SHOCK POSITION	
		CRITICAL	SUPERCRITICAL
MACH NUMBER	ON DESIGN MACH NUMBER	case 12	case 13

- Case 1: *Critical* operation at on-design Mach number and cruise altitude. (M = 3.5, H= 16000 m)
- Case 2**:** *Supercritical* operation at on-design Mach number and cruise altitude. (M = 3.5, H = 16000 m)
- Case 3: *Subcritica*l operation at on-design Mach number and cruise altitude. (M = 3.5, H = 16000 m)
- Case 4: *Critical* operation at above design Mach number and cruise altitude. (M = 4.0, H = 16000 m)
- Case 5: *Supercritical* operation at above design Mach number and cruise altitude. (M = 4.0, H = 16000 m)
- Case 6: *Subcritical* operation at above design Mach number and cruise altitude. (M = 4.0, H = 16000 m)
- Case 7: *Critical* operation at below design Mach number and cruise altitude. (M = 3.0, H = 16000 m)
- Case 8: *Supercritical* operation at below design Mach number and cruise altitude. (M = 3.0, H = 16000 m)

- Case 9: *Subcritical* operation at below design Mach number and cruise altitude. (M = 3.0, H = 16000 m)
- Case 10: *Critical* operation at *positive angle of attack*, on-design Mach number and cruise altitude. (α = 10°, M = 3.5, H = 16000 m)
- Case 11: *Supercritical* operation at *positive angle of attack*, on-design Mach number and cruise altitude. (α = 10°, M = 3.5, H = 16000 m)
- Case 12: *Critical* operation at *negative angle of attack*, on-design Mach number and cruise altitude. (α = -10°, M = 3.5, H = 16000 m)
- Case 13: *Supercritical* operation at *negative angle of attack*, on-design Mach number and cruise altitude. (α = -10°, M = 3.5, H = 16000 m)

For each case, the analytically calculated performance parameters are:

- The total pressure recovery (P_{tch}/P_{t0})
- The Capture Area Ratio (A_0/A_c)

4.1.1 Performance parameters of case 1

(M=3.5, H=16000m, α=0°, critical operation)

The on-design Mach number, critical operating condition is the design-to condition of the inlet. It is defined by shock-on-lip operation and a full capture. Thus, A_0/A_c=1. The value of the total pressure recovery is calculated by using the Rankine-Hugoniot relations given by equations (3.5) to (3.9). Solving these equations for this case yields; P_{tch}/P_{t0} = 0.6099.

4.1.2 Performance parameters of case 2

(M=3.5, H=16000m, α=0°, supercritical operation)

The on-design Mach number, supercritical operating condition is also defined by shock-on-lip operation and a full capture. Thus, A_0/A_c = 1. In order to calculate the total pressure recovery value the following calculation methodology is applied.

- The Mach number upstream of the terminal normal shock is assigned.
- As soon as the Mach number upstream of the terminal normal shock is known, the total pressure recovery value can be obtained by solving equations (3.5) to (3.9).

Solving this case for an assigned upstream terminal normal shock Mach number of 1.91 yields, P_{tch}/P_{t0} = 0.5253. Nevertheless, in order to ensure that the same case will be solved during CFD analyses, the corresponding chamber entry station static pressure value should be calculated. As will be explained in Chapter 5, this value is a required input boundary condition for the CFD analysis. The methodology applied to obtain the value of the chamber entry station static pressure along with other parameters is given in Section 4.2.2.

4.1.3 Performance parameters of case 3, case 6 and case 9

(M=3.5, H=16000m, α=0°, subcritical operation), (M=4.0, H=16000m, α=0°, subcritical operation), (M=3.0, H=16000m, α=0°, subcritical operation)

In these cases, the terminal normal shock and the oblique shocks intersect upstream of the cowl station. However, no analytical methods to estimate the capture area ratio of the subcritical operating case was found in literature. Although it is known that the capture area ratio of the subcritical operating case is less than 1, no analytical method was found in literature to obtain this ratio for these cases. If the terminal normal shock is able to attain a stable position in the supersonic diffuser, then the respective subcritical total pressure recovery value will be nearly equal to the critical total pressure recovery value of each respective case.

4.1.4 Performance parameters of case 4

(M=4.0, H=16000m, α=0°, critical operation)

This case also corresponds to a full capture, but this captured streamtube consists of uncompressed and compressed air. Thus, $A_0/A_c = 1$. In this case, when equations (3.5) to (3.9) are solved it is determined that the first oblique shock angle is 28.1°, and the second oblique shock angle is 40.18°. Therefore, it is readily determined that the intersection point of the oblique shock falls inside the captured streamtube boundary. As stated in Section 2.5.1, this may cause flow instability and estimating the value of the total pressure recovery would be meaningless, if such occurrence takes place. Since the stability state can be determined after CFD analyses, the total pressure recovery value calculated by solving equations (3.5) to (3.9) is: $P_{tch}/P_{t0} = 0.4862$

4.1.5 Performance parameters of case 5

(M=4.0, H=16000m, α=0°, supercritical operation)

For this case, the supersonic diffuser flow picture is no different than the supersonic diffuser flow picture of Case 4. Therefore the same possibility of flow instability remains valid for this case also. Since the external flow picture is no different than the external flow picture of Case 4, the capture area ratio value of this case is also the same as Case 4's. Thus, $A_0/A_c = 1$. The total pressure recovery value of this case was not estimated because there was no quick analytical method that would incorporate for the extra compression due to the possible shock reflections in the throat section.

4.1.6 Performance parameters of case 7

(M=3.0, H=16000m, α=0°, critical operation)

The capture area ratio for this case is calculated from Eqn. (4.1) of Reference [6].

$$\frac{A_0}{A_c} = \frac{\cot\delta_1 - \cot\beta_{1D}}{\cot\delta_1 - \cot\beta_1} \cdot \frac{\cot\delta_2 - \cot\beta_{2D}}{\cot\delta_2 - \cot\beta_2} \tag{4.1}$$

where β_1 and β_2 are the realized oblique shock angles at below-design Mach number operation and β_{1D} and β_{2D} are the shock-on-lip oblique shock angles corresponding to the design-to condition. Thus, A_0/A_c =0.80103. For the calculation of the total pressure recovery the same methodology as in Case 1 is applied and, P_{tch}/P_{t0} = 0.7354.

4.1.7 Performance parameters of case 8

(M=3.0, H=16000m, α=0°, supercritical operation)

The capture area ratio of this case is equal to the capture area ratio of Case 7, since the supersonic diffuser flow pictures are the same for these two cases.Thus, A_0/A_c =0.80103. For the calculation of the total pressure recovery the same methodology as in Case 2 is applied, and for an assigned terminal normal shock Mach number of 1.95; P_{tch}/P_{t0} = 0.5653.

4.1.8 Performance parameters of case 10

(M=3.5, H=16000m, α=10°, critical operation)

The capture area ratio of this case is calculated using Eqn. (4.2) [6]. The symbols used through equations (4.2) to (4.4) are shown in Figure 4.1 [6].

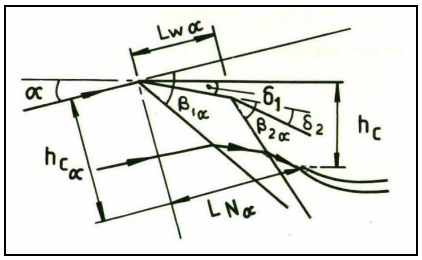

Figure 4.1 Schematic of symbols used in equations of capture area ratio at angle of attack

$$\frac{A_0}{A_c} = \frac{h_{c,\alpha}}{h_c}\frac{h_\infty}{h_{c,\alpha}} \tag{4.2}$$

where,

$$\frac{h_\infty}{h_{c,\alpha}} = \frac{\cot\delta_{1,\alpha} - \cot\beta_{1D,\alpha}}{\cot\delta_{1,\alpha} - \cot\beta_{1,\alpha}}\frac{\cot\delta_2 - \cot\beta_{2D,\alpha}}{\cot\delta_2 - \cot\beta_{2D,\alpha}} \tag{4.3}$$

The $\frac{h_{c,\alpha}}{h_c}$ term in Eqn. (4.2) is calculated from Eqn. (4.4)

$$\frac{h_{c,\alpha}}{h_c} = \frac{\sin(\beta_{1D} + \alpha)}{\sin\beta_{1D}} \tag{4.4}$$

As a result; A_0/A_c = 1.1846. For the calculation of the total pressure recovery, the same methodology as in Case 1 is applied and, P_{tch}/P_{t0} = 0.4913.

4.1.9 Performance parameters of case 11

(M=3.5, H=16000m, α=10°, supercritical operation)

The capture area ratio of this case is equal to the capture area ratio of Case 10, since the supersonic diffuser flow pictures are the same for these two cases.Thus,

A_0/A_c = 1.1846. For the calculation of the total pressure recovery the same methodology as in Case 2 is applied and for an assigned terminal normal shock Mach number of 1.5; P_{tch}/P_{t0} = 0.4569.

4.1.10 Performance parameters of case 12

(M=3.5, H=16000m, α = -10°, critical operation)

The capture area ratio of this case is also calculated using equations (4.2) to (4.4). As a result, A_0/A_c = 0.6763. For the calculation of the total pressure recovery the same methodology as in Case 1 is applied. As a result, P_{tch}/P_{t0} = 0.5266.

4.1.11 Performance parameters of case 13

(M=3.5, H=16000m, α = -10°, supercritical operation)

The capture area ratio of this case is equal to the capture area ratio of Case 12, since the supersonic diffuser flow pictures are the same for these two cases. As a result, A_0/A_c = 0.6763. For the calculation of the total pressure recovery the same methodology as in Case 1 is applied. As a result, P_{tch}/P_{t0} = 0.4016.

4.2 Calculation of Flow Parameters at Critical and Supercritical Operating Conditions

4.2.1 Calculation of flow parameters at critical operating conditions

Apart from calculating the performance parameters (A_0/A_c and P_{tch}/P_{t0}), flow parameters such as total pressure, total temperature, static pressure, static temperature, static density, Mach number, speed of sound and velocity are calculated at the stations shown in Figure 4.2.

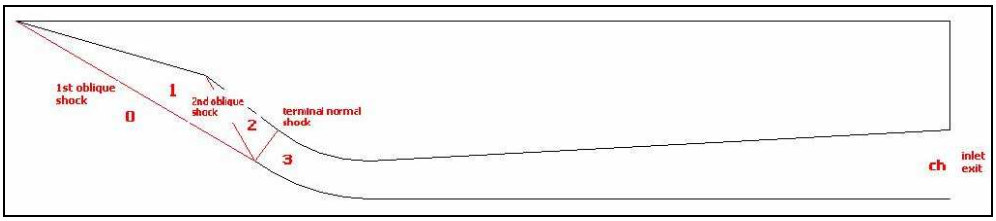

Figure 4.2 Representative inlet stations for critical operation case

The calculations are made for the critical operating regime using a *MATLAB* code that is developed especially for this purpose. In this code, equations (2.4), (2.5), isentropic relations and equations (3.5) to (3.9) are used to obtain the flow parameters at the various stations. The methodology applied to obtain the flow parameters at the various stations are given in the flowchart in Figure 4.3. The results obtained for Case 1, Case 4, Case 7, Case 10 and Case 12 are given in Appendix A.

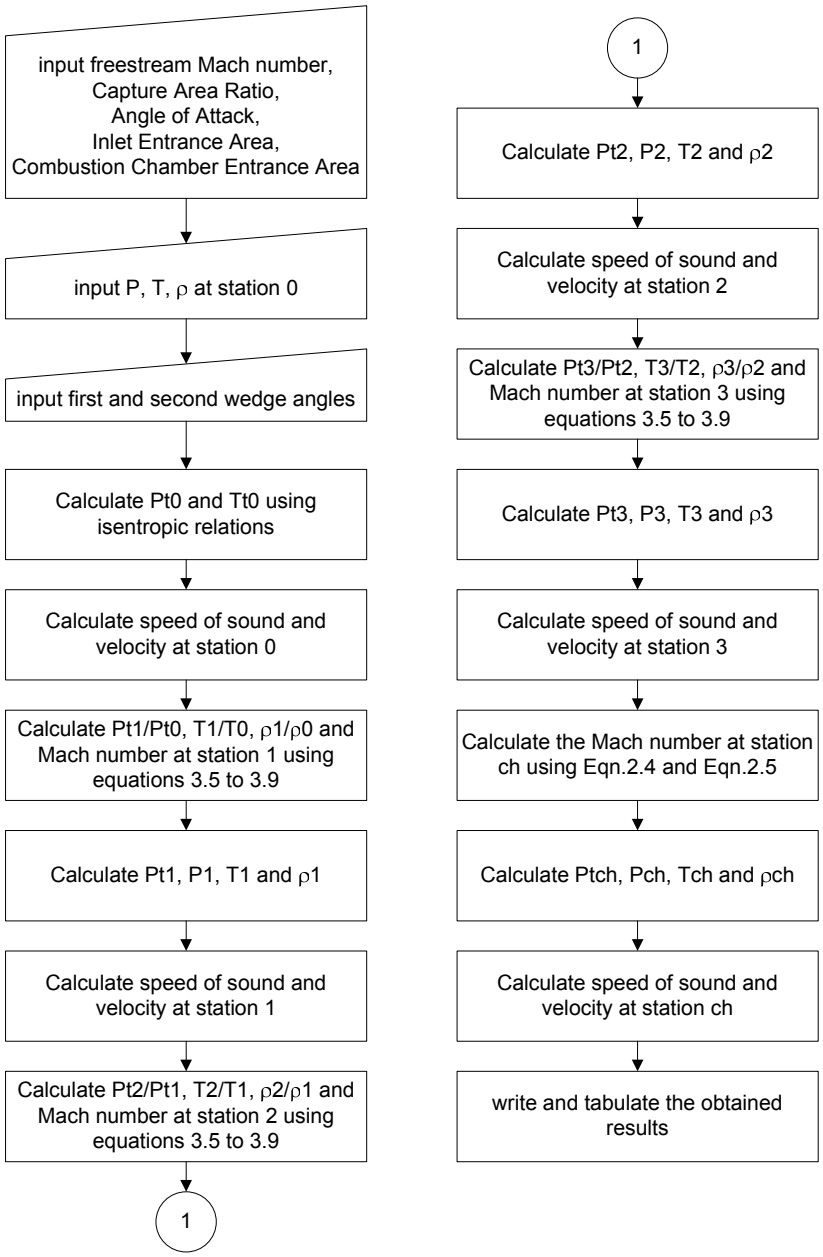

Figure 4.3 Flowchart of the methodology applied to obtain the flow parameters at critical operation

4.2.2 Calculation of flow parameters at supercritical operating conditions

The flow parameters such as; total pressure, total temperature, static pressure, static temperature, static density, Mach number, speed of sound and velocity are also calculated for supercritical operation at the stations shown in Figure 4.4.

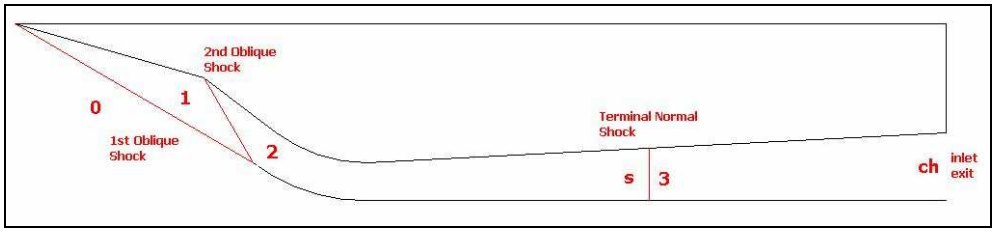

Figure 4.4 Representative inlet stations for supercritical operation case

The calculations are also made for the supercritical operating regime by using a *MATLAB* code developed especially for this purpose. As in the one used for the critical operating regime, in this code too, equations (2.4), (2.5), isentropic relations and equations (3.5) to (3.9) are used to obtain the flow parameters at the various stations. The methodology applied to obtain the flow parameters at the various stations are given in the flowchart in Figure 4.5. The results obtained for Case 2, Case 8, Case 11 and Case 13 are also given in Appendix A.

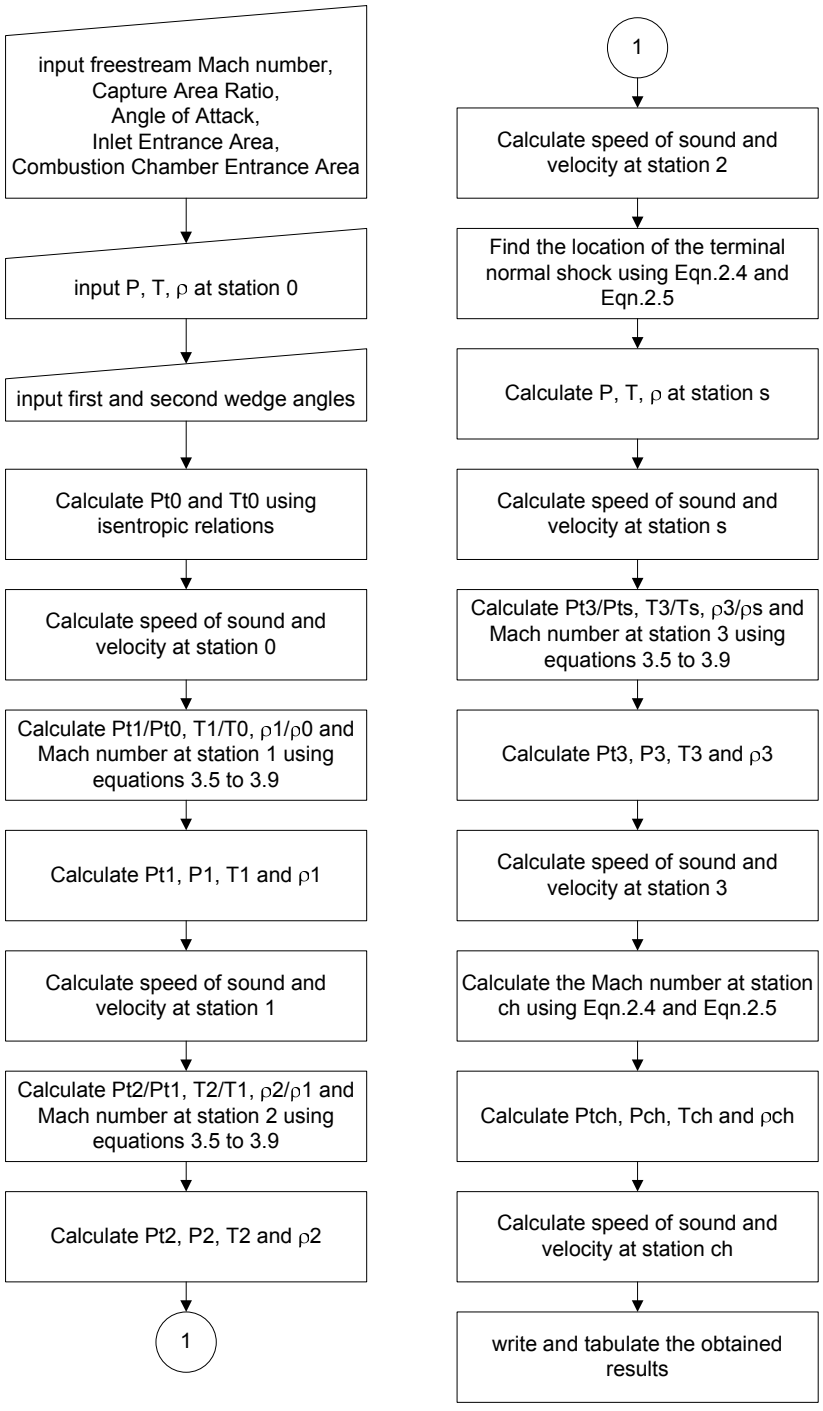

Figure 4.5 Flowchart of the methodology applied to obtain the flow parameters at supercritical operation

The capture area ratio is an input to both of the above mentioned *MATLAB* codes. Another *MATLAB* code that calculates the capture area ratio is developed. This code uses equations (4.1) to (4.4) for calculating the capture area ratio. This ratio can be calculated either for cases in which angle of attack is present or the cases in which below design Mach number operation is present.

CHAPTER 5

CFD METHOD AND FLOW SOLVER

5.1 Overview

The advantage of CFD is that the inlet flow problem can be analyzed with less time and cost than the experimental techniques. The cases to be solved with CFD analyses for the inlet flow problem are, two dimensional cases; Case 1 to Case 13 (explained in CHAPTER 4)

Viscous effects must be included if a true flow solution is desired when dealing with the inlet flow problem. The viscous effects are dominant in the subsonic diffuser, and the shock-boundary layer effects are important. The total pressure recovery when viscous effects are taken into consideration is lower than the inviscid total pressure recovery. However, in this study, the aim is to obtain the patterns and positions of the two oblique and normal shocks and the capture area ratio along with the mass flow rate of air at various operating conditions. If at these various operating conditions, the inviscid total pressure recoveries calculated analytically can be obtained, it would give a good idea about whether the design satisfies the requirements. If it is found that, even the inviscid total pressure recovery is too low to satisfy the requirements, then it can be concluded that the design will have to be revised. This will save design time and design cost through not having to deal with the long computational times involved in viscous CFD analysis. Another aim of this study is to determine whether the inlet unstarts in any of the operating conditions to be solved. This will give an idea about the robustness of the design. If it is observed that unstart is yielded even with inviscid analysis, then again it can be concluded that the design has to be revised. Similarly, this will

too save design cost and design time. Therefore, it is decided to conduct inviscid CFD analyses for the inlet flow problem. Consequently, an Euler solver with memory requirements less than Navier-Stokes solvers can be used.

In this study, for the CFD solutions a stand alone PC having a 2.6 MHz processor and 512 MB RAM is used for the solution of the two-dimensional flow.

There are various commercial and research flow solvers applicable to different fields and that use different mathematical models, space and time discretization algorithms and grid types. In this study, the commercial CFD-FASTRAN [38] flow solver is used.

5.2 Model Preparation Process in CFD-FASTRAN

The model preparation process in CFD-FASTRAN starting from the geometry generation to the submission of the run is given in the flowchart of Figure 5.1 [38, 39, 40]. The processes of the flowchart shown in Figure 5.1 are followed step by step to prepare the model of the inlet flow problem in CFD-FASTRAN.

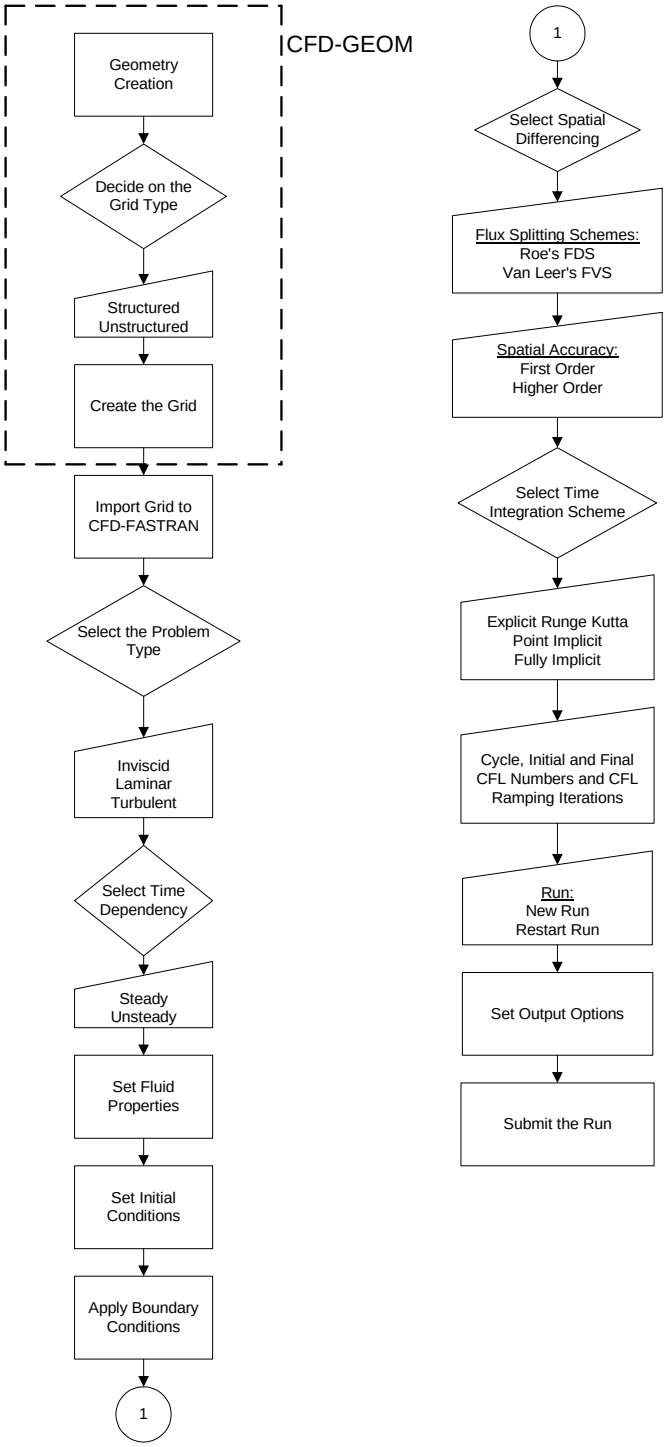

Figure 5.1 Flowchart of the model preparation process in CFD-FASTRAN

5.3 Geometry and Grid Creation

Both the geometry and the grid of the inlet flow problem is generated using CFD-GEOM. For the solution of the inlet flow problem it is decided to use a structured grid. It is very important to observe the shock wave patterns and shock wave locations in the final solution, which can be best obtained on structured grids. The effort involved for generating the grid is not a big concern, since the geometry is not a complex one. However, the flow to be observed in the final solution is a complex one. Therefore, a choice to use structured grids also decreases the computational time.

In order to determine the optimum number of elements on the grid, a grid independency study is conducted. This grid dependency study is conducted on only a single case because the computation is too CPU intensive. This selected case is Case 2, in which it is readily ensured from analytical results that the inlet remains started. The results obtained on 3 different meshes (each having different number of grids in the streamwise direction and the same number of grids in the vertical direction) are compared. The first mesh has 207 grid points in the streamwise direction and 119 grid points in the vertical direction. In the second mesh the number of elements in the streamwise direction is increased by 50 % yielding 417 grid points. In the third mesh the number of elements in the streamwise direction is increased by another 50 % yielding 627 grid points. The results of this study are presented in Section 6.1. It is observed that while the first and second meshes yield different mach contours and results, the second and third meshes yield nearly the same mach contours and results. Thus, it is determined that the second mesh is sufficient for the analyses. Therefore, it is decided to use this mesh consisting of 417 x 119 points. The mesh is shown in Figure 5.2 for the analyses. It can be seen from this figure that the grid distribution is finer around the cowl lip. This is necessary due to the fact that three shocks will intersect at the cowl lip during the inlets on-design critical operation.

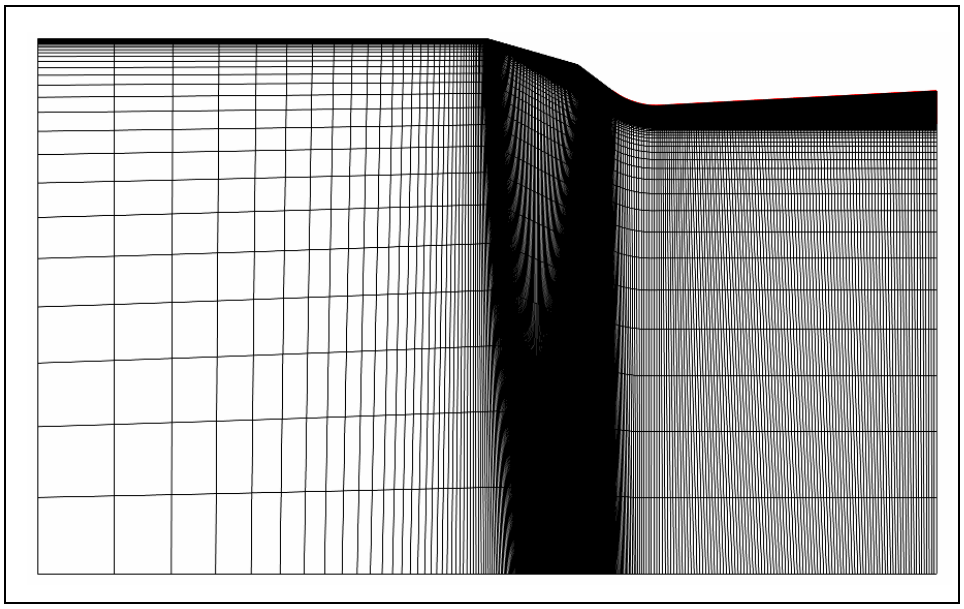

Figure 5.2 Mesh of the 2-D model (417x119 grid points)

5.4 Problem Type and Time Dependency Selection

As discussed earlier, the inviscid flow option is chosen for the problem type. The time dependency of the problem may be set to *Steady* or *Transient*. Obtaining the performance parameters of the inlet at an unstarted state would be meaningless. Therefore, the aim of this study is to obtain the flow solutions at states where the inlet remains started (where the flowfield is considered stable). Consequently, the time dependency of the problem is set to *Steady*.

5.5 Setting the Fluid Properties

The calorically perfect gas option is selected and the default value of 1.4 for the specific heat ratio of air is selected for specifying the fluid properties.

5.6 Setting the Initial Conditions

The variables that need to be initiated are the static pressure, the static temperature and the velocity. In the case of steady-state simulations, initial conditions are merely initial guesses. They do not influence the final solution but they influence the speed of convergence to the final solution [38]. Therefore, in order to obtain a faster convergence, instead of initializing the whole computational domain with freestream values different initial conditions are assigned to different domains. For this purpose the *Volume by Volume* sub-option is selected. The external flow regions are initiated with the freestream flow variable values. The interior flow regions are initiated with analytically calculated flow variable values upstream and downstream of the shocks. These values are found in Appendix A. This methodology is in perfect accordance with the multi zonal approach used. Different initial conditions are used for different cases. The zones of the computational domain for the 2-D model are given in Figure 5.3. The initial conditions for each case is given in Table 5.1.

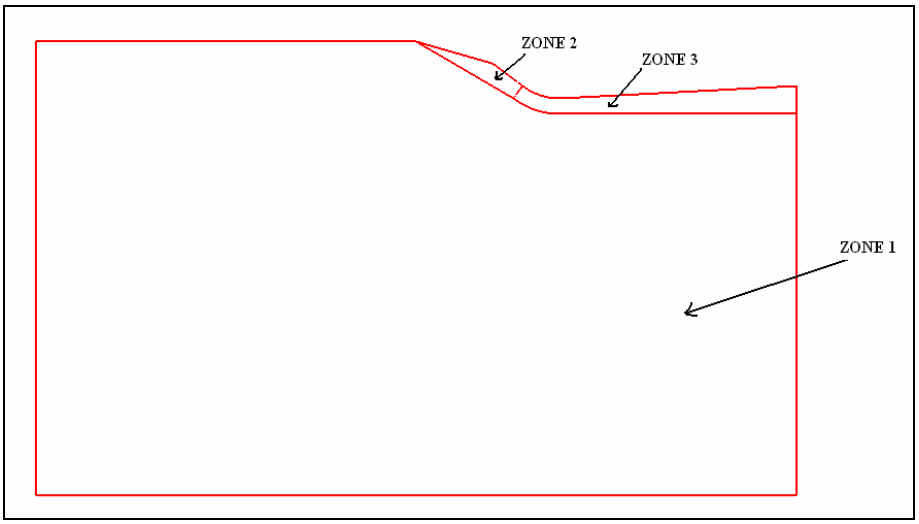

Figure 5.3 Zones of the 2-D model

Table 5.1 Initial conditions of the analyses cases

CASES	ZONES		
	Zone 1	Zone 2	Zone 3
Case 1 Case 2 Case 3	U=1032.745 m/s V=0 m/s P=10,353 Pa T=216.65 K	U=920 m/s V=0 m/s P=35,768 Pa T=326 K	U=346.7 m/s V=0 m/s P=359,763 Pa T=687.6 K
Case 4 Case 5 Case 6	U=1180.28 m/s V=0 m/s P=10,353 Pa T=216.65 K	U=1064 m/s V=0 m/s P=41,142 Pa T=345.6 K	U=353.8 m/s V=0 m/s P=596,469 Pa T=847.7 K
Case 7 Case 8 Case 9	U=885.21 m/s V=0 m/s P=10,353 Pa T=216.65 K	U=775 m/s V=0 m/s P=31,021 Pa T=307.7 K	U=354.6 m/s V=0 m/s P=191,140 Pa T=544.1 K
Case 10 Case 11	U=1017.0552 m/s V=179.3343 m/s P=10,353 Pa T=216.65 K	U=798.35 m/s V=0 m/s P=64,545 Pa T=430.26 K	U=488.55 m/s V=0 m/s P=211,754 Pa T=628.7 K
Case 12 Case 13	U=1017.0552 m/s V=-179.3343 m/s P=10,353 Pa T=216.65 K	U=998.29 m/s V=0 m/s P=17,229 Pa T=251.55 K	U=3104.18 m/s V=0 m/s P=333,062Pa T=701.5 K

5.7 Setting the Boundary Conditions

After the initial conditions are set, the next step is to set the boundary conditions. The types of boundary conditions applied to the 2-D model are given in Figure 5.4.

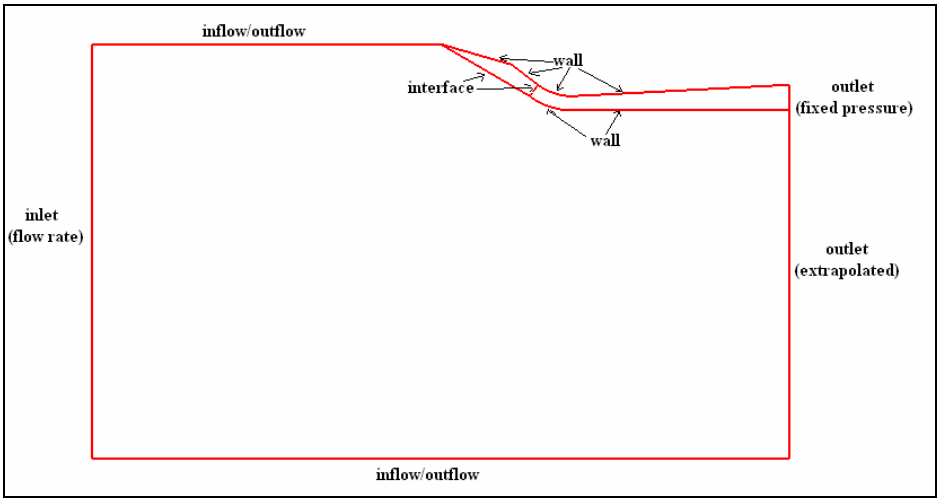

Figure 5.4 Boundary conditions applied to the 2-D model

The *Inlet* boundary condition has two options, the fixed mass flow rate and the fixed total pressure condition. The fixed mass flow rate condition in which all variables are kept constant is set for the inlet flow problem.

The *Outlet* boundary condition has two options, the fixed static pressure option and the extrapolated option. For subsonic outflows, the fixed static pressure option is used. In this option, the user specifies the pressure on the exit plane and the flow solver checks the local Mach number at boundary points using the fixed pressure condition. For local subsonic outflow the remaining flow variables are extrapolated from the interior to the exit plane. For the extrapolated option, no information is required from the user. All flow variables are extrapolated to the exit boundary from the interior domain.

The *Inflow/Outflow* boundary condition is a combination of the *Inlet* and *Outlet* boundary conditions. The CFD-FASTRAN flow solver uses internal logic to determine which boundary condition to apply. For supersonic inflows, this boundary condition uses the user specified variables. For supersonic outflows it uses the same approach as the extrapolated exit boundary condition.

The *Interface* boundary condition is used to link multiple domains to one another.

The *Wall* boundary condition has five options; adiabatic, isothermal, heat flux, aeroelastic and radiative. For the inlet flow problem the adiabatic wall boundary condition which sets the surface heat flux to zero is used.

The major challenge in the CFD analysis of an inlet flow is to determine the value of the exit pressure (back pressure) for the critical operating condition. At this condition, since the exit flow is subsonic the *Fixed Pressure Outlet* boundary condition is applied at the inlet exit. This requires the exit back pressure to be input by the user. An iterative procedure is applied in which a number of computations are performed to search for the exit back pressure value that yields critical operation. In a number of calculations, the exit back pressure is gradually increased from a value yielding supercritical operation until the back pressure value yielding critical operation is found. This procedure is also known as a root search iteration. Apart from the difficulty of having to perform many calculations for a single case there is another important drawback. This drawback is that, when the exit back pressure approaches the critical value, the shock wave system moves very slowly and a very long execution time is necessary to ensure the stability of the shock wave [15].

In the work done by Knight et al. [15] on high performance supersonic missile inlet design using automated optimization, they managed to obtain a critical back pressure tolerance less than 1 %. This means that a 1 % increase in the converged value for the back pressure would cause the inlet to unstart.

Although the boundary condition types are the same for each of the cases to be solved the values are different for each case. These values are given in Table 5.2.

Table 5.2 Boundary conditions of the analyses cases

Cases	**Boundary Conditions**		
	Inlet	Inflow / Outflow	Outlet (fixed pressure)
Case 1	U=1032.745 m/s V=0 m/s P=10,353 Pa T=216.65 K	U=1032.745 m/s V=0 m/s P=10,353 Pa T=216.65 K	Trial and error for Pexit > $(Pexit)_{case\ 2}$
Case 2			Pexit = 380,000 Pa
Case 3			Trial and error for Pexit > $(Pexit)_{case\ 1}$
Case 4	U=1180.28 m/s V=0 m/s P=10,353 Pa T=216.65K	U=1180.28 m/s V=0 m/s P=10,353 Pa T=216.65 K	Trial and error for Pexit > $(Pexit)_{case\ 5}$
Case 5			Pexit = 580,000 Pa
Case 6			Trial and error for Pexit > $(Pexit)_{case\ 4}$
Case 7	U=885.21 m/s V=0 m/s P=10,353 Pa T=216.65 K	U=885.21 m/s V=0 m/s P=10,353 Pa T=216.65 K	Trial and error for Pexit > $(Pexit)_{case\ 8}$
Case 8			Pexit = 187,966.7 Pa
Case 9			Trial and error for Pexit > $(Pexit)_{case\ 7}$
Case 10	U=1017.0552 m/s V=179.3343 m/s P=10,353 Pa T=216.65 K	U=885.21 m/s V=0 m/s P=10,353 Pa T=216.65 K	Trial and error for Pexit > $(Pexit)_{case\ 11}$
Case 11			Pexit = 297,967.9 Pa
Case 12	U=1017.0552 m/s V= -179.3343 m/s P=10,353 Pa T=216.65 K	U=1017.0552 m/s V=-179.3343 m/s P=10,353 Pa T=216.65 K	Trial and error for Pexit > $(Pexit)_{case\ 13}$
Case 13			Pexit=198,046.6 Pa

5.8 Selection of the Flux Splitting Scheme

In CFD-FASTRAN, the user has an option of using either one of two spatial differencing schemes; Roe's flux difference splitting or Van Leer's flux vector splitting. Both are upwind differencing schemes. The Van Leer's scheme may be less accurate if viscous forces or viscous effects are highly important. However, the dissipative effects of the Van Leer's scheme cause it to be more robust than the

Roe's scheme. It is known that the Van Leer's scheme has been tailored for transonic flows and should provide better transonic shock structure than Roe's scheme [38]. Since for the inlet flow problem the point of interest is obtaining the shock structure and since the solution will be realized for inviscid flow it is decided to use the Van Leer's scheme.

This scheme is frequently used in similar problems. For example, in the work done by Doyle Knight et al. to investigate the High Speed Civil Transport Inlets operability with angle of attack [18] the Van Leer's scheme was used to evaluate the inviscid flux. In the study they performed, it was decided to use the Van Leer's scheme after determining that the Roe's scheme failed due to anomalous solution.

5.9 Selection of the Spatial Accuracy

The flux splitting schemes provided in CFD-FASTRAN are spatially first order accurate. However, via several slope limiters the spatial accuracy can be increased to second or third order. Though the least accurate, first order spatial accuracy is the most robust. Therefore, for the inlet flow problem first order spatial accuracy is used.

5.10 Selection of the Time Integration Scheme and the CFL Number

In CFD-FASTRAN explicit and implicit time integration scheme options are present. The explicit scheme option is the *Runge-Kutta Explicit Scheme*. The implicit schemes are; the *Point Implicit Scheme* and the *Fully Implicit Scheme*. For the inlet flow problem, the Runge Kutta Explicit and Point Implicit schemes yield convergence problems. Therefore, a Fully Implicit Scheme is used. The initial CFL number is set to 1. However, due to convergence problems, it is not possible to increase the CFL number as the solution progresses. The final CFL number is also set to 1.

5.11 Concluding Remarks

In this chapter the CFD method and the flow solver was explained. The methodology that is applied in order to analyze the inlet flow problem was presented. In Chapter 6; the results of the 13 cases solved for the inlet flow problem are given, along with the discussions on these results.

CHAPTER 6

RESULTS AND DISCUSSION

6.1 Overview

In this chapter, the results of the aforementioned 13 cases obtained through the CFD-FASTRAN flow solver are presented. These 13 cases are sufficient to understand to some extent the flow phenomenon occurring during the inlets on-design, above-design, below-design, critical, subcritical, supercritical, positive angle of attack and negative angle of attack operations. It is possible to also obtain the values of the performance parameters at these solved cases.

For each constant Mach number; it is necessary to first obtain the solution of the supercritical case. The reason can be explained as follows: For the critical operating condition the exit pressure (back pressure) is an unknown. Nevertheless, the value of the exit back pressure must be input at the exit boundary as the *Fixed Pressure Outlet* boundary condition. Therefore, an iterative procedure called a root search iteration is applied to search for the exit back pressure value that yields critical operation. In this procedure, in a number of runs, the exit back pressure is gradually increased from a value yielding supercritical operation until the back pressure value yielding critical operation is found. This is why it is necessary to first solve the supercritical case.

Steady state, inviscid solutions are obtained for these cases using first order spatial accuracy, Van Leer's flux splitting, and fully implicit time integration schemes. The initial and final CFL numbers are equal to 1. The grid used for these cases was presented in Section 5.4 and was decided on after performing a grid independency

study. The results of the grid independency study are also presented in this chapter in detail.

The results of the 13 cases solved are compared with the analytical solutions which may be found in Appendix A.

6.2 Convergence Criterion

Convergence of a solution is monitored with the L_2-norm of the conserved variables. As the steady state solution is approached, the variation in flow properties becomes smaller and smaller. Monitoring the L_2-norm is one way of measuring these variations. Also, as the steady state solution is approached the forces and moments at the wall boundaries begin to stay constant. Therefore, the forces and moments at the wall boundaries were also checked during the solution. In the 13 cases solved for the inlet flow problem, it was possible to obtain at least 3 orders of magnitude decreases in residual levels. Figure 6.1 shows the L_2-norm of the density with a decrease of 13 orders of magnitude for a converged solution (Case 13, M=3.5, H=16000m, α = -10°, supercritical).

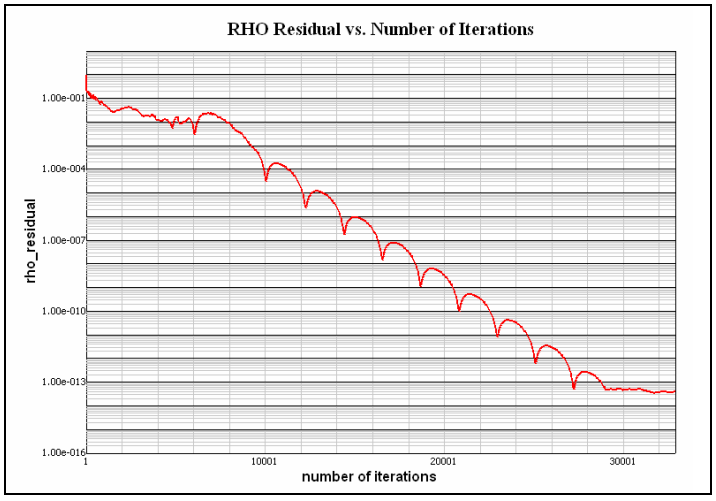

Figure 6.1 Steady state solution residual graph (case 13)

6.3 Grid Independency Study

In order to determine the grid to be used in the solution of the 13 cases of the inlet flow problem a grid independency study was conducted. As explained in Section 5.4 this study was conducted on only a single case (Case 2, M=3.5, H=16000m, α = 0°, supercritical). The solution was obtained for 3 different meshes (each having different number of grids in the streamwise direction and the same number of grids in the vertical direction). The first configuration which had 207 grid points in the streamwise direction and 119 grid points in the vertical direction, was named as *coarse grid*. In the second one the number of elements in the streamwise direction was increased by 50% yielding 417 grid points. This second grid was named as *mid resolution grid*. In the third one the number of elements in the streamwise direction was increased by another 50% yielding 627 grid points. This grid was named as *fine grid*.

Each of the 3 meshes were solved and the residuals for all flow variables were decreased by 4 orders of magnitude in the final converged solutions of each case. In Table 6.1, the number of elements of the three grids, the CPU times, the memory and number of iterations are given.

Table 6.1 Solution characteristics for grid independency study

Configuration	**Number of Elements of the Grid**	**CPU Time (sec/cycle)**	**Total CPU Time (hr)**	**Memory (MB)**	**Number of Iterations**
Coarse Configuration	22807	1.04	5.5 hours	25	18500
Mid Configuration	46007	2.24	7.5 hours	48	12000
Fine Configuration	69207	3.47	15 hours	70.5	15500

In order to compare the results obtained on these 3 meshes, the area averaged Mach number, the static pressure, and the density at stations 0, 1, 2, “s”, 3 and “ch” (these stations were presented in Section 4.2.2) are calculated for each mesh separately. The total pressure recovery, the capture area ratio, the first oblique shock wave angle, the second oblique shock wave angle, and the terminal normal shocks distance from the inlets leading edge are also calculated. These area averaged flow quantities along with the total pressure recovery, the capture area ratio, oblique shock angles, and the terminal normal shocks distance from the leading edge are compared with the analytical results of Case 2, which may be found in Appendix A. The results for the total pressure recovery, the capture area, the first and second oblique shock angles and the terminal normal shocks distance from the inlets leading edge are given in Table 6.2. The results for the area averaged values of the static pressure, the Mach number and the density are given in Figure 6.2, Figure 6.3, Figure 6.4 respectively.

Table 6.2 Comparison of the results obtained on the coarse, mid resolution and fine grids with analytical results

	Coarse Grid	**Mid Resolution Grid**	**Fine Grid**	**Analytical Results of Case 2**
Total Pressure Recovery	0.5214	0.5233	0.5247	0.5253
Capture Area Ratio	0.9694	0.9943	0.9960	1
First Oblique Shock Angle (°)	30	30	30	30
Second Oblique Shock Angle (°)	46	44	44	44
Terminal Normal Shocks Distance from Inlets Leading Edge (mm)	564	606	618	655

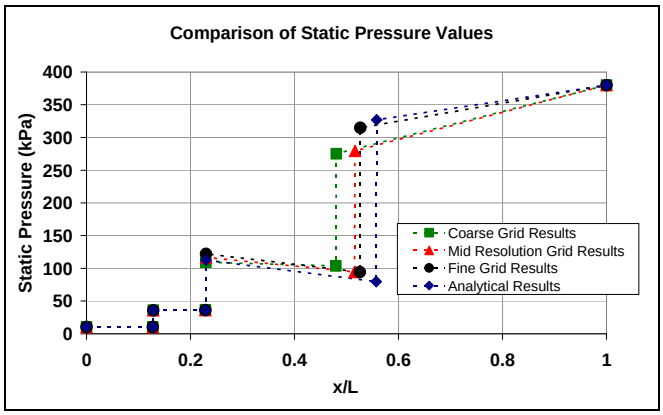

Figure 6.2 Comparison of the static pressure values obtained on the coarse, mid resolution and fine grids

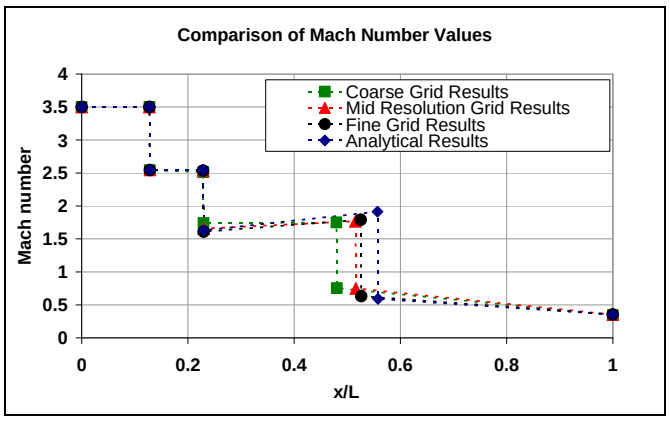

Figure 6.3 Comparison of the Mach number values obtained on the coarse, mid resolution and fine grids

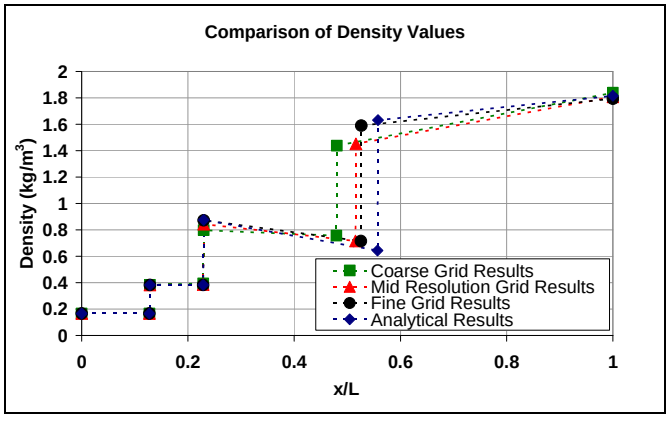

Figure 6.4 Comparison of the density values obtained on the coarse, mid resolution and fine grids

It can be seen from the results presented in Figure 6.2, Figure 6.3 and Figure 6.4, that, the solutions of the mid resolution grid and the fine grid are alike and close to the analytical results but the results of the coarse grid are quite different from the mid resolution and fine ones and analytical results. The values obtained for the terminal normal shocks distance from the inlet leading edge are close for the mid resolution and fine grids, but are different from the analytical results. This is due to the fact that the analytical results were obtained with the quasi 1-D flow assumption, whereas the CFD-FASTRAN solution is a 2-D flow solution. Therefore, the terminal normal shock stands at a more upstream distance due to the 2-D effects in the CFD-FASTRAN flow solution.

In order to choose which grid to perform the analyses on, it is also necessary to investigate and compare the resulting flowfields of the three meshes. In Figure 6.5, the Mach number contours of the coarse, mid resolution and fine grids are given. It can be observed that the contours of the mid resolution and fine grids are nearly overlapping, but the contours of the coarse grid is far away from the contours of the mid resolution and fine grids.

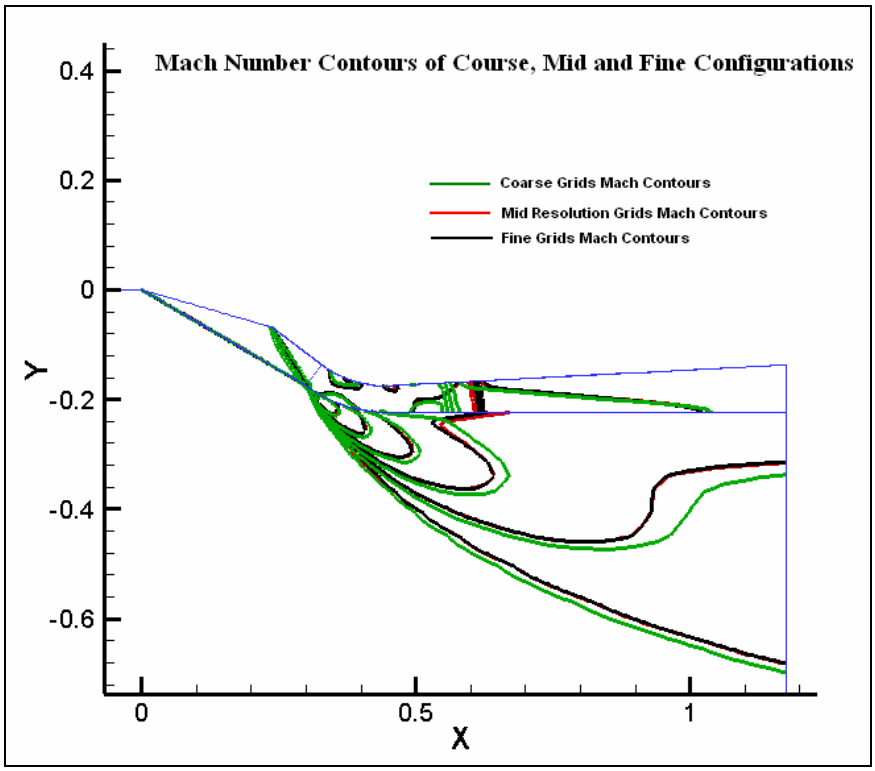

Figure 6.5 Mach number contours of coarse, mid resolution and fine grids

From the results given in Table 6.2, Figure 6.2, Figure 6.3, Figure 6.4 and Figure 6.5, it seems reasonable to choose the mid resolution grid as the grid to be used in the rest of the analyses. This is because the mid resolution grid yields nearly the same results as the fine grid, but the former has the advantage of a lower total CPU time.

6.4 Results of Case 1 to Case 13

For each of the cases in which it was possible to obtain a converged final solution, the inlets performance parameters, namely, the total pressure recovery, the capture area ratio, and the steady state flow distortion are calculated from the results of the converged solution. These performance parameters, are obtained by calculating the area averaged values of the related flow variables by evaluating line integrals at the

related cross sections. The values obtained are compared to the analytical solutions of the corresponding case.

The initial conditions and the boundary conditions applied along with the flow solver settings for each case were previously presented in Chapter 5.

From the flowfield, the first and second oblique shock angles and the coordinates of the intersection point of the two shocks are also calculated for each case and compared to the analytical solution. The aim of performing this comparison is to determine the accuracy of the CFD-FASTRAN solution.

Other variables that are calculated for each case and compared to the analytical solution are the terminal normal shocks distance from the inlets leading edge and the area averaged Mach number, the static pressure and the density at stations 0, 1, 2, “s”, 3 and “ch”.

6.4.1 Case 2 results

(M=3.5, H=16000m, $\alpha = 0°$, supercritical)

In the final converged solution the residuals for all flow variables were decreased by 4 orders of magnitude, with 12,000 iterations costing at a total CPU time of 7.5 hours. In Figure 6.6 the Mach number contours of the final converged solution are shown. The passage from purple colored contours to orange colored contours show the first oblique shock wave and the passage from orange colored contours to green contours shows the second oblique shock wave. The normal shock is located at the passage from green contours to blue contours. It can be seen from Figure 6.6 that the intersection point of the two oblique shock falls on the cowl lip and the terminal normal shock is located in the subsonic diffuser. In Table 6.3, the results for the total pressure recovery, the capture area, the steady state flow distortion, the first and second oblique shock angles and the terminal normal shocks distance from the inlets leading edge are given. The results for the area averaged values of the static

pressure, the Mach number and the density are given in Figure 6.7, Figure 6.8 and Figure 6.9 respectively.

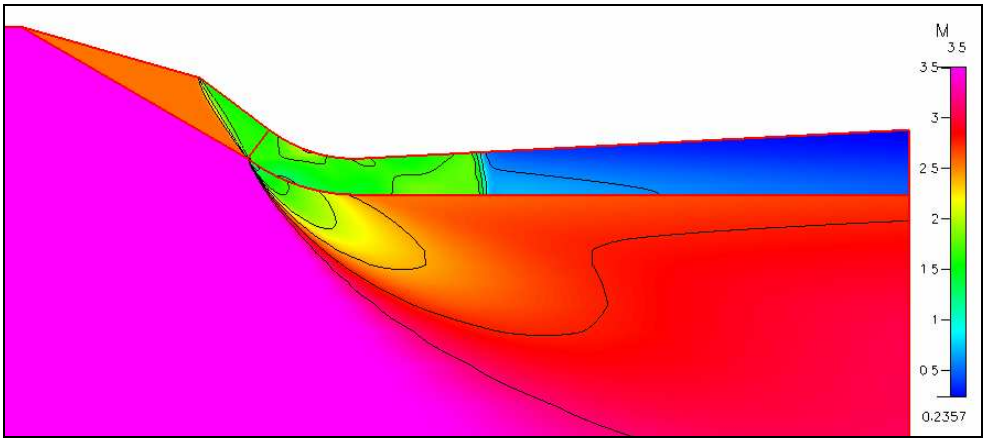

Figure 6.6 Mach number contours of the solution of case 2

Table 6.3 CFD-FASTRAN and analytical results comparison of case 2

	CFD FASTRAN Results of Case 2	**Analytical Results of Case 2**
Total Pressure Recovery	0.5233	0.5253
Capture Area Ratio	0.9943	1
Steady State Flow Distortion	0.12	-
First Oblique Shock Angle (°)	30.22	30.22
Second Oblique Shock Angle (°)	43.79	43.61
Intersection point of the two oblique shocks (mm) [with respect to inlet leading edge (0,0)]	(299.739,-174.625)	(300.428,-175.026)
Terminal Normal Shocks Distance from Inlets Leading Edge (mm)	606	655

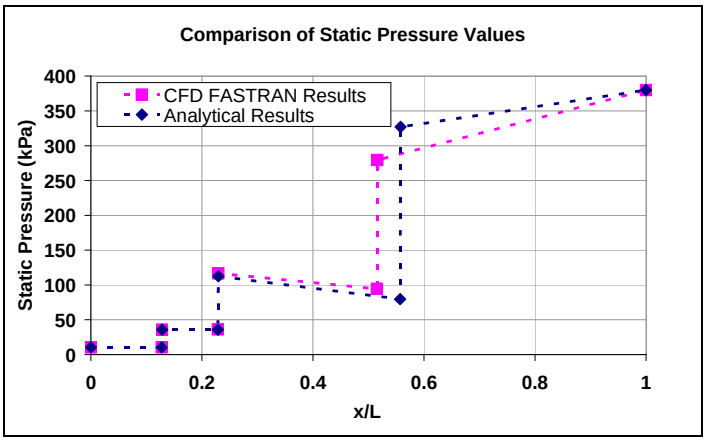

Figure 6.7 Comparison of the static pressure values for case 2

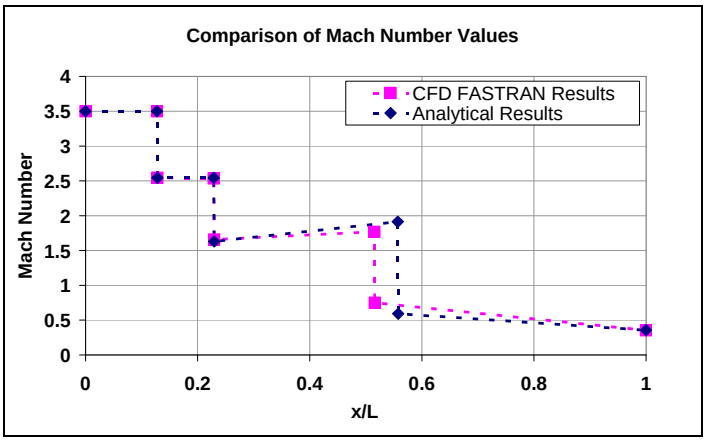

Figure 6.8 Comparison of the Mach number values for case 2

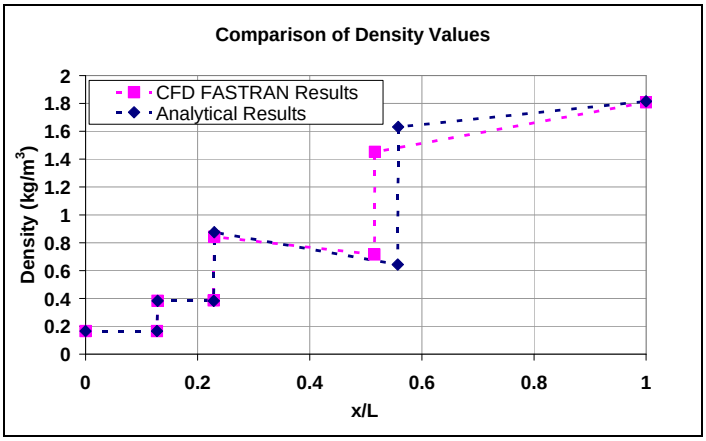

Figure 6.9 Comparison of the density values for case 2

From the results in Table 6.3 and Figure 6.6, it is seen that the first and second oblique shock angles and the coordinates of the intersection point of the two oblique shocks are identical to the analytical results. This is an indication that the CFD-FASTRAN solution is accurate.

The capture area ratio value is approximately the same as the analytical result with only a 0.5% difference. This indicates that, at on-design Mach number operating regime (keeping in mind that the solution is inviscid) the exact amount of flow required by the engine can be delivered by the inlet. The steady state flow distortion is very low, which is an expected result since the solution is an inviscid solution. The total pressure recovery is nearly the same as the analytical result with only a 0.4% difference. The exit Mach number is nearly the same as the analytical result with only a 0.7% difference. Therefore, one could expect the inviscid exit Mach number to be the same as the analytically calculated exit Mach number, and the inviscid total pressure recovery to be the same as the analytically calculated total pressure recovery during the on-design Mach number supercritical operation of the inlet.

The terminal normal shocks distance from the inlets leading edge is different from the analytical results. This is due to the fact that the analytical result is obtained with the quasi 1-D flow assumption whereas the CFD-FASTRAN solution is a 2-D flow solution therefore the terminal normal shock stands at a more upstream position due to the 2-D effects in the CFD-FASTRAN flow solution.

6.4.2 Case 1 results

(M=3.5, H=16000m, $\alpha = 0°$, critical)

In this case a root search iteration was performed in order to obtain the back pressure value that yields critical operation. In a total of 7 runs the back pressure value, specified as the fixed pressure outlet boundary condition, was increased from 380,000 Pa (back pressure value yielding supercritical operation) until the back pressure value yielding critical operation was obtained. The back pressure

values for which the solutions were obtained are 420,000 Pa; 430,000 Pa; 434,000 Pa; 452,500 Pa; 435,000 Pa; 434,200 Pa and 434,500 Pa. The difficulty encountered in this procedure was that as the exit pressure approached the critical value, the shock wave system moved very slowly, and oscillations in residuals and convergence problems were encountered and long execution times were necessary to establish a stationary shock wave. This is why this root search iteration process took a total CPU time of 101 hours. At the end of the root search iteration, it is determined that a back pressure value of 434,500 Pa yields critical operation at the on-design Mach number. With this back pressure value the terminal normal shock is positioned only 4 mm downstream of the cowl lip plane. However, it is also determined that if this back pressure value is increased to 435,000 Pa the terminal normal shock is ejected upstream of the entrance channel. It was managed to obtain a back pressure tolerance of 0.1 %. This means that a 0.1% increase in the back pressure value of 434,500 Pa will cause the terminal normal shock to be ejected from the entrance plane.

In the final converged solution of Case 1 the residuals were decreased by 4 orders in a total of 35,000 iterations. In Figure 6.10 the Mach number contours of the final converged solution are shown. In this figure the passage from purple colored contours to orange colored contours shows the first oblique shock wave and the passage from orange colored contours to green contours shows the second oblique shock wave. It can be seen that the supersonic diffuser flow picture of this case is the same as the one obtained for Case 2. The normal shock is located at the passage from green contours to blue contours. It is seen from the flowfield that the normal shock is located at the throat.

In Table 6.4, the results for the total pressure recovery, the capture area, the steady state flow distortion, the first and second oblique shock angles and the terminal normal shocks distance from the inlets leading edge are given. The results for the area averaged values of the static pressure, the Mach number and the density are given in Figure 6.11, Figure 6.12 and Figure 6.13 respectively.

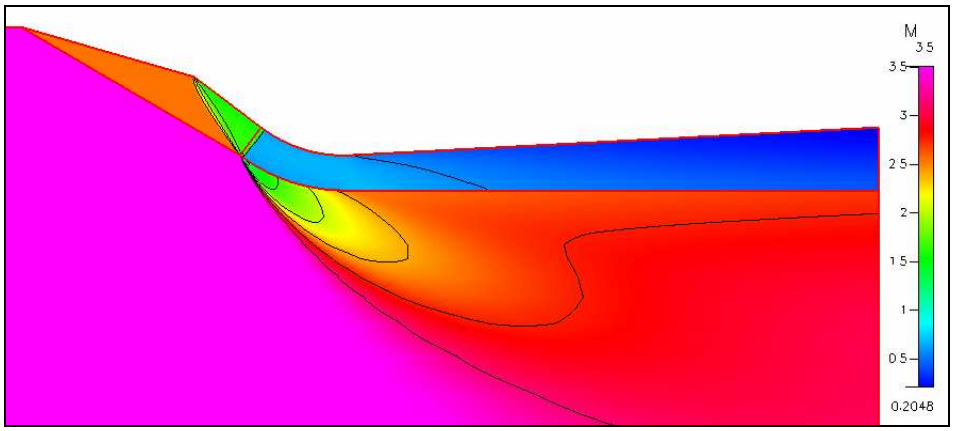

Figure 6.10 Mach number contours of the solution of case 1

Table 6.4 CFD-FASTRAN and analytical results comparison of case 1

	CFD FASTRAN Results of Case 1	**Analytical Results of Case 1**
Total Pressure Recovery	0.5909	0.6099
Capture Area Ratio	0.9943	1
Steady State Flow Distortion	0.10	-
First Oblique Shock Angle (°)	30	30
Second Oblique Shock Angle (°)	44	44
Intersection point of the two oblique shocks (mm) [with respect to inlet leading edge (0,0)]	(299.739,-174.625)	(300.428,-175.026)
Terminal Normal Shocks Distance from Inlets Leading Edge	4 mm downstream of the cowl lip plane	@ the cowl lip plane

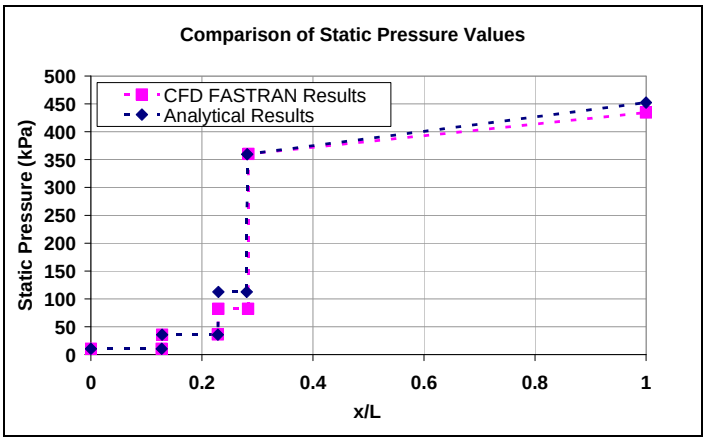

Figure 6.11 Comparison of the static pressure values for case 1

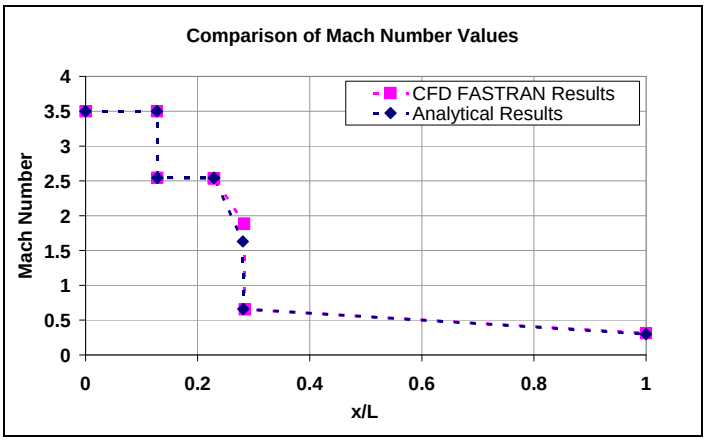

Figure 6.12 Comparison of the Mach number values for case 1

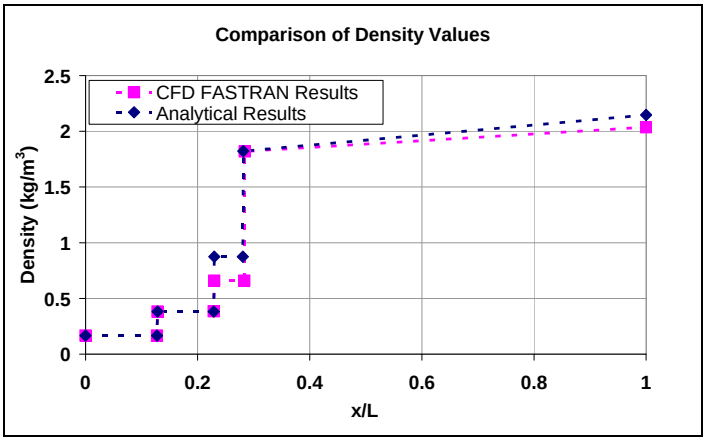

Figure 6.13 Comparison of the density values for case 1

The results in Table 6.4 and Figure 6.10, show that the first and second oblique shock angles and the coordinates of the intersection point of the two oblique shocks, moreover, the supersonic diffuser flow picture are the same as the one obtained for the on design Mach number supercritical case (Case 2). This verifies that, the supersonic diffuser flow is not affected by the movement of the terminal normal shock from the subsonic diffuser to the inlets cowl lip plane. Due to this fact, the value of the capture area ratio is also the same as the one obtained for Case 2.

The steady state flow distortion is very low: This is an expected result since the solution is an inviscid solution. The total pressure recovery is close to the analytical result with a 3.2% difference. The exit Mach number is close to the analytical result with a 4.8% difference. Therefore, it is reasonable to expect the inviscid exit Mach number to be slightly higher than the analytical value and the inviscid total pressure recovery to be slightly lower than the analytical value. The differences in these values are not major differences and are not significant enough to degrade the performance of the inlet during the on-design critical operation. It can be finally concluded that the inlet design is verified for the design-to condition since Case 1 is the case that represents the design-to condition.

6.4.3 Case 3 results

(M=3.5, H=16000m, $\alpha = 0°$, subcritical)

It was stated in Section 6.4.2 that when the exit back pressure is increased from 434,500 Pa by only 0.1% to 435,000 Pa the terminal normal shock is ejected from the entrance channel to an upstream station. However, with such a back pressure value (435,000 Pa) it is not possible to obtain a converged solution. This is due to the fact that it is not possible for the terminal normal shock to maintain a stable position upstream of the cowl lip plane and the flow is unsteady. Consequently, inlet unstart occurs. This phenomenon can be due to the interaction of the slip line

emanating from the triple shock intersection point with the cowl boundary which causes the pressure slope to presume a positive value as explained in Section 2.5.1.

This indicates that, at on-design Mach number the performed inlet design is a zero subcritical stability design. Which is perfectly reasonable since the inlet was designed to obtain maximum performance at the design-to condition. It was discussed in Section 2.5.1 that the inlet designs which have subcritical stability yield critical total pressure recovery values less than that can be achieved with “no stability” designs.

The divergence history of the solution of Case 3 in the form of Mach number contours is given in Figure 6.14.

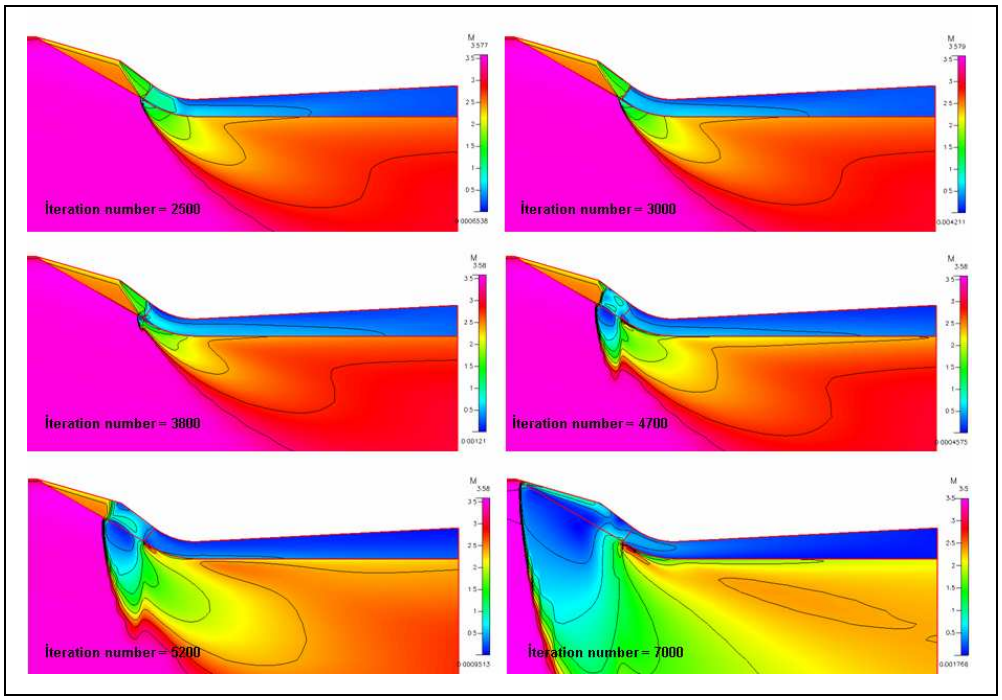

Figure 6.14 Divergence history of case 3

6.4.4 Case 5 results

(M=4.0, H=16000m, α = 0°, supercritical)

It is readily depicted from the analytical solution of this case that the intersection point of the two oblique shocks falls inside the entry stream tube boundary. Therefore, it can be expected that the slip plane emanating from the shock intersection point will interact with the cowl boundary, the flow will become unstable and inlet buzz will occur causing the inlet to unstart as discussed in Section 2.5.1. In fact, this is exactly what is obtained from the solution of this case. It was not possible to obtain a converged solution for this case due to the occurrence of the phenomenon described above. The divergence history of the solution of Case 5 in the form of Mach number contours is given in Figure 6.15.

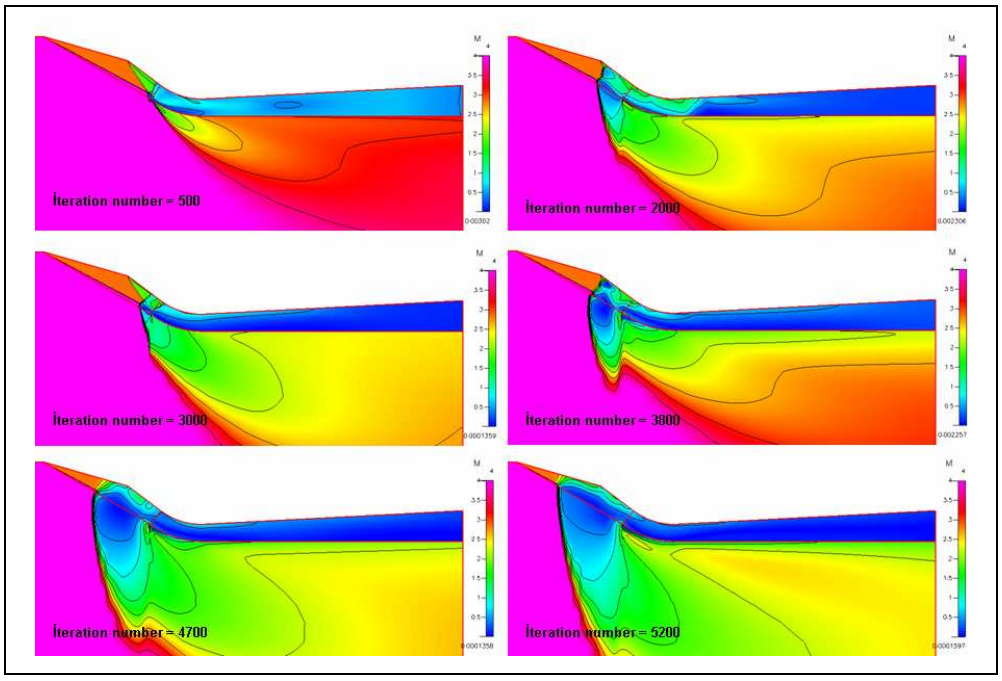

Figure 6.15 Divergence history of case 5

6.4.5 Case 4 results

(M=4.0, H=16000m, $\alpha = 0°$, critical)

If it were possible to obtain a converged solution for Case 5, then it would be possible and meaningful to perform a root search iteration for this case and to obtain the back pressure value yielding critical operation at above design Mach number. However, under these circumstances it is readily known that a converged solution will not be obtained for this case.

6.4.6 Case 6 results

(M=4.0, H=16000m, $\alpha = 0°$, subcritical)

Because of the same reasons as that of Case 4, it is readily known that a converged solution will not be obtained for this case. Therefore, Case 6 is not solved.

6.4.7 Case 8 results

(M=3.0, H=16000m, $\alpha = 0°$, supercritical)

Unlike the previous two cases, a converged solution was obtained for this case. A total of 12,000 iterations resulted in 5 orders of magnitude decrease in the residuals, taking 7.5 hours of CPU time. In this case, although the shock intersection point is not on the cowl lip it is possible to obtain a converged solution because the flow remains steady. This is due to the fact that the shock intersection point falls outside of the entrance streamtube boundary as predicted.

In Figure 6.16 the Mach number contours of the final converged solution are shown. In this figure the first oblique shock occurs at the passage from purple colored contours to orange colored contours. The second oblique shock occurs at the passage from orange colored contours to green colored contours. It can be seen that the intersection point of the oblique shocks falls below the cowl lip, outside of the entrance streamtube. The normal shock is located at the subsonic diffuser, where the contours pass from green color to blue color. In Table 6.5, the results for

the total pressure recovery, the capture area, the steady state flow distortion, the first and second oblique shock angles and the terminal normal shocks distance from the inlets leading edge are given. The results for the area averaged values of the static pressure, the Mach number and the density are given in Figure 6.17, Figure 6.18 and Figure 6.19 respectively.

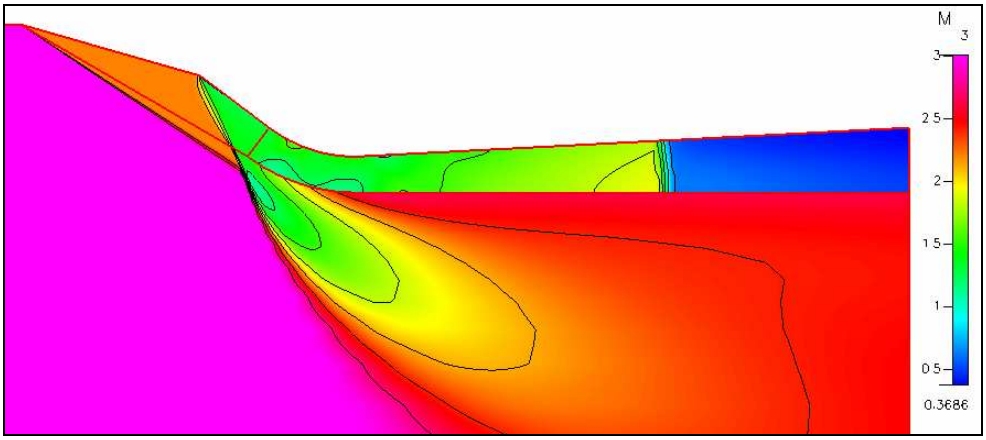

Figure 6.16 Mach number contours of the solution of case 8

Table 6.5 CFD-FASTRAN and analytical results comparison of case 8

	CFD FASTRAN Results of Case 8	**Analytical Results of Case 8**
Total Pressure Recovery	0.5617	0.5653
Capture Area Ratio	0.6803	0.8010
Steady State Flow Distortion	0.08	-
First Oblique Shock Angle(°)	33	33
Second Oblique Shock Angle (°)	50	49.5
Intersection point of the two oblique shocks (mm) [with respect to inlet leading edge (0,0)]	(294.416,-196.778)	(295.077,-193.756)
Terminal Normal Shocks Distance from Inlets Leading Edge (mm)	635	655

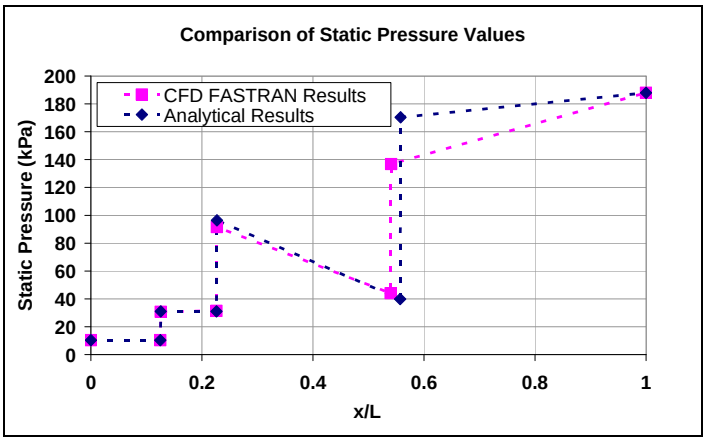

Figure 6.17 Comparison of the static pressure values for case 8

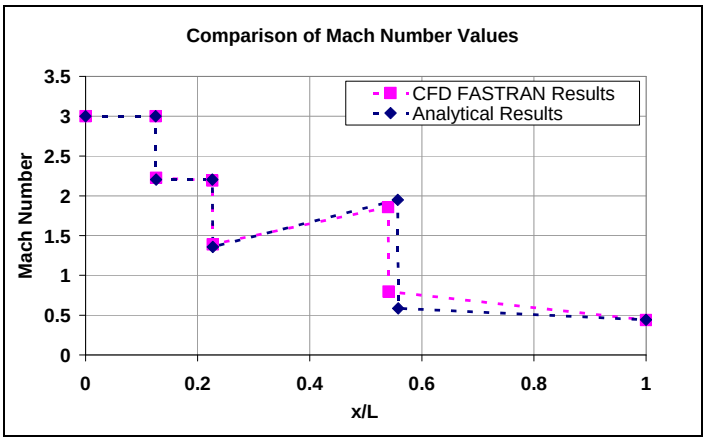

Figure 6.18 Comparison of the Mach number values for case 8

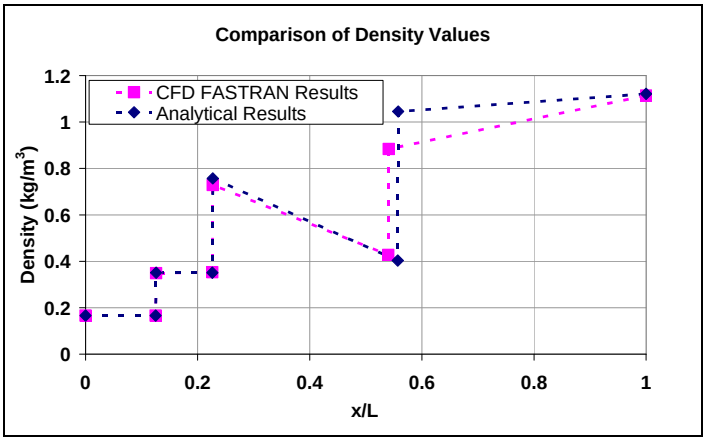

Figure 6.19 Comparison of the density values for case 8

From the results presented in Table 6.5 and Figure 6.16, it is determined that the first and second oblique shock angles and the coordinates of the intersection point of the two oblique shocks are nearly the same as the analytical results.

The capture area ratio value is 17.7% less than the analytical result. This indicates that, at below-design Mach number operating regime, the amount of flow spillage is more than that predicted through analytical procedures. The steady state flow distortion is very low, which is an expected result since the solution is an inviscid solution. The total pressure recovery is nearly the same as the analytical result with only a 0.6% difference. The exit Mach number is nearly the same as the analytical result with only a 2% difference. It is shown by these calculations that one could expect the inviscid exit Mach number to be the same as the analytically calculated exit Mach number, and the inviscid total pressure recovery to be the same as the analytically calculated total pressure recovery during the below-design Mach number supercritical operation of the inlet.

However, the terminal normal shocks distance from the inlets leading edge is different from the analytical results. This is due to the fact that the analytical result is obtained with the quasi 1-D flow assumption whereas the CFD-FASTRAN solution is a 2-D flow solution therefore the terminal normal shock stands at a more upstream distance due to the 2-D effects in the CFD-FASTRAN flow solution.

6.4.8 Case 7 results

(M=3.0, H=16000m, $\alpha = 0°$, critical)

In this case a root search iteration is performed in order to obtain the back pressure value that yields critical operation. In a total of 7 runs the back pressure value, is increased from 187,966.7 Pa, until the back pressure value yielding critical operation is obtained. The back pressure values for which the solution is obtained are 220,000 Pa, 247,785.8 Pa, 260,272.4 Pa, 253,000 Pa, 257,000 Pa, 255,000 Pa,

and, 254,000 Pa respectively. The difficulty encountered in this procedure was that as the exit pressure approached the critical value, the shock wave system moved very slowly and oscillations in residuals and convergence problems occurred. Long execution times were necessary to ensure the stability of the shock wave. This is why this root search iteration process took a total CPU time of 118.5 hours. At the end of the root search iteration it was determined that a back pressure value of 254,000 Pa yields critical operation at the on-design Mach number. With this back pressure value the terminal normal shock is positioned only 5 mm downstream of the cowl lip plane. Nevertheless, it was also determined that, if this back pressure value is increased to 255,000 Pa, the terminal normal shock is ejected upstream of the entrance channel. Therefore, it was possible to obtain a back pressure tolerance of 0.4 %. This means that a 0.4% increase in the back pressure value of 254,000 Pa will cause the terminal normal shock to be ejected from the entrance plane.

In the final converged solution of Case 7 the residuals were decreased by 4 orders at a total of 35,000 iterations. In Figure 6.20 the Mach number contours of the final converged solution are shown. It is seen from this figure that the terminal normal shock is located at the cowl lip plane, where the contours pass from green color to blue color. The first and second oblique shocks and their intersection point are located at the same positions as in Case 8 (passage from purple to orange color and the passage from orange to green color). No change in the supersonic diffuser flow picture has occurred when compared to the flow picture of Case 8. In Table 6.6, the results for the total pressure recovery, the capture area, the steady state flow distortion, the first and second oblique shock angles and the terminal normal shocks distance from the inlets leading edge are given. The results for the area averaged values of the static pressure, the Mach number and the density are given in Figure 6.21, Figure 6.22 and Figure 6.23 respectively.

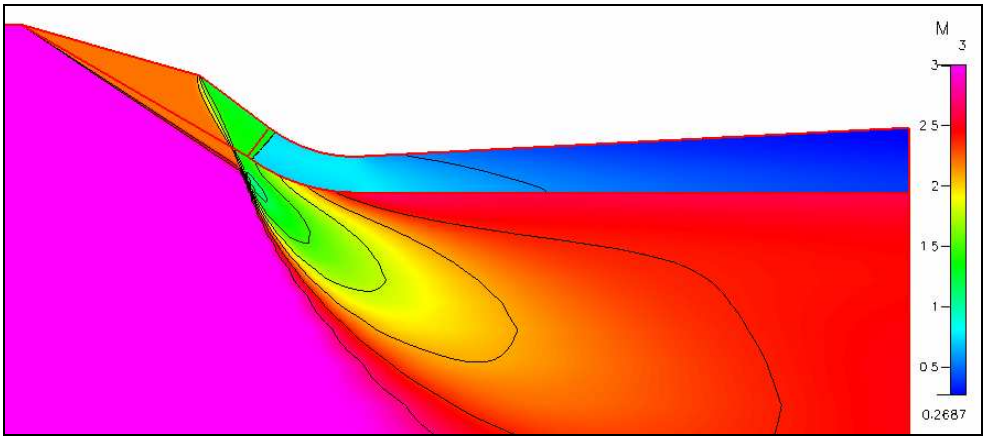

Figure 6.20 Mach number contours of the solution of case 7

Table 6.6 CFD-FASTRAN and analytical results comparison of case 7

	CFD FASTRAN Results of Case 7	**Analytical Results of Case 7**
Total Pressure Recovery	0.7176	0.7354
Capture Area Ratio	0.6803	0.8010
Steady State Flow Distortion	0.05	-
First Oblique Shock Angle (°)	33	33
Second Oblique Shock Angle (°)	50	49.5
Intersection point of the two oblique shocks (mm) [with respect to inlet leading edge (0,0)]	(294.416,-196.778)	(295.077,-193.756)
Terminal Normal Shocks Distance from Inlets Leading Edge	5 mm downstream of the cowl lip plane	@ the cowl lip plane

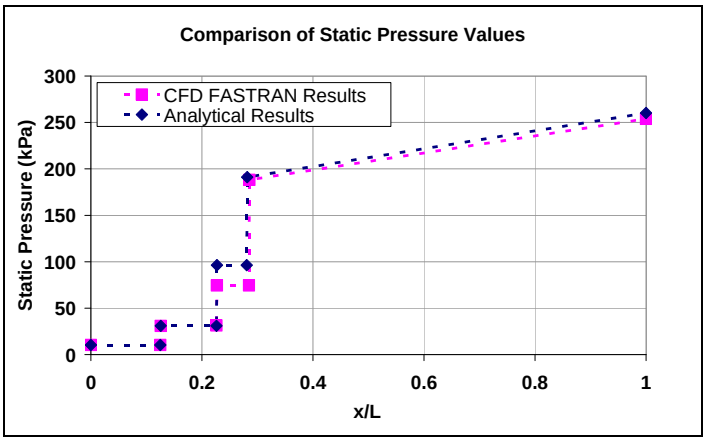

Figure 6.21 Comparison of the static pressure values for case 7

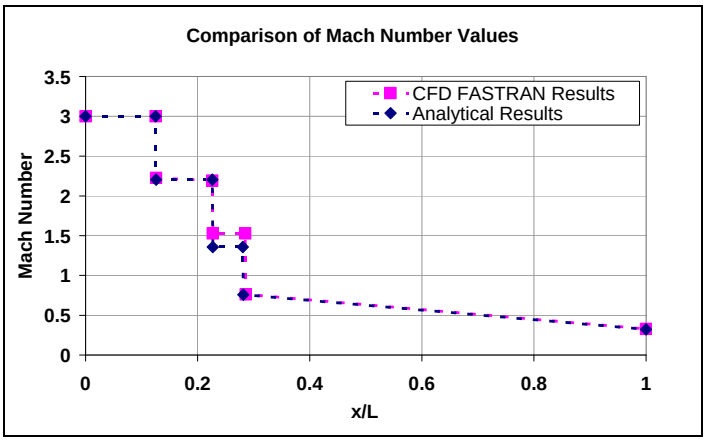

Figure 6.22 Comparison of the Mach number values for case 7

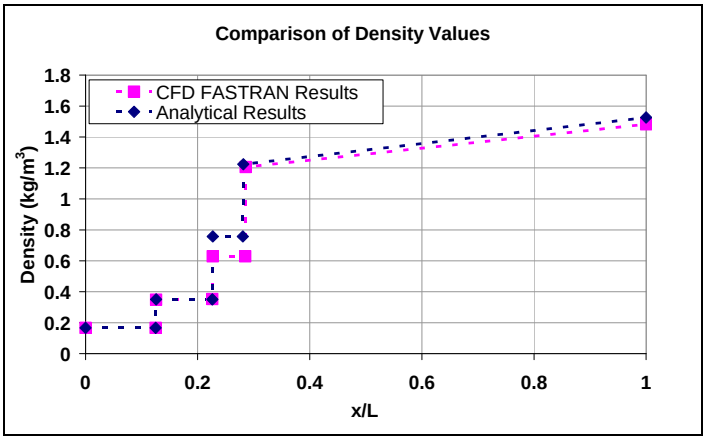

Figure 6.23 Comparison of the density values for case 7

The fact that the supersonic diffuser flow picture is the same as the one obtained for the below design Mach number supercritical case (Case 8), is clearly seen from the results in Table 6.6 and Figure 6.20. This verifies that, the supersonic diffuser flow is not affected by the movement of the terminal normal shock from the subsonic diffuser to the inlets cowl lip plane. Due to this fact, the value of the capture area ratio is also the same as the one obtained for Case 8.

The steady state flow distortion is very low, which is an expected result since the solution is an inviscid solution. The total pressure recovery is close to the analytical result with a 2.5% difference. The exit Mach number is close to the analytical result with a 1.8% difference. Therefore, it is reasonable to expect the inviscid exit Mach number to be slightly higher than the analytical value and the inviscid total pressure recovery to be a little more lower than the analytical value.

6.4.9 Case 9 results

(M=3.0, H=16000m, $\alpha = 0°$, subcritical)

It was stated in Section 6.4.8 that when the exit back pressure is increased from 254,000 Pa by only 0.4% to 255,000 Pa the terminal normal shock is ejected from the entrance channel to an upstream station. Although it was not possible to obtain a converged solution for the on-design Mach number subcritical operating case (Case 3) it was possible to obtain a converged solution for this one. The terminal normal shock manages to maintain a stable position ahead of the entrance channel while the flow remains steady. This shows that, the inlet designed at the on-design Mach number has a subcritical stability margin at this flight condition. This is perfectly reasonable since the inlet does exhibit maximum performance (in terms of total pressure recovery and capture area ratio) at this condition. It was explained in Section 2.5.1 that the inlet designs which have subcritical stability; yield critical total pressure recovery values less than that can be achieved with “no stability” designs.

In the final converged solution the residuals were decreased by 4 orders of magnitude, 35,000 iterations are realized at a total CPU time of 22 hours. In Figure 6.24 the Mach number contours of the final converged solution are shown. The first and second oblique shocks and their intersection point (intersection of purple, orange and green colored contours) is clearly seen in this figure. This intersection point falls below the cowl lip and outside of the entrance streamtube boundary. The terminal normal shock at the passage from green to blue color is located upstream of the cowl lip. In Table 6.7, only the calculated results from the CFD-FASTRAN solution (for the total pressure recovery, the capture area, the steady state flow distortion, the first and second oblique shock angles and the terminal normal shocks distance from the inlets leading edge) are presented since there are no analytical results for this case. The results for the area averaged values of the static pressure, the Mach number and the density are given in Figure 6.25, Figure 6.26 and Figure 6.27 respectively.

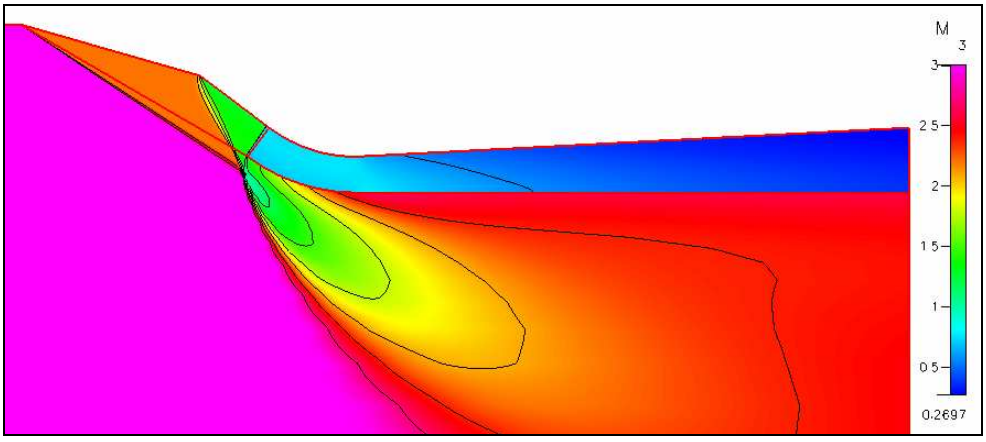

Figure 6.24 Mach number contours of the solution of case 9

Table 6.7 CFD-FASTRAN results of case 9

	CFD FASTRAN Results of Case 9
Total Pressure Recovery	0.7179
Capture Area Ratio	0.6740
Steady State Flow Distortion	0.05
First Oblique Shock Angle (°)	33
Second Oblique Shock Angle (°)	50
Terminal Normal Shocks Distance from Inlets Leading Edge	5 mm upstream of the cowl lip plane

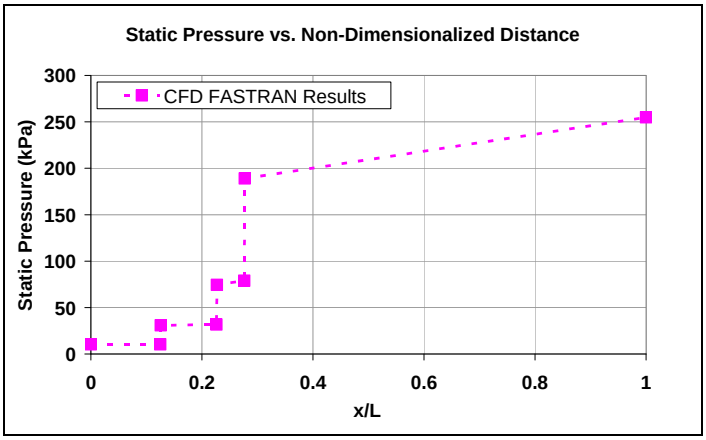

Figure 6.25 Static pressure vs. non-dimensional distance for case 9

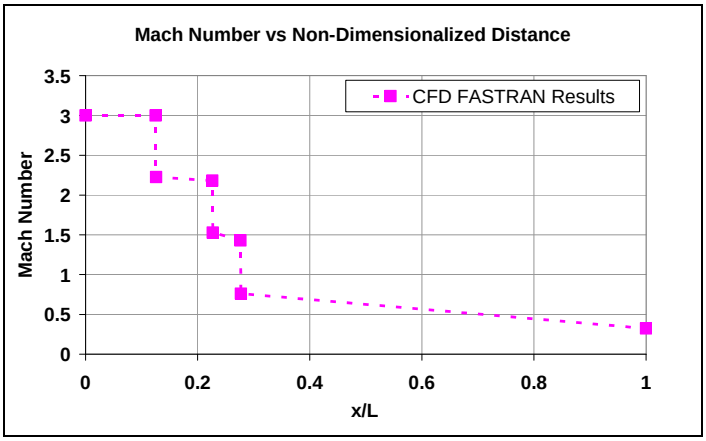

Figure 6.26 Mach number vs. non-dimensional distance for case 9

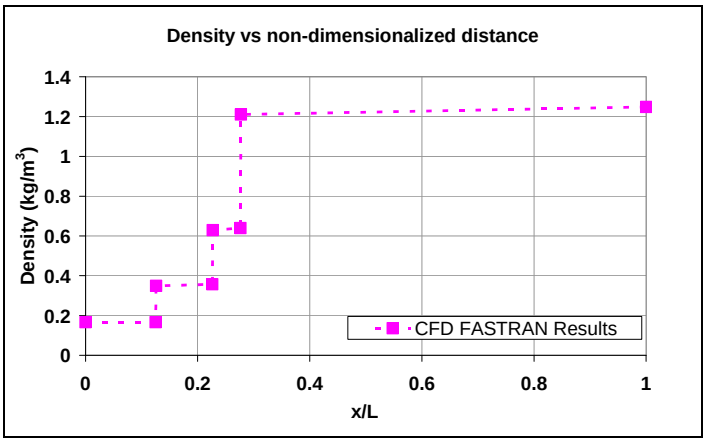

Figure 6.27 Density vs. non-dimensional distance for case 9

From the results presented in Table 6.7 and Figure 6.24, it is noticed that the capture area ratio of the below design subcritical operation case is only 0.9% less than the capture area ratio of the below design critical operation case. Thus, it can be concluded that no extra flow spillage occurs when the operating regime changes from critical to subcritical at below design Mach number of 3.0. It was mentioned in Section 2.5.1 that in subcritical operating condition, as long as the terminal normal shock maintains a stable position in the supersonic diffuser, the subcritical total pressure recovery remains nearly the same as the critical total pressure recovery value. With the solution of this case, this phenomenon is proved since the total pressure recovery value of this below design Mach number subcritical case (Case 9) is identical to the total pressure recovery value of the below design Mach number critical case (Case 7).

6.4.10 Case 11 results

(M=3.5, H=16000m, $\alpha = 10°$, supercritical)

In the final converged solution the residuals were decreased by 9 orders of magnitude, through 35,000 iterations costing at a total CPU time of 22 hours. The

convergence history of the solution of Case 11 in the form of Mach number contours is given in Figure 6.28.

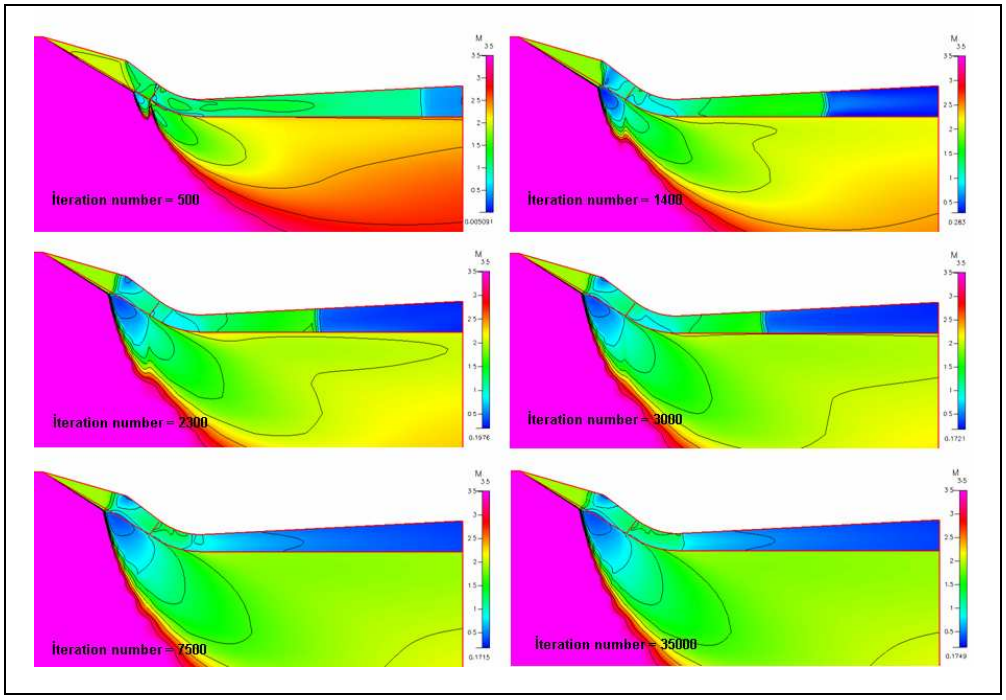

Figure 6.28 Convergence history of the solution of case 11

It can be seen from Figure 6.28 that the merger of the two oblique shocks is ejected outside of the inlet in the final solution. This occurs due to the interaction of the slip line with the cowl lip. The slip line interacting with the cowl lip causes a circulatory flow to occur at the cowl lip. This causes flow spillage and the merger of the two oblique shocks to be ejected from the inlet.

Because the resulting flowfield is very different from the predicted result, it is meaningful to only calculate the capture area ratio, the total pressure recovery, the steady state flow distortion and the Mach number at the inlet exit. These values are presented in Table 6.8.

Table 6.8 CFD-FASTRAN results of case 11

	CFD FASTRAN Results of Case 11	**Analytical Results of Case 11**
Station ch Exit Mach Number	M = 0.3408	M = 0.5299
Total Pressure Recovery	0.4074	0.4569
Capture Area Ratio	0.7477	1.1846
Steady State Flow Distortion	0.01	-

6.4.11 Case 10 results

(M=3.5, H=16000m, α = 10°, critical)

Due to the nature of the solution obtained in Case 11, it is not possible to perform a root search iteration to obtain the critical back pressure value. Therefore, this case is not solved.

6.4.12 Case 13 results

(M=3.5, H=16000m, α = -10°, supercritical)

In solution of this case the residuals are decreased by 13 orders of magnitude, with 32,800 iterations and a total CPU time of 20.5 hours. In Figure 6.29 the Mach number contours of the final converged solution are shown. In this figure, the passage from purple to red color is where the first oblique shock is located. It is noticed that the first oblique shock falls outside the cowl. Contrary to the first oblique shock, the second oblique shock falls inside the cowl at the passage from red to yellow and green colors. The normal shock is located at the subsonic diffuser at the passage from yellow and orange to blue color.

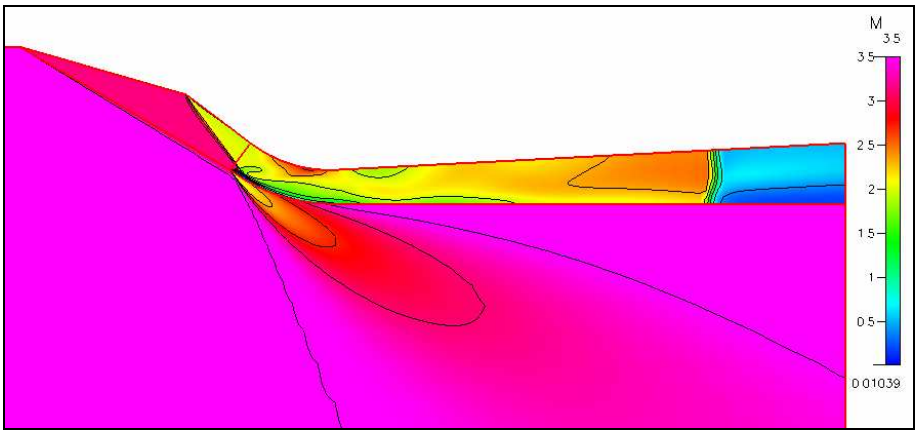

Figure 6.29 Mach number contours of the solution of case 13

Zooming to the cowl lip region a subsonic circulatory flow is observed. This is shown in Figure 6.30. The reason for this occurrence can be explained as follows: The second oblique shock falls just downstream of the entrance plane on to the cowl wall. However, the flow behind this second oblique shock is not aligned with the cowl surface and therefore, flow circulation occurs in this region.

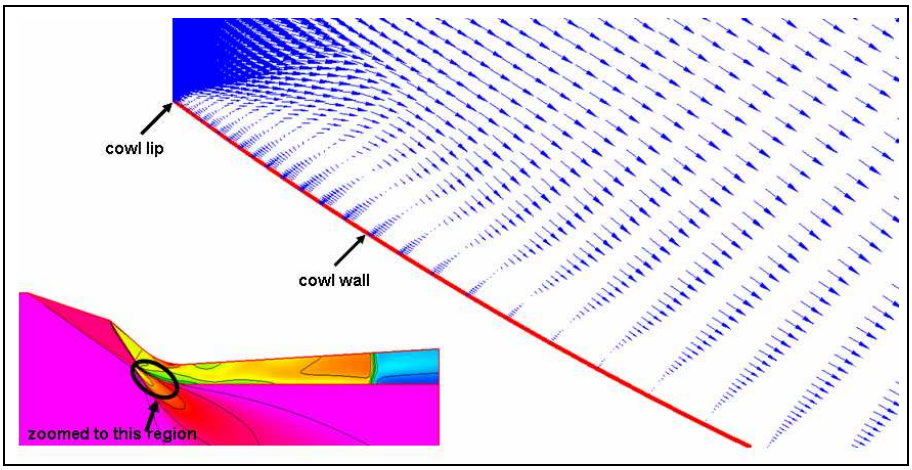

Figure 6.30 Circulatory flow region near the cowl lip region

In Table 6.9, the results for the total pressure recovery, the capture area, the steady state flow distortion, the first and second oblique shock angles and the terminal normal shocks distance from the inlets leading edge are presented. The results for

the area averaged values of the static pressure, the Mach number and the density are given in Figure 6.31, Figure 6.32 and Figure 6.33.

Table 6.9 CFD-FASTRAN and analytical results comparison of case 13

	CFD FASTRAN Results of Case 13	**Analytical Results of Case 13**
Total Pressure Recovery	0.2927	0.2896
Capture Area Ratio	0.6760	0.6763
Steady State Flow Distortion	0.21	-
First Oblique Shock Angle (°)	21	21
Second Oblique Shock Angle (°)	38.5	38
Intersection point of the second oblique shock and the cowl wall (mm) [with respect to inlet leading edge (0,0)]	No intersection. 2nd oblique shock intercepts the cowl @ (301.818,-158.288)	No intersection. 2nd oblique shock intercepts the cowl @ (329.160,-193.600)
Terminal Normal Shocks Distance from Inlets Leading Edge (mm)	983	1100

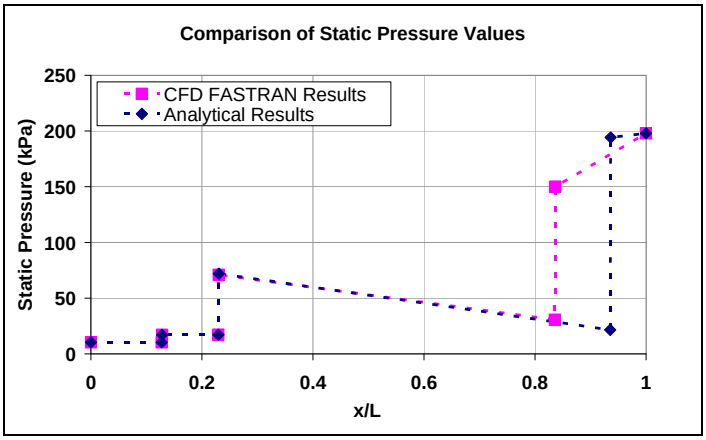

Figure 6.31 Comparison of the static pressure values for case 13

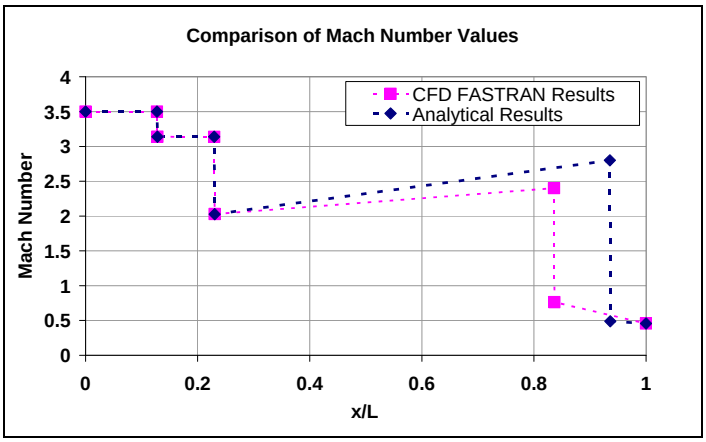

Figure 6.32 Comparison of the Mach number values for case 13

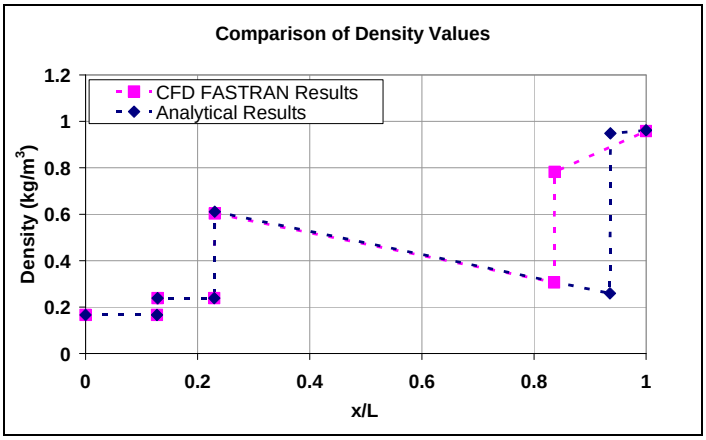

Figure 6.33 Comparison of the density values for case 13

From the results given in Table 6.9 and Figure 6.29, it can be interpreted that the first and second oblique shock angles are nearly the same as the analytical results. This is an indication that the CFD-FASTRAN solution is accurate.

The capture area ratio value is identical to the analytical result. This indicates that, at on-design Mach number negative angle of attack supercritical operating regime, the amount of flow spillage is the same as predicted with analytical procedures. The steady state flow distortion is very low, as expected, since the solution is an inviscid solution. The total pressure recovery is nearly the same as the analytical

result with only a 1% difference. The exit Mach number is identical to the analytical result. Hence, one could expect the inviscid exit Mach number to be the same as the analytically calculated exit Mach number, and the inviscid total pressure recovery to be the same as the analytically calculated total pressure recovery during the on-design Mach number negative angle of attack supercritical operation of the inlet.

The terminal normal shocks distance from the inlets leading edge is different from the analytical results. This is due to the fact that the analytical result is obtained with the quasi 1-D flow assumption whereas the CFD-FASTRAN solution is a 2-D flow solution. Therefore, the terminal normal shock stands at a more upstream distance due to the 2-D effects in the CFD-FASTRAN flow solution.

6.4.13 Case 12 results

(M=3.5, H=16000m, α = -10°, critical)

In this case a root search iteration was performed in order to obtain the back pressure value that yields critical operation. In a total of 7 runs, the back pressure value, was increased from 198046.6Pa until the back pressure value yielding critical operation was obtained. The back pressure values for which the solution is obtained are 230,000 Pa, 260,000 Pa, 275,000 Pa, 290,000 Pa, 293,000 Pa, 291,500 Pa, 290,500 Pa respectively. The difficulty encountered in this procedure was that as the exit pressure approached the critical value, the shock wave system moved very slowly and oscillations in residuals and convergence problems were encountered. Long execution times were necessary to ensure the stability of the shock wave. This is again the reason for the root search iteration process taking a total CPU time of 144 hours. At the end of this root search iteration it was determined that the terminal normal shock presumes its most upstream position with a back pressure value of 290,500 Pa. However this most upstream position of the terminal normal shock is not the critical position. When this back pressure

value is increased by only 0.3% the terminal normal shock is ejected upstream of the entrance plane. Although the back pressure tolerance obtained is 0.3%, the terminal normal shock is not positioned in critical position as can be seen in Figure 6.34. This indicates that the transient passage from supercritical operation to subcritical operation is extremely narrow, and the inlet has no subcritical stability at this case. One phenomenon triggering this occurrence can be the second oblique shock falling downstream of the cowl lip on the cowl wall and the formation of the circulatory flow (as was shown in Figure 6.30).

In the final converged solution the residuals were decreased by 3 orders of magnitude. Mach number contours of the final converged solution are shown in Figure 6.34. The supersonic diffuser flow picture remains the same when compared to the flow picture of Case 13. Once again, the first oblique shock is located outside the cowl at the passage form purple to red color. The second oblique shock at the passage from red to yellow color falls inside the cowl lip. Nevertheless, the normal shock is not located at the cowl plane. It’s positioned slightly downstream of the constant area throat in the subsonic diffuser. In Table 6.10, the results for the total pressure recovery, the capture area, the steady state flow distortion, the first and second oblique shock angles and the terminal normal shocks distance from the inlets leading edge are presented. The results for the area averaged values of the static pressure, the Mach number and the density are given in Figure 6.35, Figure 6.36, Figure 6.37.

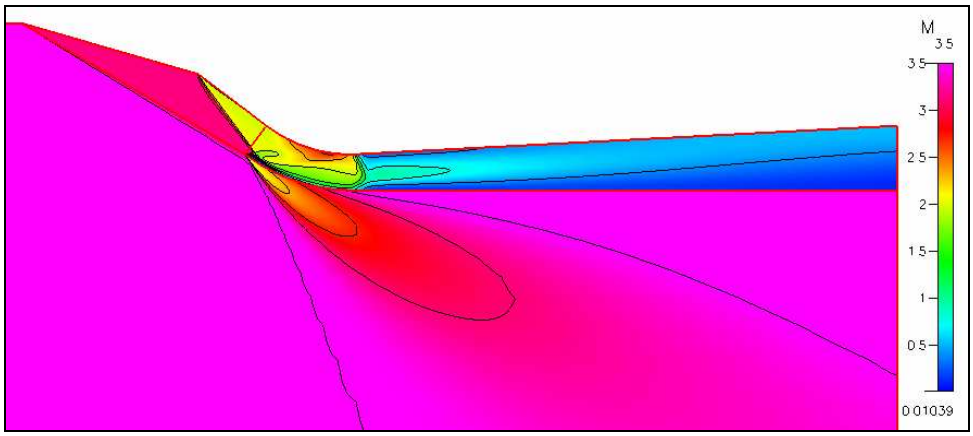

Figure 6.34 Mach number contours of the solution of case 12

Table 6.10 CFD-FASTRAN and analytical results comparison of case 12

	CFD FASTRAN Results of Case 12	**Analytical Results of Case 12**
Total Pressure Recovery	0.3999	0.5266
Capture Area Ratio	0.6760	0.6763
Steady State Flow Distortion	0.19	-
First Oblique Shock Angle (°)	21	21
Second Oblique Shock Angle (°)	38.5	38
Intersection point of the second oblique shock and the cowl wall (mm) [with respect to inlet leading edge (0,0)]	No intersection. 2nd oblique shock intercepts the cowl @ (301.818,-158.288)	No intersection. 2nd oblique shock intercepts the cowl @ (329.160,-193.600)
Terminal Normal Shocks Distance from Inlets Leading Edge (mm)	134 mm downstream of the cowl lip plane	@ the cowl lip plane

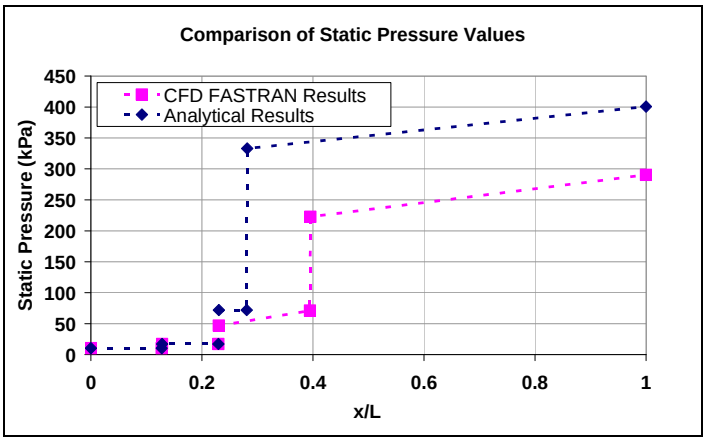

Figure 6.35 Comparison of the static pressure values for case 12

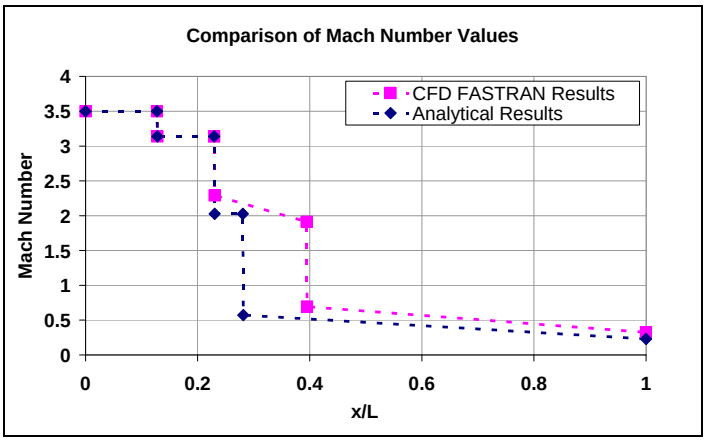

Figure 6.36 Comparison of the Mach number values for case 12

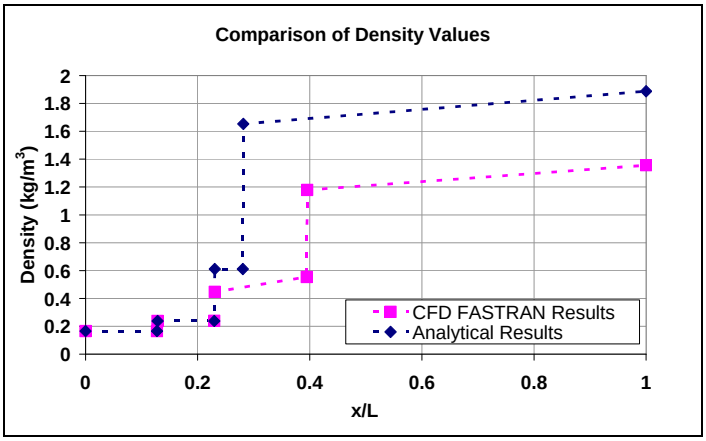

Figure 6.37 Comparison of the density values for case 12

It can obviously be seen from the results presented in Table 6.10 and Figure 6.34 that the first and second oblique shock angles and, the supersonic diffuser flow picture is the same as the one obtained for the on design Mach number negative angle of attack supercritical case (Case 13). This verifies that, the supersonic diffuser flow is not affected by the movement of the terminal normal shock from the subsonic diffuser to the inlets cowl lip plane. Due to this fact, the value of the capture area ratio is also the same as the one obtained for Case 13.

It would not be reasonable to compare the other flow parameter results obtained with CFD FASTRAN with the analytical results since the solution of this case does not exactly yield critical operation.

6.5 Final Discussion on the Results

In order to understand the on-design and off-design behavior of the flow through the designed inlet analytical and CFD analyses of the aforementioned 13 cases, namely, subcritical, critical, and supercritical operations at below design, on design, and above design Mach numbers were carried out. Analyses for on design Mach number, critical and supercritical operation at both positive and negative angle of attack values were also performed. Flow visualizations were done for these cases. In addition the relevant performance parameters were obtained. With these results, it is shown that the design-to total pressure recovery is obtained at on-design Mach number critical operation. It is also demonstrated that, the maximum mass flow rate of air (or capture area ratio) is obtained at the on-design Mach number. Furthermore, the exact amount of air required can be delivered to the engine at the on-design Mach number. The inlet design is validated for the design-to condition. It is shown that the supersonic diffuser flow picture remains unchanged when the terminal normal shock moves from a supercritical position to a critical position. It is also demonstrated that as long as the terminal normal shock maintains a stable position in the supersonic diffuser, the subcritical total pressure

recovery remains nearly the same as the critical total pressure recovery value. It is also determined that at the on-design Mach number the designed inlet exhibits zero subcritical stability, but a maximum performance. It is demonstrated that the value of the exit Mach number is dependant on the terminal normal shocks position. Thus, it can be concluded that shock position control would ease obtaining the desired exit Mach numbers. It is also proved that even in inviscid flow cases when the intersection point of the two oblique shocks falls inside of the entrance streamtube boundary, inlet flow instability occurs and the inlet unstarts. It is also understood that for the designed inlet, major performance degradation is experienced at on-design Mach number during both negative and positive angle of attack operation. It is also shown that, at the below-design Mach number operation, there is an increase in performance in terms of total pressure recovery and a degradation in performance in terms of capture area ratio when compared to on-design Mach number operation. Nevertheless, it is determined that, the designed inlet exhibits subcritical stability at below design Mach number operation.

CHAPTER 7

CONCLUSION

The present study is devoted to the understanding of air inlets of supersonic missiles. At first glance although the problem seems to be very simple, when one starts to go deep into its physics, it will not take long to realize how complicated the problem is. The proper functioning of a supersonic air inlet cannot be separated from the rest of the system. It is not only the inlet problem that one has to resolve but the integrity of the total system must be considered in order to grasp the physics of the problem. Hence, an air inlet is not a simple opening in front of an air breathing engine, but it is just another component of the engine. Therefore, understanding the behavior of an air inlet is very difficult, and one should consider numerous factors for its proper functioning.

The study is initiated by an understanding of the physics of the problem. Similar studies performed by other researches are investigated and their findings are critically analyzed within the light of the present investigation. The constraints imposed by the total system (missile) design specifications and the inlet design requirements derived from the engine design requirements are determined. These requirements state that; the inlet should capture the exact amount of air required by the ramjet engine; the inlet should accomplish the diffusion of air with a minimum loss in total pressure, the inlet should deliver the air to the engine with a tolerable amount of flow distortion and the inlet should contribute the least possible external drag to the system. Next, the design-to condition is selected. Since the major portion of the flight is spent in the cruise the design-to condition is chosen as the cruise condition. After performing the competitor study, the inlet design parameters (the family, the geometry, the supersonic diffuser form, the supersonic compression

complexity, the supersonic compression direction, the location on the vehicle body, the number of inlets and the interface with the combustor) are selected. Then, the inlet is sized using analytical methods (two dimensional shock wave equations and one dimensional gas dynamics equations). Since the inlet was sized for the design-to condition it was extremely important to investigate the performance, the flowfield behavior and the stability of the inlet at various off-design operating conditions. These analyses were first done by using analytical methods (two dimensional shock wave equations and one dimensional gas dynamics equations). After obtaining the analytical results, CFD analyses are performed. The advantage of CFD analyses over the analytical methodology is that it makes possible the visualization of the entire flowfield, and the determination of the stability condition of the flow, while providing more accurate and reliable results.

For the analysis of the physics of the problem, an analysis matrix is formed where the Mach number effect versus the terminal normal shock position is investigated. As far as the Mach number effect is considered the problem is analyzed for above, on or below design Mach numbers. For each of these three cases, the location of the terminal normal shock determined the operating regime of the inlet as being subcritical, critical or supercritical. As it was previously described, when the terminal normal shock is located at the throat the operating regime is called critical, whereas if the normal shock is located upstream or downstream of the throat the operating regimes are called subcritical or supercritical respectively. These analyses are also repeated for positive and negative angles of attack of the inlet for the on design Mach number condition where the effects of critical and supercritical conditions are investigated.

The CFD tool used for the present investigations is a commercial CFD code called CFD-FASTRAN. The use of this code has proven to be very efficient since most of the flow physics are captured. Although the code has the capability of solving both the Euler or the Navier Stokes equations with a choice of different turbulence models only the Euler equations are solved for the present investigations. Solving

the inviscid flow revealed most of the expected physical phenomenon faced in inlets except for shock boundary layer interactions. The steady state solutions are obtained for flows where no instability effects. For flows with instabilities, no steady state solutions were obtained. Hence for flows where no steady state solutions were possible, it was concluded that the phenomenon called inlet buzz occurred. This phenomenon was explained as being the flow instability observed in the supersonic diffuser in the form of an oscillation of the shock-wave system.

The evaluation of the results obtained for zero angle of attack revealed the following findings:

- As expected, the best operating condition is the on design Mach number critical operating regime (which is the design-to condition). At this condition the maximum mass flow rate, the design-to total pressure recovery and, the desired combustion chamber entrance Mach number are obtained. However, it is found that at this condition the inlet has no subcritical stability.

- At above design Mach number, unstable operation is encountered.

- At below design Mach number, there is an increase in performance in terms of total pressure recovery and a degradation in terms of capture area ratio. However, at below design Mach number the designed inlet exhibits subcritical stability. During below design Mach number operation, the subcritical total pressure recovery level is nearly the same as the critical total pressure recovery level. At below design Mach number operation the exit Mach number is increased when compared to on design Mach number operation.

- The total pressure recovery at the critical operating regime is higher than the total pressure recovery at the supercritical operating regime.

- The capture area ratio is the same for the critical and supercritical operating regimes.

For positive and negative angles of attack the following conclusions can be drawn:

- Major performance degradation in terms of both total pressure recovery and capture area ratio is experienced. The exit Mach numbers are higher when compared to the on design Mach number operation.

All these studies presented here showed that the best operating conditions of the air inlet is obtained for the design-to condition. For operations outside this condition the inlet performance is degraded to various extends. Either the inlet works but very poorly, or it does not work at all. Hence, one can say that the operating conditions of the inlet must be determined precisely before starting the design and the design of the inlet must be done accordingly. As it was stated previously the operating conditions of an inlet is very sensitive and even the slightest modifications on these parameters alter the performance of the inlet significantly. In order to alleviate this problem various solutions can be thought of such as implementing variable geometry devices or adjusting the fuel flow very accurately with very sensitive metering. These solutions are expensive solutions that require great design effort.

The results obtained in this work need to be verified in the future. Hence it would be desirable if these results are verified with experimental results. As a matter of fact all of the CFD results need to be checked with experimental results. Without experimental verification it will not be very safe to implement the conclusions to practical applications.

In particular, considering the sensitivity of the operational regime of the air inlet to changes in parameters and the geometry, it will be a prudent thing to perform experimental verification in order to cover the full flow envelope. In the present

investigation, the effects of viscosity were neglected in order to get a first order of magnitude analysis for the problem. However, the computations with viscosity would also bring up the question of appropriate turbulence modeling to be used with the viscous calculations. At this stage Euler solutions were thought to be sufficient enough since the present studies were targeted towards a preliminary analysis of the air inlet. In the future a detailed viscous analysis must be done in order to incorporate the effects of viscosity in the subsonic diffuser. The current design can be improved by implementing variable geometry devices (for example an adjustable ramp) that could compensate for the performance degradations at various off-design conditions. The stability margin of the inlet flow can be analyzed in detail via unsteady CFD analyses.

REFERENCES

[1] DKM Industries Business Group., Aerospace Systems Design Laboratory., Georgia Institute of Technology., *DKM119 Fast Attack, Air Launched Air to Ground Misssile, A Proposal to the AIAA Missile Systems Technical Comitee,* June 1999

[2] Bendot, J.G. et al., *Ramjet Air Induction System Design For Tactical Missile Application,* AGARD-LS-136, October 1984

[3] Mahoney, J.J., *Inlets for Supersonic Missiles*, AIAA Education Series, January 1991

[4] Fluid Dynamics Panel Working Group 13, *Air Intakes for High Speed Vehicles*, AGARD-AR-270, September 1991

[5] Nelsen, J., *Sandia Uses CFD Software with Adaptive Meshing Capability to Optimize Complex Inlet Design*, FLUENT Journal Article JA060, 1999

[6] Seddon, J., and Goldsmith E.L., *Intake Aerodynamics*, Collins Professional and Technical Books, 1985

[7] Fleeman, E.L., *Technologies for Future Precision Strike Missile Systems – Missile Design Technology*, RTO-EN-018, July 2001

[8] Goldsmith, E.L., *Some Aspects of Intake Design, Performance and Integration With The Airframe,* AGARD-CP-498

[9] Azevedo D.J. et al., *Prediction of Inviscid Stagnation Pressure Losses in Supersonic Inlet Flows*, AIAA Journal, Vol.28, No.10, December 1989

[10] Safarik P., and Polak A., *Optimal Shock Wave Parameters for Supersonic Inlets*, Journal of Propulsion and Power, Vol.12, No.1, February 1996

[11] Ahsun U., et al., *Design of an Actively Stabilized Near-Isentropic Inlet*, AIAA Journal, September 2003

[12] Bourdeau C., Blaize M., and Knight D., *Performance Analysis for High-Speed Missile Inlets*, Journal of Propulsion and Power, Vol.16, No.6, December 2000

[13] Blaize M., and Knight D., *Automated Optimization of Two-Dimensional High Speed Missile Inlets*, 36th AIAA Aerospace Sciences Meeting, January 1998

[14] Blaize M., Knight D., and Rasheed K., *Automated Optimal Design of Two-Dimensional Supersonic Missile Inlets*, Journal of Propulsion and Power, Vol.14, No. 6, December 1998

[15] Knight D., et al., *High Performance Supersonic Missile Inlet Design Using Automated Optimization*, 6th AIAA/NASA/ISSMO Symposium on Multidisciplinary Analysis and Optimization, July 1996

[16] Knight D., et al., Three Dimensional Optimization of Supersonic Inlets, 35th AIAA/ASME/SAE/ASEE Joint Propulsion Conference and Exhibit, June 1999

[17] Connors, J.F., *Some Aspects of Supersonic Inlet Stability*, NACA RM E55L16a, February 1956

[18] Pordal, H.S., *Transient Behavior of Supersonic Flow Through Inlets*, AIAA Journal, Vol.30, No.3, March 1992

[19] Pamadi, B.N et al., *Subcritical Flow Studies on Two-Dimensional External Compression Supersonic Inlets*, Journal of Propulsion and Power Vol.8, No.4, August 1992

[20] Rodi, P.E., and Trexler, C.A., *Unsteady Pressure Behavior in a Ramjet/Scramjet Inlet*, Journal of Propulsion and Power Vol.12, No.3, June 1996

[21] Miller, D.N., and Smith B.R., *CFD Based Simulation of Inlet Unstart Phenomena: Toward Supersonic Inlet Flow Control Techniques*, 4th ASME/JSME Joint Fluids Engineering Conference, July 2003

[22] Mayer, D.W., and Paynter G.C., *Boundary Conditions for Unsteady Supersonic Inlet Analyses*, AIAA Journal, Vol.32, No.6, June 1994

[23] Knight D., et al., *Investigations of High-Speed Civil Transport Inlet Unstart at Angle of Attack*, Journal of Aircraft, Vol.35, No.6, December 1998

[24] Knight D., et al., *Numerical Simulation of High Speed Civil Transport Inlet Operability with Angle of Attack*, AIAA Journal, Vol.36, No.7, July 1998

[25] Tindell, R.H., and Hill, W.G., *CFD Analysis of the X-29 Inlet at High Angle of Attack*, Journal of Aircraft, Vol.30, No.4, August 1993

[26] Chan, J.J., and Liang S.M., *Numerical Investigation of Supersonic Mixed Compression Inlet Using an Implicit Upwind Scheme*, Journal of Propulsion and Power, Vol. 8, No.1, February 1992

[27] Holland, S.D., and Perkins, J.N., *Inviscid Parametric Analysis of Three-Dimensional Inlet Performance*, Journal of Aircraft, Vol.31, No.3, June 1994

[28] Smart, M.K., *Optimization of Two-Dimensional Scramjet Inlets*, Journal of Aircraft, Vol.36, No.2, April 1999

[29] Hsia, Y.C., et al., *Inviscid Analysis of a Dual Mode Scramjet Inlet*, Journal of Propulsion and Power, Vol.7, No.6, December 1991

[30] Ng, W.F., Ajmani, K., and Taylor, A.C., *Turbulence Modeling in a Hypersonic Inlet*, AIAA Journal, Vol.27, No.10, October 1989

[31] Cockrell, E.C., and Huebner, L.D., *Generic Hypersonic Inlet Module Analysis*, AIAA 91-3209, AIAA 9th Applied Aerodynamics Conference, September 1991

[32] Ender, T.R, McClure, E.K., and Mavris, D.N., *Development of an Integrated Parametric Environment for Conceptual Hypersonic Missile Sizing*, AIAA 2002-5856, Aircraft Technology, Integration, and Operations 2002 Technical Forum, October 1992

[33] Anderson J.D., *Fundamentals of Aerodynamics second edition*, McGraw Hill, 1991

[34] Delery., J., *Air Intakes for Aircraft and Missiles*, notes from the course given at Sup-Aero

[35] Zucrow, M.J., and Hoffman, J.D. *Gas Dynamics Volume I*, John Wiley & Sons, 1976

[36] Burdette G.W. and Meyers, G.W., *Solid Fuel Ramjet Composition*, United States Patent, Patent Number 5320692, June 1994

[37] U.S. Standard Atmosphere, 1976, http://tpsx.arc.nasa.gov/cgi-perl/alt.pl, December 2004

[38] CFD- FASTRAN™ User Manual, Version 2003, CFD Research Corporation, 2003

[39] Bahar, C., *Euler Solutions for A Medium Range Cargo Aircraft*, A Thesis Submitted to the Graduate School of Natural and Applied Sciences of The Missle East Technical University, January 2001

[40] CFD- FASTRAN™ Theory Manual, Version 2002, CFD Research Corporation, 2002

APPENDIX A

ANALYTICALLY CALCULATED FLOW PARAMETERS RESULTS

Table A.1 Analytically calculated flow parameters results of case 1

CASE1					
FLOW PROPERTIES					
A0/Ac	1				
Ptch/Pt0	0.6099				
beta1(deg)	30.22				
beta2(deg)	43.61				
coordinates of intersection point of the 2 oblique shocks (mm) Note: (0,0) is the inlets leading edge	(300.428,-175.026)				
FLOW PROPERTIES at STATIONS	**STATIONS**				
	0	**1**	**2**	**3**	**ch**
Mach Number	3.5	2.5446	1.6304	0.6595	0.3
Speed of Sound (m/s)	295.07	361.78	442.85	525.68	543.20
Velocity (m/s)	1032.745	920.57	722.04	346.70	162.96
Static Pressure (Pa)	10353	35768.5	122587.5	359763.3	452511.1
Total Pressure (Pa)	789647.1	654921.9	545102.2	481666.6	481666.6
Static Temperature (K)	216.65	325.69	487.99	687.63	734.23
Density (kg/m^3)	0.16647	0.38258	0.87511	1.82259	2.14702
Total Temperature (K)	747.4425	747.4425	747.4425	747.4425	747.4425
mass flow rate of air (kg/s)	4.5136	4.5136	4.5136	4.5136	4.5136
Direction of Velocity Vector with horizontal (degrees)	0	-16	-37	-37 (at first tangent)	0

Table A.2 Analytically calculated flow parameters results of case 4

CASE4					
FLOW PROPERTIES					
A0/Ac	1				
Ptch/Pt0	0.4862				
beta1(deg)	28.1				
beta2(deg)	40.18				
coordinates of intersection point of the 2 oblique shocks (mm) Note: (0,0) is the inlets leading edge	(299.079,-159.693)				
FLOW PROPERTIES at STATIONS	**STATIONS**				
	0	**1**	**2**	**3**	**ch**
Mach Number	4.0	2.8572	1.8479	0.6061	0.2334
Speed of Sound (m/s)	295.07	372.70	466.15	583.67	601.44
Velocity (m/s)	1180.280	1064.88	861.42	353.78	140.40
Static Pressure (Pa)	10353	41142.9	156251.2	596469.8	735863.3
Total Pressure (Pa)	1571950	1217816	966042.0	764318.7	764318.7
Static Temperature (K)	216.65	345.65	540.70	847.70	900.12
Density (kg/m^3)	0.16647	0.41466	1.00669	2.45117	2.84796
Total Temperature (K)	747.4425	747.4425	747.4425	747.4425	747.4425
mass flow rate of air (kg/s)	4.5136	4.5136	4.5136	4.5136	4.5136
Direction of Velocity Vector with horizontal (degrees)	0	-16	-37	-37 (at first tangent)	0

Table A.3 Analytically calculated flow parameters results of case 7

CASE 7					
FLOW PROPERTIES					
A0/Ac	0.80103				
Ptch/Pt0	0.7354				
beta1(deg)	33.29				
beta2(deg)	49.47				
coordinates of intersection point of the 2 oblique shocks (mm) Note: (0,0) is the inlets leading edge	(295.077,-193.756)				
FLOW PROPERTIES at STATIONS	**STATIONS**				
	0	**1**	**2**	**3**	**ch**
Mach Number	3.0	2.2039	1.3574	0.7584	0.3222
Speed of Sound (m/s)	295.07	351.67	422.08	467.61	488.70
Velocity (m/s)	885.210	775.03	572.95	354.62	157.45
Static Pressure (Pa)	10353	31021.7	96386.0	191140.4	260272.4
Total Pressure (Pa)	380293.9	333633.5	288884.6	279680.3	279680.3
Static Temperature (K)	216.65	307.73	443.30	544.09	594.28
Density (kg/m^3)	0.16647	0.35118	0.75743	1.22380	1.52570
Total Temperature (K)	606.62	606.62	606.62	606.62	606.62
mass flow rate of air (kg/s)	3.6155	3.6155	3.6155	3.6155	3.6155
Direction of Velocity Vector with horizontal (degrees)	0	-16	-37	-37 (at first tangent)	0

Table A.4 Analytically calculated flow parameters results of case 10

CASE 10					
FLOW PROPERTIES					
A0/Ac	1.1846				
Ptch/Pt0	0.49132				
beta1(deg)	42.01 (with respect to flow!)				
beta2(deg)	60.15				
coordinates of intersection point of the 2 oblique shocks (mm) Note: (0,0) is the inlets leading edge	(261.219,-163.291)				
FLOW PROPERTIES at STATIONS	**STATIONS**				
	0	**1**	**2**	**3**	**ch**
Mach Number	3.5	1.9199	1.0292	0.9720	0.47828
Speed of Sound (m/s)	295.07	415.83	497.87	502.65	535.95
Velocity (m/s)	1032.745	798.35	512.43	488.56	256.33
Static Pressure (Pa)	10353	64545.1	198044.0	211754.1	331744.7
Total Pressure (Pa)	789647.1	446016.7	387990.4	387972.5	387972.5
Static Temperature (K)	216.65	430.26	616.79	628.70	714.74
Density (kg/m^3)	0.16647	0.52259	1.11855	1.17331	1.61693
Total Temperature (K)	747.4425	747.4425	747.4425	747.4425	747.4425
mass flow rate of air (kg/s)	5.3467	5.3467	5.3467	5.3467	5.3467
Direction of Velocity Vector with horizontal (degrees)	10	-16	-37	-37 (at first tangent)	0

Table A.5 Analytically calculated flow parameters results of case 12

CASE 12					
FLOW PROPERTIES					
A0/Ac	0.67626				
Ptch/Pt0	0.5266				
beta1(deg)	20.97 (with respect to flowl)				
beta2(deg)	37.92				
coordinates of intersection point of the 2 oblique shocks (mm) Note: (0,0) is the inlets leading edge	no intersection 2nd oblique shock intercepts cowl at (329.16,-193.6)				
FLOW PROPERTIES at STATIONS	**STATIONS**				
	0	**1**	**2**	**3**	**ch**
Mach Number	3.5	3.1398	2.0272	0.5729	0.2299
Speed of Sound (m/s)	295.07	317.95	406.07	530.96	545.19
Velocity (m/s)	1032.745	998.29	823.18	304.18	125.34
Static Pressure (Pa)	10353	17229.0	71969.4	333062.5	400802.0
Total Pressure (Pa)	789647.1	779131.8	587188.0	415826.8	415826.8
Static Temperature (K)	216.65	251.55	410.30	701.51	739.62
Density (kg/m^3)	0.16647	0.23860	0.61104	1.65394	1.88780
Total Temperature (K)	747.4425	747.4425	747.4425	747.4425	747.4425
mass flow rate of air (kg/s)	3.0524	3.0524	3.0524	3.0524	3.0524
Direction of Velocity Vector with horizontal (degrees)	-10	-16	-37	-37 (at first tangent)	0

Table A.6 Analytically calculated flow parameters results of case 2

CASE 2						
FLOW PROPERTIES						
A0/Ac	1					
Ptch/Pt0	0.5253					
beta1(deg)	30.22					
beta2(deg)	43.61					
teminal normal shocks distance from inlets leading edge (mm)	655.644					
coordinates of intersection point of the 2 oblique shocks (mm) Note: (0,0) is the inlets leading edge	(300.428,-175.026)					
FLOW PROPERTIES at STATIONS	**STATIONS**					
	0	**1**	**2**	**s**	**3**	**ch**
Mach Number	3.5	2.5446	1.6304	1.9139	0.5930	0.356
Speed of Sound (m/s)	295.07	361.78	442.85	416.37	529.76	541.25
Velocity (m/s)	1032.745	920.57	722.04	796.90	314.12	192.67
Static Pressure (Pa)	10353	35768.5	122587.5	79620.8	326993.3	380000.1
Total Pressure (Pa)	789647.1	654921.9	545102.2	545102.2	414786.4	414786.4
Static Temperature (K)	216.65	325.69	487.99	431.40	698.30	729.00
Density (kg/m^3)	0.16647	0.38258	0.87511	0.64296	1.63121	1.81598
Total Temperature (K)	747.4425	747.4425	747.4425	747.4425	747.4425	747.4425
mass flow rate of air (kg/s)	4.5136	4.5136	4.5136	4.5136	4.5136	4.5136
Direction of Velocity Vector with horizontal (degrees)	0	-16	-37	0	0	0

Table A.7 Analytically calculated flow parameters results of case 8

CASE 8						
FLOW PROPERTIES						
A0/Ac	0.80103					
Ptch/Pt0	0.5653					
beta1(deg)	33.29					
beta2(deg)	49.47					
teminal normal shocks distance from inlets leading edge (mm)	655.35					
coordinates of intersection point of the 2 oblique shocks (mm) Note: (0,0) is the inlets leading edge	(295.077,-193.756)					
FLOW PROPERTIES at STATIONS	**STATIONS**					
	0	**1**	**2**	**s**	**3**	**ch**
Mach Number	3.0	2.2039	1.3574	1.9500	0.5862	0.44217
Speed of Sound (m/s)	295.07	351.66	422.08	372.12	477.60	484.37
Velocity (m/s)	885.210	775.03	572.95	725.64	279.97	214.17
Static Pressure (Pa)	10353	31021.7	96386.0	39902.3	170366.3	187966.7
Total Pressure (Pa)	380293.9	333633.5	288884.6	288884.6	214973.5	214973.5
Static Temperature (K)	216.65	307.70	443.30	344.57	567.61	583.79
Density (kg/m^3)	0.16647	0.35118	0.75743	0.40342	1.04561	1.12165
Total Temperature (K)	606.62	606.62	606.62	606.62	606.62	606.62
mass flow rate of air (kg/s)	3.6155	3.6155	3.6155	3.6155	3.6155	3.6155
Direction of Velocity Vector with horizontal (degrees)	0	-16	-37	0	0	0

Table A.8 Analytically calculated flow parameters results of case 11

CASE 11						
FLOW PROPERTIES						
A0/Ac	1.1846					
Ptch/Pt0	0.4569					
beta1(deg)	42.01 (with respect to flow!)					
beta2(deg)	60.15					
teminal normal shocks distance from inlets leading edge (mm)	929.84					
coordinates of intersection point of the 2 oblique shocks (mm) Note: (0,0) is the inlets leading edge	(261.219,-163.291)					
FLOW PROPERTIES at STATIONS	**STATIONS**					
	0	**1**	**2**	**s**	**3**	**ch**
Mach Number	3.5	1.9199	1.0292	1.5000	0.7011	0.5299
Speed of Sound (m/s)	295.07	415.83	497.87	455.14	522.97	533.30
Velocity (m/s)	1032.745	798.35	512.43	682.72	366.65	282.58
Static Pressure (Pa)	10353	64545.1	198044.0	105689.8	259820.7	297967.9
Total Pressure (Pa)	789647.1	446016.7	387990.4	387990.4	360753.5	360753.5
Static Temperature (K)	216.65	430.26	616.79	515.48	680.54	707.70
Density (kg/m^3)	0.16647	0.52259	1.11854	0.71427	1.33001	1.46674
Total Temperature (K)	747.4425	747.4425	747.4425	747.4425	747.4425	747.4425
mass flow rate of air (kg/s)	5.3467	5.3467	5.3467	5.3467	5.3467	5.3467
Direction of Velocity Vector with horizontal (degrees)	10	-16	-37	0	0	0

Table A.9 Analytically calculated flow parameters results of case 13

CASE 13						
FLOW PROPERTIES						
A0/Ac	0.67626					
Ptch/Pt0	0.2896					
beta1(deg)	20.97 (with respect to flowl)					
beta2(deg)	37.92					
teminal normal shocks distance from inlets leading edge (mm)	1100.754					
coordinates of intersection point of the 2 oblique shocks (mm) Note: (0,0) is the inlets leading edge	no intersection 2nd oblique shock intercepts cowl at (329.16,-193.6)					
FLOW PROPERTIES at STATIONS	**STATIONS**					
	0	**1**	**2**	**s**	**3**	**ch**
Mach Number	3.5	3.1398	2.0272	2.8000	0.4882	0.4582
Speed of Sound (m/s)	295.07	317.95	406.07	342.01	535.46	536.91
Velocity (m/s)	1032.745	998.29	823.18	957.63	261.41	246.00
Static Pressure (Pa)	10353	17229.2	71969.4	21636.9	194299.2	198046.6
Total Pressure (Pa)	789647.1	779131.8	587188.0	587188.0	228709.7	228709.7
Static Temperature (K)	216.65	251.55	410.30	291.06	713.44	717.32
Density (kg/m^3)	0.16647	0.23860	0.61104	0.25897	0.94875	0.96181
Total Temperature (K)	747.4425	747.4425	747.4425	747.4425	747.4425	747.4425
mass flow rate of air (kg/s)	3.0524	3.0524	3.0524	3.0524	3.0524	3.0524
Direction of Velocity Vector with horizontal (degrees)	-10	-16	-37	0	0	0